

AN ULTRAVIOLET SULFUR DIOXIDE
DETECTION USING AN OPEN-PATH
OPTICAL FIBER BASED SENSOR FOR
ENCLOSED BUILDING MONITORING
APPLICATION



ZUL RASYIED BIN AB. RASAT

اونيورسيتي مليسيا قهغ

UNIVERSITI MALAYSIA PAHANG

MASTER OF ENGINEERING
(ELECTRONIC)

UNIVERSITI MALAYSIA PAHANG

UNIVERSITI MALAYSIA PAHANG

DECLARATION OF THESIS AND COPYRIGHT

Author's Full Name : ZUL RASYIED BIN AB. RASAT

Date of Birth : 890926-03-5117

Title : AN ULTRAVIOLET SULFUR DIOXIDE DETECTION USING
AN OPEN-PATH OPTICAL FIBER BASED SENSOR FOR
ENCLOSED BUILDING MONITORING APPLICATION

Academic Session : SEMESTER 1 2020/2021

I declare that this thesis is classified as:

- CONFIDENTIAL (Contains confidential information under the Official Secret Act 1997)*
- RESTRICTED (Contains restricted information as specified by the organization where research was done)*
- OPEN ACCESS I agree that my thesis to be published as online open access (Full Text)

I acknowledge that Universiti Malaysia Pahang reserves the following rights:

1. The Thesis is the Property of Universiti Malaysia Pahang
2. The Library of Universiti Malaysia Pahang has the right to make copies of the thesis for the purpose of research only.
3. The Library has the right to make copies of the thesis for academic exchange.

Certified by:

(Student's Signature)

890926-03-5117

(Supervisor's Signature)

ASSOC. PROF. TS. DR. HADI
MANAP

New IC Number

Date: 16th JANUARY 2021

Supervisor's Name

Date: 16th JANUARY 2021

NOTE : * If the thesis is CONFIDENTIAL or RESTRICTED, please attach a thesis declaration letter.

SUPERVISOR'S DECLARATION

We hereby declare that we have checked this thesis and in our opinion, this thesis is adequate in terms of scope and quality for the award of the degree of Master of Engineering (Electronic).

(Supervisor's Signature)

Full Name : ASSOC. PROF. TS. DR. HADI BIN MANAP

Position : SENIOR LECTURER

Date : 16th JANUARY 2021

(Co-supervisor's Signature)

Full Name : ASSOC. PROF. DR. MUHAMMAD SHARFI BIN NAJIB

Position : SENIOR LECTURER

Date : 16th JANUARY 2021

STUDENT'S DECLARATION

I hereby declare that the work in this thesis is based on my original work except for quotations and citations which have been duly acknowledged. I also declare that it has not been previously or concurrently submitted for any other degree at Universiti Malaysia Pahang or any other institutions.

(Student's Signature)

Full Name : ZUL RASYIED BIN AB. RASAT

ID Number : MEL14001

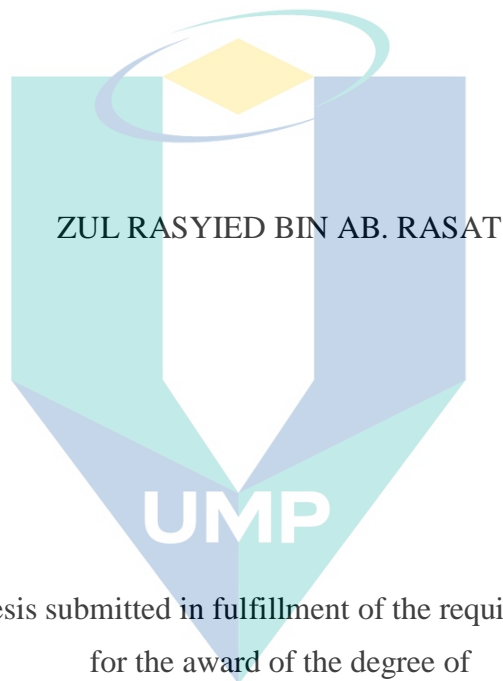
Date : 16th JANUARY 2021

UMP

اونيورسيتي ملايسيا قهغ

UNIVERSITI MALAYSIA PAHANG

AN ULTRAVIOLET SULFUR DIOXIDE DETECTION USING AN OPEN-PATH
OPTICAL FIBER BASED SENSOR FOR ENCLOSED BUILDING MONITORING
APPLICATION



Thesis submitted in fulfillment of the requirements
for the award of the degree of
Master of Engineering (Electronic)

اونيورسيتي ملايسيا قهغ

UNIVERSITI MALAYSIA PAHANG

Faculty of Electrical and Electronic Engineering Technology

UNIVERSITI MALAYSIA PAHANG

JANUARY 2021

ACKNOWLEDGEMENTS

In the name of Allah, the Most Beneficent, the Most Merciful. All the praise be to Allah, Lord of Alamin. Prayers and peace be upon our Prophet, Muhammad, his family and all of his companions. I am very grateful to Allah because of His grace, these studies have been carried out successfully.

First of all, a million thanks addressed to my beloved parent, Mr. Ab. Rasat Bin Mohd Ali and Roslina Binti Sulaiman, who has been given never ending support on everything I'm been doing. Their love is unconditional and selfless. May Allah have mercy on my parents, bless them and allow me to serve them. Ameen.

In this opportunity, I would like to express gratitude and infinite thanks to Assoc. Prof. Ts. Dr. Hadi Bin Manap, my research supervisor who has provided instruction, guidance, criticism, encouragement and advice that is meaningful to me from an early stage planning and up to the final stage of this study completed successfully.

Appreciation also to Assoc. Prof. Dr. Muhammad Sharfi Bin Najib, as my Co-Supervisor for cooperation, commitment, caring, sharing of knowledge and experience during my master study at Universiti Malaysia Pahang.

Special thanks to Assoc. Prof. Dr. Mohd Mawardi Bin Saari and all the staff at Faculty of Electrical & Electronic Engineering Technology who has given their cooperation and supports to me up to this day.

Not to mention, I am deeply thankful and blessed for the special, unique, amazing people in my life especially my friends, Dr. Amirul Mukmin, Dr. Mohamad Suhaimi and Dr. Nasrul Hadi who support me, uplift me, comfort me and bring joy to my soul as they share a piece of their own in the precise magical moment it needed to happen. My being truly loves yours.

Finally, thanks to all those who have been involved either directly or indirectly in helping to complete this thesis.

UNIVERSITI MALAYSIA PAHANG

ABSTRAK

Tesis ini menerangkan pengesanan Sulfur Dioksida (SO_2) di rantau UV. Peningkatan kawasan bandar menjadikan permintaan tenaga bertambah tinggi, oleh itu lebih banyak lagi seperti kilang bahan api fosil, alam sekitar, industri automotif dan berasaskan kimia perlu dikendalikan dan dibina. Kebanyakan sensor SO_2 yang boleh didapati secara komersial adalah berasaskan penyerapan kimia yang merupakan komponen kimia yang akan bertindak balas dengan SO_2 dan menukar sifat parameter elektrik seperti konduktansi, rintangan atau kapasitansinya. Oleh itu, kepekatan gas akan diukur dengan perubahan sifat elektrik. Jenis penderia ini mempunyai beberapa kelemahan seperti kuasa input yang tinggi, resolusi rendah, suhu tinggi dan kelembapan ketahanan, sukar untuk mencapai kepekaan, selektiviti dan kekhususan dalam kehadiran gas campuran. Oleh itu, perkembangan penderia gentian optik berasaskan SO_2 yang baru adalah untuk memutuskan panjang gelombang optimum untuk SO_2 untuk bekerja pada langkah seterusnya. Sistem penderia yang diterangkan dalam tesis ini adalah jenis berasaskan gentian optik terbuka. Ia bergantung kepada spektrum penyerapan cahaya oleh gas SO_2 . Penyerapan mengambil peranan dalam sel penyerapan gas yang diperbuat daripada keluli tahan karat dalam bentuk silinder. Pembinaan sistem penderia perlu menggunakan bahan yang tahan lama dan dapat bertahan dalam keadaan cuaca yang paling sukar. Mentol deuterium-halogen digunakan sebagai sumber cahaya di mana ia dapat memberikan cahaya UV dengan panjang gelombang bermula dari 190nm hingga 2000nm. Spektrometer digunakan sebagai penderia untuk mengesan spektrum sumber cahaya yang dihubungkan dengan perisian analisis. Kemudian penyerapan optimum dianalisis untuk mendapatkan panjang gelombang yang terbaik untuk andaian dalam rantau 200 nm hingga 235 nm dengan menggunakan 50 cm panjang sel sebagai panjang sel optimum. Didapati bahawa puncak tertinggi penyerapan keratan rentas adalah $1.81248\text{E}-18 \text{ cm}^2/\text{molekul}$ berpusat pada panjang gelombang 215.65 nm. Hasil ujian silang sensitiviti SO_2 dengan CO_2 dan O_2 menunjukkan bahawa ia tidak mempengaruhi pengukuran di rantau ini. Hasil pengukuran kepekatan telah mengesahkan terdapat pengurangan 3.38 ppm daripada kepekatan asal SO_2 dalam tangki yang disediakan oleh pengeluar. Oleh sebab penyelidikan ini dilakukan di dalam ruang tertutup makmal, maka ianya hamper menyamai ujikaji aplikasi di dalam bangunan tertutup. Kerja-kerja masa hadapan untuk penderia ini akan melihat pemasangan dan pengujian penderia ke dalam ruang tertutup industri makanan atau ruang tertutup industri pembuatan asid sulfurik dan dengan menggunakan pemantauan masa nyata dengan perisian LabVIEW. Ujian lanjut akan melihat pelbagai campuran gas yang lebih luas dan menguji gas lain dalam julat UV.

UNIVERSITI MALAYSIA PAHANG

ABSTRACT

This thesis describes the detection of Sulfur Dioxide (SO₂) in the UV region. Increasing urban areas make the energy demand highly increased, thus more such as fossil fuel plant, environment, automotive and chemical-based industries need to be operated and constructed. Most of the commercially available SO₂ sensors are chemical absorption-based which is a chemical component that will react with SO₂ and change the electrical parameter properties such as its conductance, resistance or capacitance. Hence, the concentration of gas will be measured by the changes in electrical properties. This type of sensor has several weaknesses such as high input power, lower resolution, higher temperature and humidity dependence, difficult to achieve sensitivity, selectivity, and specificity in the presence of mixture gases. Therefore, the development of a new SO₂ based fiber optic sensor is to decide the optimum wavelength for the SO₂ to work on the next step. The system of sensors mentioned in this dissertation is a fiber-based open path device. It is dependent on the spectral of absorption of light by the SO₂ gas. The absorption takes roles in the gas absorption cell made from stainless steel in a cylinder shape. The sensor system architecture requires durable material and can survive the most rigorous weather conditions. A deuterium-halogen bulb is used as the light source where it can provide UV light with a wavelength starting from 190nm to 2000nm. The spectrometer is used as a detector to detect the light source spectral interfaced with analysis software. Then the optimum absorption is analysed to get the best wavelength for assumption within the region of 200 nm to 235 nm by using 50 cm cell length as the optimum cell length. It is found that the highest peak of absorption cross section is 1.81248E-18 cm²/molecules centered at a wavelength of 215.65 nm. The findings of CO₂ and O₂ cross-sensitivity experiments for SO₂ indicate that measurements in this field have no effect. The concentration measurement result has validate there is 3.38 ppm less than the original concentration of SO₂ in the tank provided by the manufacturer. As this experiment has been done in the confined space in the lab, it is already similar to enclosed building application. Future work for this sensor will look at installing and testing the sensor into the enclosed room of food preservation or enclosed space of sulfuric acid manufacture industry and by using real-time monitoring with LabVIEW software. Further tests will look at a wider variety of gas mixtures and testing other gases within the UV range.

اوتیور سیتی ملیسیا فہم

UNIVERSITI MALAYSIA PAHANG

TABLE OF CONTENT

DECLARATION

TITLE PAGE

ACKNOWLEDGEMENTS **ii**

ABSTRAK **iii**

ABSTRACT **iv**

TABLE OF CONTENT **v**

LIST OF TABLES **ix**

LIST OF FIGURES **x**

LIST OF SYMBOLS **xii**

LIST OF ABBREVIATIONS **xiii**

LIST OF APPENDICES **xiv**

CHAPTER 1 INTRODUCTION **1**

1.1 Preamble 1

1.2 Environmental Pollution 1

1.2.1 Categories of Pollution 2

1.3 Global SO₂ Emission 3

1.4 Major SO₂ Polluting Sectors 6

1.4.1 Coal Combustion 6

1.4.2 Oil and Gas Refining/Power Generation 7

1.4.3 Smelters 7

1.4.4 SO₂ Emission in Malaysia 8

1.5 Legislative Action to Reduce SO₂ Emission 10

1.5.1	Gothenburg Protocol	12
1.5.2	Malaysia's Air Quality Standard	14
1.6	SO ₂	16
1.6.1	Exposure Effects and Properties of SO ₂	16
1.6.2	Production and Uses of SO ₂	18
1.7	Problem Statement	20
1.8	Objectives of the Research	21
1.9	Scope and Limitations of the Research	21
1.10	Thesis Outline	21
CHAPTER 2 LITERATURE REVIEW		23
2.1	Introduction	23
2.2	Light	23
2.2.1	Types of Spectroscopy Techniques	24
2.2.2	Absorption Spectroscopy of UV	26
2.3	Beer Lambert Law	29
2.4	Review on SO ₂ Sensor	31
2.4.1	Microfluidic sensor	32
2.4.2	Metal Oxide Semiconductor Sensor (MOS)	33
2.4.3	Electrochemical Sensor	36
2.4.4	Optical Fiber Sensor	37
2.5	Optical Fiber Review	37
2.5.1	Advantages of Optical Fiber	38
2.6	Classification of Optical Fiber Sensor	39
2.6.1	Location of Modulation Principle	40
2.7	Open-path Optical Technique	41

2.8	Summary	45
-----	---------	----

CHAPTER 3 METHODOLOGY **46**

3.1	Introduction	46
-----	--------------	----

3.2	Development of Sensor System	46
-----	------------------------------	----

3.2.1	UV Light Source	46
-------	-----------------	----

3.2.2	Optical UV Detector	50
-------	---------------------	----

3.2.3	Spectrometer	52
-------	--------------	----

3.2.4	Gas Cell	55
-------	----------	----

3.2.5	UVNS Optical Fibre	56
-------	--------------------	----

3.2.6	UV Lens	58
-------	---------	----

3.3	Generic Design of Experimental Setup	59
-----	--------------------------------------	----

3.4	Flowchart of Optical Fiber Sensor Development	60
-----	---	----

3.5	Data Collection Process	61
-----	-------------------------	----

3.5.1	Calculation of Beer-Lambert Law	61
-------	---------------------------------	----

3.5.2	Flowchart of Experimental Process	62
-------	-----------------------------------	----

3.6	Spectrometer Calibration	63
-----	--------------------------	----

3.7	Summary	65
-----	---------	----

CHAPTER 4 RESULTS AND DISCUSSION **66**

4.1	Introduction	66
-----	--------------	----

4.2	Results of Spectrometer Calibration	67
-----	-------------------------------------	----

4.2.1	Experimental Setup	67
-------	--------------------	----

4.3	Spectral Line Results and Discussions	68
-----	---------------------------------------	----

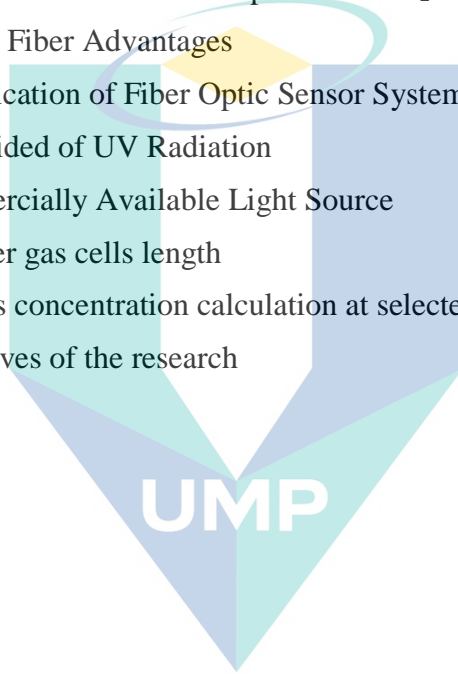
4.3.1	Result of 10 cm Cell Length	69
-------	-----------------------------	----

4.3.2	Result of 25 cm Cell Length	70
-------	-----------------------------	----

4.3.3	Result of 50 cm Cell Length	71
4.3.4	Result of 75 cm Cell Length	72
4.3.5	Result of 100 cm Cell Length	73
4.3.6	Summary on Different Types Cell Length	74
4.4	Cross Sensitivity Experiment	76
4.4.1	Cross Sensitivity with O ₂	77
4.4.2	Cross Sensitivity with CO ₂	78
4.4.3	Summary on Cross Sensitivity Experiment	80
4.5	Concentration Measurement	81
CHAPTER 5 CONCLUSION		83
5.1	Introduction	83
5.2	Conclusions	83
5.3	Future Work	84
REFERENCES		85
APPENDIX A LIST OF PUBLICATIONS		106
APPENDIX B DH2000-BAL SPECIFICATION SHEET		107
APPENDIX C SPECTROMETER SPECIFICATION SHEET		108
APPENDIX D UVNS OPTICAL FIBRE SPECIFICATION SHEET		112
APPENDIX E COLLIMATING LENS		114
APPENDIX F SPECTROMETER CALIBRATION		116

LIST OF TABLES

Table 1.1	Seven categories of pollution	2
Table 1.2	Top ten countries with the highest SO ₂ emitters	4
Table 1.3	Top 10 SO ₂ emission hotspots worldwide (kt/yr) for 2018	5
Table 1.4	Worldwide ambient air quality standards for SO ₂	10
Table 1.5	Ambient air quality standards of SO ₂ in SEA ($\mu\text{g}/\text{m}^3$)	15
Table 1.6	Effects of SO ₂ on human health	17
Table 1.7	Physical and Chemical Properties of SO ₂	18
Table 2.1	Optical Fiber Advantages	39
Table 2.2	Classification of Fiber Optic Sensor System	40
Table 3.1	Subdivided of UV Radiation	47
Table 3.2	Commercially Available Light Source	48
Table 3.3	Cylinder gas cells length	56
Table 4.1	SO ₂ gas concentration calculation at selected wavelength	81
Table 5.1	Objectives of the research	84



اونيورسيتي مليسيا قهغ

UNIVERSITI MALAYSIA PAHANG

LIST OF FIGURES

Figure 1.1	Major sectors which contribute to 2018 SO ₂ emissions	3
Figure 1.2	The world's top 10 coal combustion hotspots for SO ₂ emissions in 2018	6
Figure 1.3	Top 10 SO ₂ emission hotspots in 2018 for oil & gas refining/power generation worldwide	7
Figure 1.4	The world's top 10 smelters of SO ₂ emission hotspots (kt/yr) in 2018.	8
Figure 1.5	Emission of SO ₂ Dioxide by Sources in Malaysia (Metric Tonnes)	9
Figure 1.6	20 years pollution control for SO _x and other EMEP monitoring pollutants	12
Figure 1.7	Trends in SO ₂ emissions in Europe from 1990 to 2011	13
Figure 1.8	Contributions to the 1990-2011 decrease in SO _x emissions in Europe	14
Figure 1.9	Skeletal Formula of SO ₂	16
Figure 1.10	SO ₂ Cycle	19
Figure 2.1	Electromagnetic spectrum diagram show different properties throughout the frequency and wavelength range	24
Figure 2.2	Bonding and anti-bonding energy transition	27
Figure 2.3	Absorption cross section for SO ₂ in the UV region	29
Figure 2.4	Light absorption intensity over path-length.	30
Figure 2.5	Optical Fiber Basic Structure	38
Figure 2.6	Block Diagram of Basic Optical fiber Principle	39
Figure 2.7	Extrinsic and intrinsic fiber optic sensor	41
Figure 2.8	Third derivatives of (a) NH ₃ spectral lines (b) H ₂ O spectral line	42
Figure 2.9	Schematic diagram of DOAS sensor system	43
Figure 2.10	Scheme of the differential absorption lidar (DIAL) system.	44
Figure 3.1	Electromagnetic Spectrum	47
Figure 3.2	DH2000-BAL Light Source	49
Figure 3.3	Comparison of Ultra Violet light source intensity performance	49
Figure 3.4	Internal structure of the miniature spectrometer	53
Figure 3.5	Interface of SpectraSuite	54
Figure 3.6	Different Length of Gas Cell	55
Figure 3.7	Transmission properties comparison between two UVNS fibres	57
Figure 3.8	UVNS Optical Fiber Cable	57
Figure 3.9	UV Lens Holder	58

Figure 3.10	Generic Design of Experimental Setup to measure UV absorption of SO ₂	59
Figure 3.11	Theoretical SO ₂ absorption lines	62
Figure 3.12	HG-1 Mercury Lamp	64
Figure 3.13	Calibration Experimental Setup	64
Figure 4.1	Calibration coefficients data for spectrometer	67
Figure 4.2	Pictorial diagram of experimental setup	68
Figure 4.3	Spectral line of 10 cm cell length	69
Figure 4.4	Spectral line of 25 cm cell length	70
Figure 4.5	Spectral line of 50 cm cell length	71
Figure 4.6	Spectral line of 75 cm cell length	72
Figure 4.7	Spectral line of 100 cm cell length	73
Figure 4.8	Initial experimental result compared with theoretical lines	75
Figure 4.9	Reading of spectrometer when UV light source is switched on/off	76
Figure 4.10	Pictorial diagram of O ₂ cross-sensitivity experimental setup	77
Figure 4.11	O ₂ absorption lines compared to SO ₂ gas	78
Figure 4.12	Pictorial diagram of CO ₂ cross-sensitivity experimental setup	79
Figure 4.13	CO ₂ absorption lines as compared to SO ₂ gas	80

UMP

اونيورسيتي ملايسيا قهغ

UNIVERSITI MALAYSIA PAHANG

LIST OF SYMBOLS

E	Energy of a photon
h	Planck's Constant
c	Speed of light in vacuum
ν	Frequency of a photon
λ	Wavelength
A	Absorbance
T	Transmittance
ppm	Concentration of test species in parts-per-million
ppb	Concentration in parts-per-billion
σ	Absorption cross section
ω	Molecular weight of the test species
ρ	Density of the test species
N_A	Avogadro's Constant
I	Transmitted intensity
I_o	Incident intensity
I_b	Background intensity
R	Ideal gas constant
n	Number of moles
l	Optical path length
atm	Unit for atmosphere's pressure
K	Unit for temperature in Kelvin
N	The number of molecules in a unit volume (molecules.cm ⁻³)
eV	Unit for photon's energy

LIST OF ABBREVIATIONS

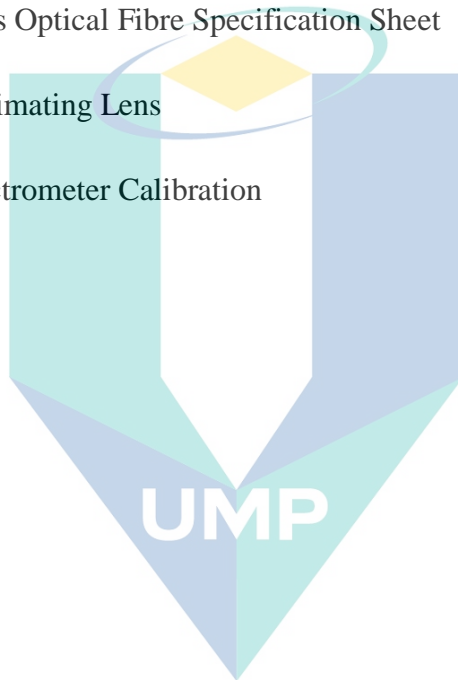
<i>SNR</i>	Signal-to-noise ratio
<i>P2P</i>	Peak to peak
<i>LED</i>	Light Emitting Diode
<i>UV</i>	Ultraviolet
<i>NIR</i>	Near Infra Red
<i>FWHM</i>	Full width half maximum
<i>SD(noise)</i>	The standard deviation of noise
<i>UVNS</i>	Ultra Violet Non Solarising
<i>CCD</i>	Charge Coupled Device
<i>PDA</i>	Photodiode Array
<i>PMT</i>	Photomultiplier Tube
<i>MFC</i>	Mass Flow Controller
<i>SMA</i>	Sub-Miniature version A
<i>VI</i>	Virtual Instrument
<i>SO₂</i>	Sulfur Dioxide
<i>O₂</i>	Oxygen
<i>N₂</i>	Nitrogen
<i>CO₂</i>	Carbon Dioxide

اونيورسيتي ملايسيا قهغ

UNIVERSITI MALAYSIA PAHANG

LIST OF APPENDICES

Appendix A:	List of Publications	106
Appendix B:	Dh2000-Bal Specification Sheet	107
Appendix C:	Spectrometer Specification Sheet	108
Appendix D:	Uvns Optical Fibre Specification Sheet	112
Appendix E:	Collimating Lens	114
Appendix F:	Spectrometer Calibration	116



اونيورسيتي ملايسيا قهغ

UNIVERSITI MALAYSIA PAHANG

CHAPTER 1

INTRODUCTION

1.1 Preamble

The development of an open path optical fibre sensor to detect Sulfur Dioxide (SO₂) gas is illustrated in this study. Using an open-path technique it operates in the UV region. The chapter will clarify the environmental issue and rationale for developing a new SO₂ sensor in relation to SO₂. The discussion will lead to SO₂ sensor problem statement, goals, scopes and expected outcome of this research then the content of this thesis is delineated.

1.2 Environmental Pollution

The world before urbanization and industrialization is vastly different than it was today. Since the world starting to have mass production on every product needed by human, there were many factor contribute to environmental issue. Late 20th century (Shonnard and Allen, 2010), peoples become aware and concern about their environment and the issue of the environment had evolved into a widespread issue which is greatly discussed all over the world. Environmental problems are anthropogenic implications for the biophysical environment (Sahney, Benton and Ferry, 2010). Climate change, overpopulation, resource depletion, toxicants, waste, pollution, environmental degradation and health are some issues from many environmental issues. The sources causing environmental issues come from several industries that produce human needs such as automotive, oil and gas, agriculture, medicine, etc.

The improper waste management of these industries contributes to major pollution and degradation of the environment in many cities, particularly in developing countries. Worst, it will affect the earth ecosystem and human life which is very infectious, toxic or radioactive. Environmental definition means the environment or conditions in which a person, animal or plant lives or operates (*Environment: Definition of Environment in Oxford Dictionary (British & World English)*, no date). The meaning of pollution meanwhile is the presence or introduction into the environment of a

substance that has harmful or toxic effects (*Pollution: Definition of Pollution in Oxford Dictionary (British & World English)*, no date). Therefore, the definition of environmental pollution is the presence in the environment of substances which have a harmful effect on living or non-living things surrounding organisms or groups of organisms.

1.2.1 Categories of Pollution

Pollution is divided into two parts; Point Source Pollution (PS) and Non-point Source Pollution (NPS). According to EPA Victoria (*Point and nonpoint sources of water pollution*, no date), PS is any single identifiable source of pollution which is can be easily tracked back to its source. It immediately destroys habitats and kill organism on large scale. As an example chemicals coming out of pipes, oil spills from ships, smoke from a factory etc. Meanwhile NPS is the type of pollution that comes from diffuse source and cannot easily tracked back to its sources. Common example for this types of pollution is forestry, agriculture, urban, land disposal etc. NPS is not same with PS as it does not always immediately destroy habitats and usually destroyed over longer periods of time. Atmospheric, water, radioactive, agrochemicals, soil, noise, thermal, land and etc. are some types of pollution occurred nowadays as showed in Table 1.1 (Inaoka, 2005).

Table 1.1 Seven categories of pollution

Category	Major Causes	Major Symptoms	Examples
Atmospheric pollution	Smoke, dust, exhaust fume, toxic substances (SO ₂ and NO ₂)	Asthma, bronchitis	Photochemical smog, "Yokkaichi Asthma"
Water pollution	Polluted waste water, waste fluids, sludge, household sewage, sewage discharge, agricultural chemicals	Noxious odors, poisoning	Minamata Disease, "Itai-itai" Disease (cadmium poisoning), PCB poisoning
Soil	Arsenic, heavy metals		Poisoning
Noise	Factories, construction work, road traffic, trains and aircraft, advertising	Headaches, insomnia, depression, hearing loss, impaired development	Osaka airport noise
Vibration	Factories, construction work, road traffic, trains and aircraft	Dizziness, discomfort, structural damage to homes	Shinkasen (bullet train) vibration
Ground subsidence	Upwelling of groundwater, gravel quarrying, coal mining	Structural damage buildings	Koto ward, Tokyo

Source: Inaoka, (2005)

Polluted environment is very unhealthy to live in if it has high concentration of toxic levels of chemicals in the land, air and water. Pollutants may be liquid – oil spills, pesticides and detergent; gases – CFCs, carbon monoxide, methane and ammonia; or solid – tin, iron and metals. Any substance that harmful and pollute something is called pollutant (Daly and Zannetti, 2007). In case of SO₂ emission, it's been categorized under the atmospheric pollution. The global emission of SO₂ will be discussed further in the next sub-chapter.

1.3 Global SO₂ Emission

Department of the Environment and Heritage of Australian Government calculated that about 99% of the SO₂ in the atmosphere comes from human source (Australian Government Department of the Environment and Heritage, 2005). Principle wellspring of SO₂ outflows are from compost producers, control plants, treatment facilities, wood and paper factories, metal smelters, and other industrial processes (Xu *et al.*, 2016). Dahiya and Myllyvirta said 60% of the satellite's total emissions are anthropogenic (Dahiya and Myllyvirta, 2019). Figure 1.1 from the report shows major sectors contributing to the world's SO₂ emissions in 2018, with high coal combustion efficiency contributing 31% to power generation, manufacturing, smelters, oil and gas refining or combustion, 10% and 19% respectively.

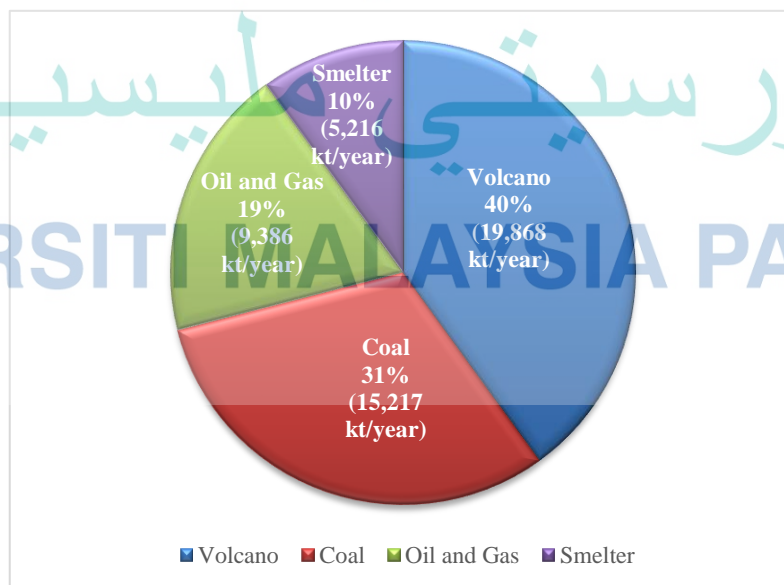


Figure 1.1 Major sectors which contribute to 2018 SO₂ emissions

Source: Dahiya and Myllyvirta, (2019)

Worldwide SO₂ emission crested in the mid 1970s and diminished until 2000 and afterward expanded from 2000 to 2005 because of expanded discharges in China, international shipping, and developing countries in general (Mohajan, 2014). Currently, India is the world's largest producer of SO₂ recorded by Dahiya and Myllyvirta, contributing over 15% of the worldwide anthropogenic outflows that have recently overtaken Russia and China (Dahiya and Myllyvirta, 2019). Table 1.2 below shows the Top ten countries with the highest SO₂ emitters.

Table 1.2 Top ten countries with the highest SO₂ emitters

Country	SO ₂ emission from hotspots in 2018 (kt/yr)
India	4,586
Russia	3,683
China	2,578
Mexico	1,897
Iran	1,820
Saudi Arabia	1,783
South Africa	1,648
Ukraine	979
U.S.A	967
Turkey	919

Source: Dahiya and Myllyvirta, (2019)

As reported by Li et al., since 2007, emissions in China have declined by 75% while those in India have increased by 50% (Li *et al.*, 2017). With these changes, India is now surpassing China as the world's largest emitter of anthropogenic SO₂. The results suggest that India may soon become, if it is not already, the world's top emitter of SO₂. The report also added that, the essential purpose behind India's high SO₂ outflow yield is the development of coal-based power age over the previous decade and five of the top 50 SO₂ emission hotspots from coal or power generation industry across the world are in India. Table 1.3 below shows top 10 SO₂ emission hotspots worldwide (kt/yr) for 2018.

Table 1.3 Top 10 SO₂ emission hotspots worldwide (kt/yr) for 2018

Hotspot name	SO ₂ emissions (kt/yr)
Norilsk	1,898
Kriel	714
Zagroz	614
Rabigh	515
Singrauli	507
Cantarell	461
Matimba	412
Reforma	407
Shaiba	398
Das Island	397

Source: Dahiya and Myllyvirta, (2019)

Table 1.3 also shows the Norilsk smelter site in Russia remains the world's largest anthropogenic SO₂ pollution hotspot, preceded by the Kriel region in the province of Mpumalanga in South Africa and Zagroz in Iran. Many areas with high coal consumption or oil and gas refining and combustion such as Rabigh in Saudi Arabia and Singrauli in India have been catching up with the top three hotspots over the past decade and their emissions have dramatically increased. This is caused primarily by increasing coal combustion efficiency, oil refining / consumption, and in part by slow implementation or adoption of stringent emission standards.

Through Dahiya and Myllyvirta's Greenpeace Environment Trust report, it reported that there are 12 coal-fired power stations in South Africa's Mpumalanga province, making the province the world's largest SO₂ emission hotspot from generation power. Saudi Arabia is the highest SO₂ emitter in the Middle East with the province of Makkah home to the worst hotspots due to the region's polluting oil power plants, industries and refinery facilities. Across Europe, Russia, Serbia and Bulgaria are on the list of the world's worst 20 countries releasing SO₂. Previous reports by the United States Environmental Protection Agency showed a gradual decline across levels of SO₂ in the United States (US EPA, n.d).

1.4 Major SO₂ Polluting Sectors

1.4.1 Coal Combustion

More than 51% of gross anthropogenic SO₂ emissions in high-coal regions for electricity generation and industry are released. (International Energy Agency, 2016). Coal combustion is the main pollution source in these regions with smaller oil refineries contributions, smelters and others (Chakraborty *et al.*, 2008). Data from NASA MEASURE reveals that coal power plants are one of the major generating industries in India, China, Indonesia, Thailand, Mexico, South Africa, Bulgaria and Australia. (NASA., 2016). Many states and regions such as China, India, South Africa and Indonesia have imposed or enhanced emission standards for SO₂ in recent years. (Xu, 2011; Singh and Issar, 2017). Regulations and their enforcement differ, however, between countries, and emissions standards remain in many places much too weak to effectively improve air quality. This shift in emission regulation and different efficiencies in the management of SO₂ pollution contribute to varying emissions from the same power plant capability in different regions. Figure 1.2 below shows the world's top 10 coal combustion hotspots for SO₂ emissions in 2018.

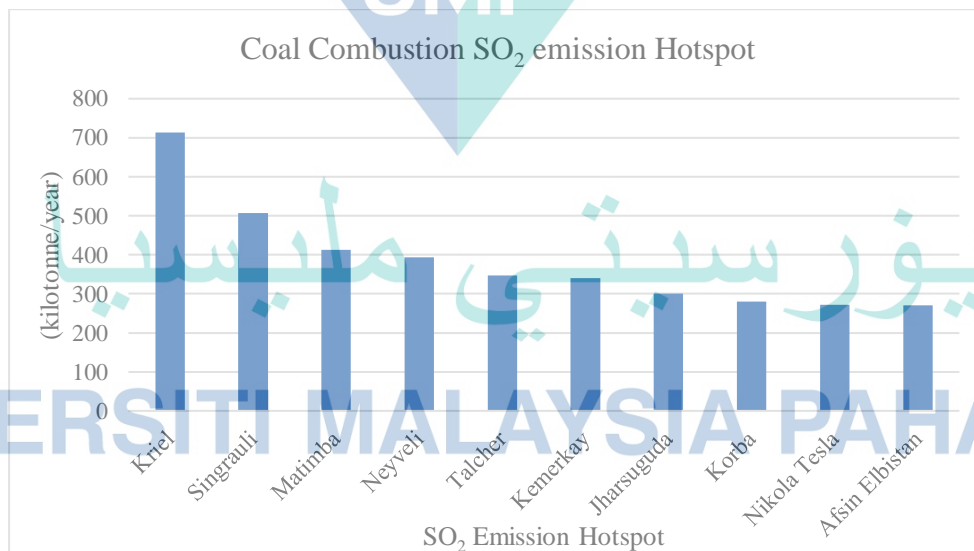


Figure 1.2 The world's top 10 coal combustion hotspots for SO₂ emissions in 2018

Source: Wang and Chen, (2016); Makgato and Chirwa, (2017); Dahiya and Myllyvirta, (2019)

1.4.2 Oil and Gas Refining/Power Generation

Greenpeace Environment Trust reports that oil and gas refining and generation industries/power are pumping large amounts of SO₂ into the atmosphere in Mexico, Saudi Arabia, Iran, the United Arab Emirates (UAE), Russia, Uzbekistan, and Venezuela. (Dahiya and Myllyvirta, 2019). NASA Ozone Monitoring Instrument (OMI) hotspots display the areas of oil refining and gas facilities (NASA, no date). OMI captured more than 40 regions with clusters of oil and gas refining. Figure 1.3 shows the top 10 SO₂ emission hotspots in 2018 for oil & gas refining/power generation worldwide. Mexico has several of the highest points of SO₂, including Cantrell, Reforma and Salina Cruz, resulting from oil refining and gas production clusters (Dahiya and Myllyvirta, 2019). Many major oil refining/combustion pollution hotspots in the Middle East and North Africa (MENA) areas have been found.

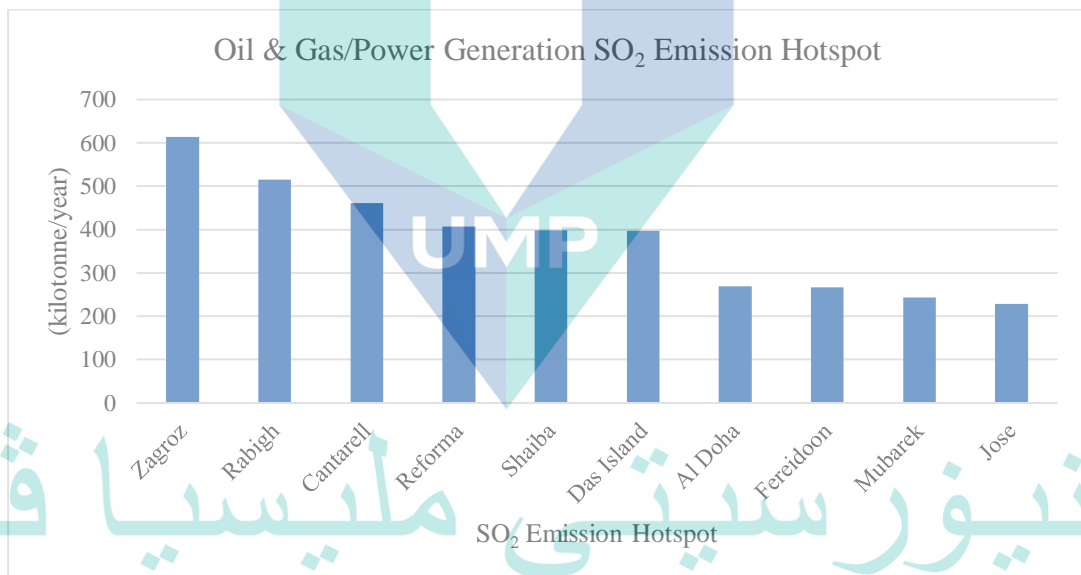


Figure 1.3 Top 10 SO₂ emission hotspots in 2018 for oil & gas refining/power generation worldwide

Source: Dahiya and Myllyvirta, (2019); Tiwari, Bajpai and Dewangan, (2019)

1.4.3 Smelters

Metal smelters are typically located near steel mines in clusters where raw metal ores can be mined. The operation of these smelters, especially those which do not have appropriate pollution control instruments, emits SO₂ into the air and can be monitored by NASA OMI. (NASA, no date). Smelters are the main contributors to SO₂ in many of the largest hotspots detected (Gwimbi, 2017). Emission levels for these hotspots are shown

in Figure 1.4 below. Norilsk in Russia continues to be the world's largest emitting city, with Sarchshmeb in Iran, Ilo in Peru, Cuba's Nicaro, Uzbekistan, and Russia's Karabash in Russia (Khokhar, Platt and Wagner, 2008; Gwimbi, 2017).

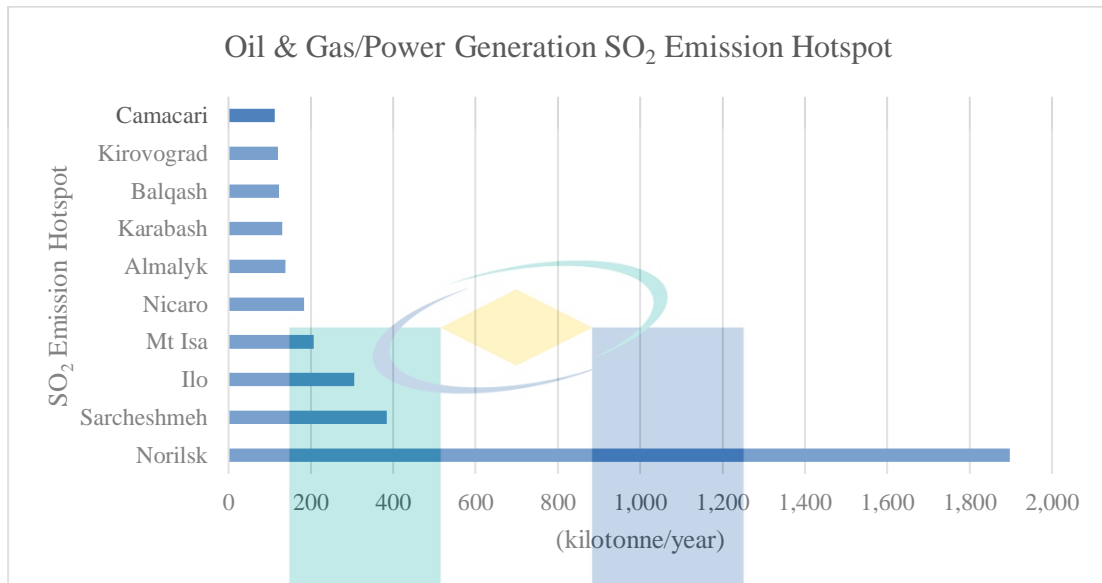


Figure 1.4 The world's top 10 smelters of SO₂ emission hotspots (kt/yr) in 2018.

Source: Khokhar, Platt and Wagner, (2008); Dahiya and Myllyvirta, (2019)

1.4.4 SO₂ Emission in Malaysia

As there are no volcanic activities in Malaysia, emissions of SO₂ are mainly generated through combustion of SO₂ with fossil fuel, especially coal and oil (Salahudin, Abdullah and Newaz, 2013). The combustion of fossil fuel in a power plant has become the largest source of SO₂ and is also produced by combustion of vehicle fuel (Salahudin, Abdullah and Newaz, 2013; Binyehmed, Abdullah and Zainal, 2016). Another source to SO₂ emissions in Malaysia comes from manufacturing activities (Salahudin, Abdullah and Newaz, 2013). Department of the Environment (DOE) of Malaysia reported that fossil fuel combustion from 41 power stations in Malaysia generates 48% of the total SO₂ or 78,416 metric tons, industrial operations such as metal processing contributed 23% or 36,938 metric tons of released SO₂, motor vehicle combustion produces 8% or 12,865 metric tons of SO₂ and the remaining 21% with 33,694 metric tonnes contribute from others as stated in Figure 1.5.

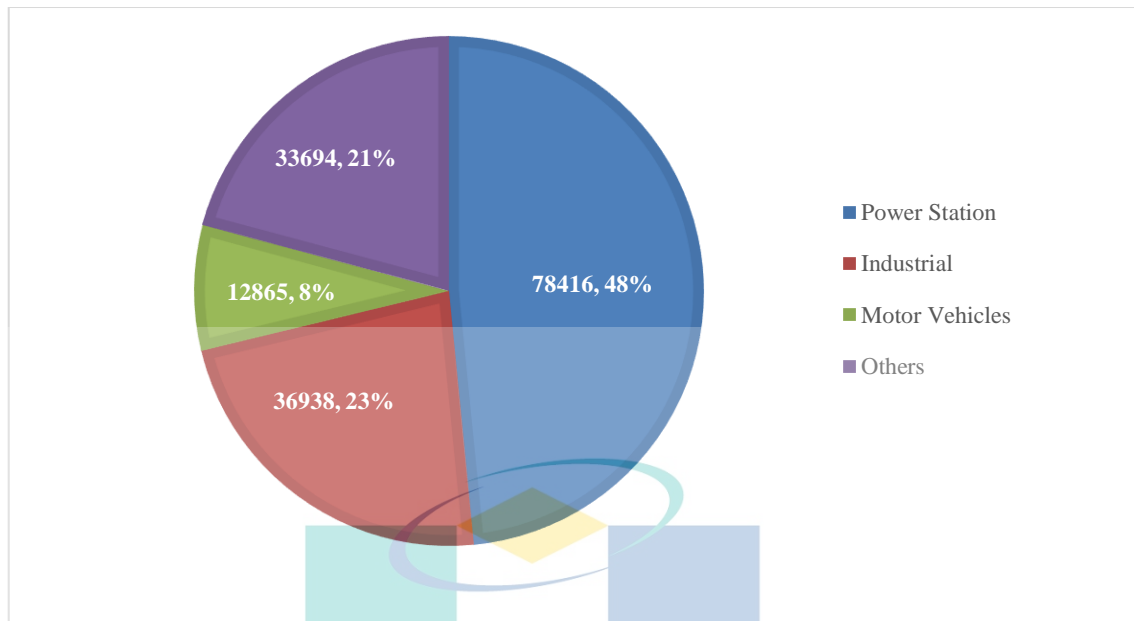


Figure 1.5 Emission of SO₂ Dioxide by Sources in Malaysia (Metric Tonnes)

Source: DOE's Report | Department of Environment, (no date)

Figure 1.5 also shows the amount of SO₂ dioxide has been released to the ambient environment together with its percentage. Motor vehicles contribute the lowest emission of SO₂ dioxide. However, for an enclosed car park, motor vehicle might be the main contributor to the emission of SO₂ dioxide. For motor vehicles, the amount of emission is depends on type of fuel used because different fuel will give varies range of SO₂ content (Colls and Tiwary, 2010).

However in Malaysia, there are some incident of leaked SO₂. In July 1997 at 7:00 pm, 49 members of the public complained of dizziness, sore throat, eyes irritation and tightness of chest after exposed to sulphur dioxide while traveling on the road about 100 meter 90m the sulfuric acid factory in Teluk Kalong Kemaman. The incident was caused by leaked SO₂ from return pipe of scrubber circulation tank in the factory. The problem had occurred due to carelessness of the operator to inspect the level of water in the scrubber circulation tank during the operation (Azmi, Mohd Kamil and Balkis, 2002). Beside, in the case of Sungai Kim Kim, Johor, Fareez Azman from Astro Awani reported that there are several gas has been founded instead of methane gas which is hydrogen chloride, benzene, hydrogen cynide and SO₂ that lead to more than 300 victims showing the gas poisoning symptom (Azman, 2019).

1.5 Legislative Action to Reduce SO₂ Emission

Each country in the industrialized world has established SO₂ air quality standards. These standards and recommendations fall into two groups, primary standards for the prevention of negative health effects in human populations and secondary standards for the conservation of people's well-being including soil, water, vegetation, visibility and climate. A study by Vahlsing and Smith on the national air quality standards and recommendations found that 76 of the 192 UN Member States have approved SO₂ mandatory or optional 24-hour limit values. (Vahlsing and Smith, 2012). For those countries the average daily limit was 182 µg/m³ (95% CI 158-205 µg/m³).

Table 1.4 compares and contrasts the standards established by a small number of the countries that have openly listed their values online or answered a questionnaire by mail. 91% of the 24 countries that answered the questionnaire said it aimed at updating its SO₂ air quality standards using the WHO air quality guidelines. The current WHO Air Quality Guideline values for SO₂ for a 10-minute measuring time of 500 µg/m³, and for a 24-hour period of 20 µg/m³ have been defined.

Table 1.4 Worldwide ambient air quality standards for SO₂

Country/Region	1-hr average (µg/m ³ /ppb)	24-hr average (µg/m ³ /ppb)	Annual (µg/m ³ /ppb)	Year
Canada	838/315	279/105	56/21	1998
China	500/191	150/57	60/23	2010
Japan	/100	/40	n/a	1973
United States	200/75	n/a	n/a	2010
India	n/a	80/30	50/19	2008
Australia	532/200	213/80	53/20	1998
European Union	350/134	125/48	20/8	2005

Source: Vahlsing and Smith, (2012)

In 1980, with the implementation of Council Directive 80/779/EEC (Council of the European Union, 1980), the EU started to enforce air quality standards for SO₂. This directive identified limits of 140 and 400 µg/m³ for annual and 30-minute periods, respectively. These values have been revised downwards when the Air Quality Framework Directive for the first daughter was published in 1999 (99/30/EEC) (EC, 1999). The new hourly SO₂ limit of 350 µg/m³ and a daily limit of 125 µg/m³ were designed

to protect human health in urban areas; however the annual limit of $20 \mu\text{g}/\text{m}^3$ was directed at Europe's sensitive ecosystems (EC, 2000). The Directive stipulated that conformity is necessary by 2010, and that the hourly and daily limits should not exceed 24 and 3 times a year respectively. In addition, a warning level of $500 \mu\text{g}/\text{m}^3$ was established which would lead to an immediate adverse human health impact with short and transient exposures.

In order to measure progress, an annual limit of tolerances and a 1-hour limit values were established, which gradually reduced the number of allowable exceedances from the year of initiation until the date of attainment of 2010. The tolerance limits enabled the Commission to identify the areas with the worst air quality. SO_2 's initial 50% tolerance limits were allowed, but every Member State needed annual action plans detailing how they intended to comply as the Directive entered into force. A new Air Quality Directive was published in 2008 which merged the first three Daughter Directives with retained SO_2 limits, but allowed Member States to seek a five-year compliance extension (EC, 2008).

A complex legislative history is linked to the development of the EU limit standards, including the introduction of legislation restricting combustion-related emissions. A number of different emission limits were released, restricting the release of SO_2 from both the environment and stationary sources during combustion. These include the Integrated Pollution Prevention and Control Directive (2008/1/EC), which reduces industrial emissions and makes possible the application of best technology in the combustion process for solid and fluid fuels (European Parliament and Council, 2008). Similarly, the NEC Directive (2001/81/EC) defined SO_2 emission limits for each Member States which had to be met by 2010 (European Parliament And The Council Of The European Union, 2001).

The first NEC Directive was designed to reduce SO_2 emissions to a level almost 50% below the maximum cap of 8297 kilotons per year. As part of the Clean Air Plan for Europe in 2013, a new NEC Directive was planned but delayed due to a lengthy debate on the emissions targets. The law is expected to introduce drastic cuts, with a projected 81% (based on 2005 levels) reductions in SO_2 emissions to 1530 kilotons per year by 2030. A pair of Fuel Quality Directives (1998/70/EC and 1999/32/EC) were eventually released, which initially decreased petrol's SO_2 content to 150 mg/kg, diesel fuel to 350

mg/kg and marine gas oil to 0.2% (The European Parliament and the Council of the European Union, 1998; EC, 1999). There were two further directives adopted in 2003 which initially restricted the SO₂ content of petroleum, diesel fuel, and gas oils to 50 mg/kg; these, however, were again amended in 2009 to create the current 10 mg/kg limit (EC, 2003, EC, 2009).

1.5.1 Gothenburg Protocol

The Gothenburg Protocol of 1999, implemented by the UN Economic Commission for Europe (UNECE, 2007), is a final piece of legislation with a direct impact on SO_x pollution and transport. The Protocol was included in the 1979 Long-Range Transboundary Air Pollution Convention (CLRTAP), which 47 European nations, Canada, the United States and the European Union have ratified. The original protocol came into force in 2005 and was scheduled for completion by 2010. The Treaty established stationary emission limits for SO₂. The objective was to reduce the SO_x emissions by 63% by limiting to 0.2% by July 2000 the SO₂ content of gas fuel used by power stations and other power-generating installations and 0.1% by January 2008. In Europe, for the Monitoring and Evaluation of Long-Range Transmission of Air Pollutants (EMEP), a Co-operative Program was established to monitor progress through the establishment of a monitoring network and the creation of an inventory reporting protocol (UNECE, 1984). As of 2010, the European Union achieved an 82 percent decrease in SO_x emissions (European Environment Agency, 2016). Figure 1.6 shows these achievements, particularly as regards smaller declines in other targeted pollutants, which clearly shows the noticeable reductions in SO_x.

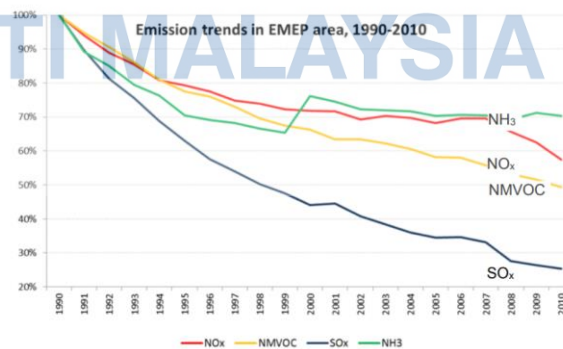


Figure 1.6 20 years pollution control for SO_x and other EMEP monitoring pollutants

Source: EMEP, (2013)

The revised Gothenburg Protocol set new targets for reducing emissions from 2005 (UNECE, 2012) was adopted in 2012. The aim of this amendment was to further reduce SO₂ emissions by 59% by 2020. The EU is also amending the Emissions Ceiling Directive and mandating an additional 81% reduction by 2030 in SO₂ emission ceilings (EPRS, 2015). The net effect of these new legislative pieces is to ensure that further reductions in the environmental SO₂ level are evident in the future and that the very real possibility that such modifications will override any advantages of further reductions in limit values.

The implementation of the previous legislation together have had a major impact on European airborne SO₂ levels and a majority of 28 member countries witnessed a decrease of more than 70 % between 1990 and 2011 (Vestreng *et al.*, 2009; Guerreiro, Foltescu and de Leeuw, 2014). This has resulted in a cumulative decrease of 74% of SO_x emissions from the 33 Member States of the European Environment Agency (Iceland, Liechtenstein, Norway, Switzerland and Turkey are not EU Member States), as shown in Figure 1.7 (EEA, 2014).

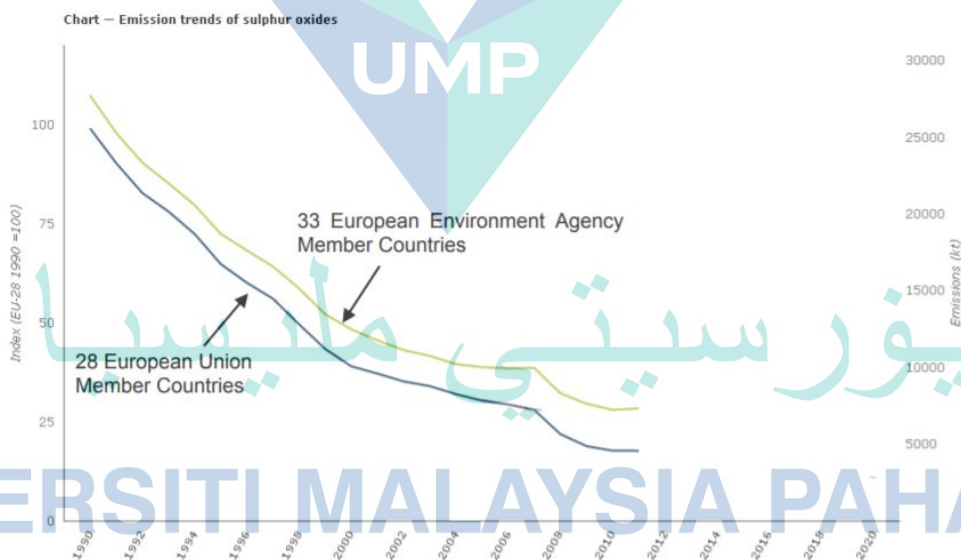


Figure 1.7 Trends in SO₂ emissions in Europe from 1990 to 2011

Source: EMEP, (2013)

The SO₂ emission level goals of all 28 EU Member States for 2010 were achieved primarily due to substantial emission reductions in the electricity production and industrial energy use sectors of 76% and 72%, as shown by Figure 1.8. Emissions

reductions led to airborne levels below EU limits and in 2011 SO₂ exposures were not exceeded; but 46% of the population were exposed to SO₂ levels exceeding the WHO daily air quality guideline value of 20 µg/m³.

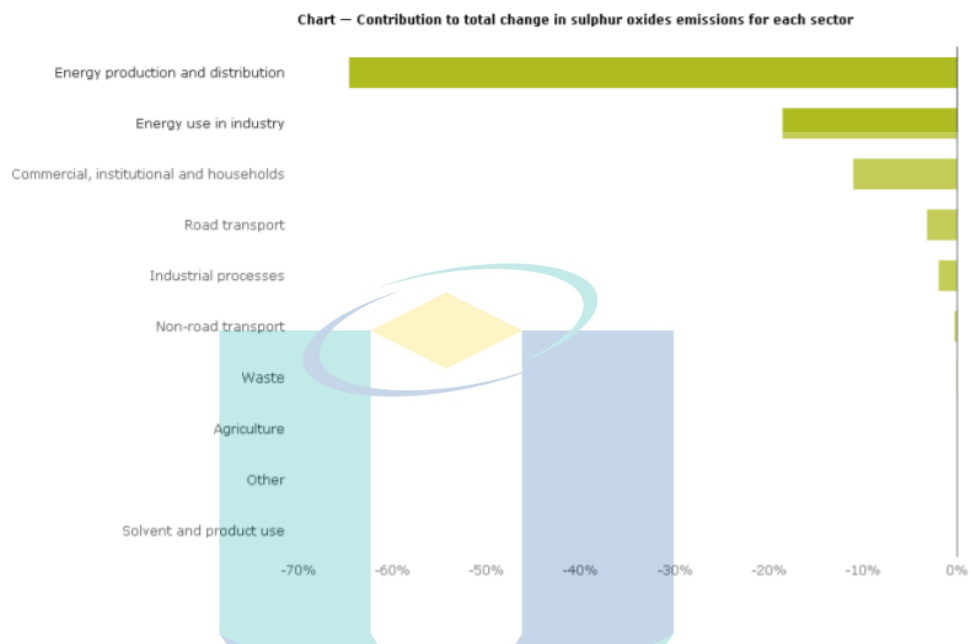


Figure 1.8 Contributions to the 1990-2011 decrease in SO_x emissions in Europe
Source: EEA, (2014)

The decreases in European SO₂ emissions reflect those from other parts of the world. Modeling studies have shown that there have been noticeable declines in anthropogenic SO₂ release for the period 2000 to 2010 in many countries, including the USA, Canada, Korea and Latin America (Amann, Klimont and Wagner, 2013; Ray and Kim, 2014). These same models also predict that global SO₂ emissions will decline by as much as 10 percent more in 2030 in the absence of new legislation (Amann, Klimont and Wagner, 2013). This would be much higher in India and China where SO₂ emissions have risen steadily or fluctuated because of trade-offs between economic growth and environmental policy (Lu, Zhang and Streets, 2011). This figure would be significantly higher.

1.5.2 Malaysia’s Air Quality Standard

Even though some standards are consistent with interim targets of the World Health Organization (WHO), compliance processes are limited and concentration levels are often surpassed. Coal combustion for electricity and industrial processes today

constitute the most fuel-related sources of SO₂ emissions in Southeast Asia (SEA) with around three-quarters of the total SO₂ emissions of SO₂ at 3.9 million tons (Mt). Nearly half of the emissions of SO₂ from coal-fired power are emitted in Indonesia alone—approximately equal to its share in the local coal-fired power fleet.

As early as 1978 Malaysia developed industry and transformation emission standards covering existing as well as new installations. Certain industries are subject to specific dust restrictions (e.g. asphalt concrete, cement plants, nitric acid or sulfuric acid production). A major threat in terms of air pollution is the combination of rapid economic and energy demand growth with a growing urbanisation and reliance on the conventional use of biomass. In several countries in the SEA region, air quality standards are in place as shown in Table 1.5.

Table 1.5 Ambient air quality standards of SO₂ in SEA (µg/m³)

Country/Region	SO ₂	
	24 Hour	Annual
Brunei Darussalam	n/a	n/a
Cambodia	300	100
Indonesia	365	60
Lao PDR	300	100
Malaysia	105 (0.04ppm)	n/a
Myanmar	n/a	n/a
Philippines	180	80
Singapore	50 (20)	15
Thailand	300	100
Vietnam	125	50

Source: Clean Air Asia, (2016)

The national environmental quality requirements in Malaysia usually adhere to the provisional goals of WHO and are regularly revised in compliance with environmental quality (clean air) legislation dating from the late 1970s. Malaysia has a history of air quality management, well-developed monitoring systems and a criterion for good air quality is set in the Environmental Strategy Plan 2011-2020. Today, Malaysia's energy demand is largely met by natural gas (43%), oil (35%), and coal (17%) with further small bio-energy and hydropower contributions. At COP21, Malaysia made a voluntary pledge to reduce the level of greenhouse gas emissions by 35 percent from the 2005 rate by 2030. The main characteristics of the 2014 Roadmap of Emission Intensity Reduction to minimize the level of CO₂ in 2030 by 40 percent relative to 2005 and Renewable Energy Policy and Action Plan 2010.

1.6 SO₂

SO₂ consists of one sulfur atom and two oxygen atom linked by double bond which is has a bent structure with bond length 143.2 pm as show in Figure 1.9 (King, 2005). Its molecular formula is SO₂. Both Sulfur and Oxygen is an element of Group 16 in periodic table. It is an omnivorous air pollutant and toxic gas which needs measures to prevent and control adequate public health protection.

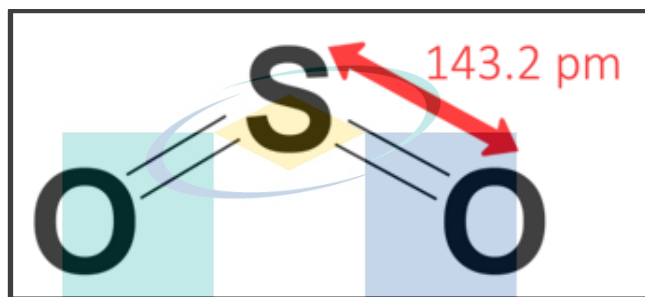


Figure 1.9 Skeletal Formula of SO₂

SO₂ is a colorless gas with a strong suffocating pungent odor, non-inflammable, irritant, and is heavier than air at Standard Temperature and Pressure (STP). (*Sulfur Dioxide*, no date; Perry, 2011). In water, alcohol and ether, it is extremely soluble. SO₂ easily dissolves into sulfuric acid in water. One well known fact is that these gasses are the main cause of acid rain.

1.6.1 Exposure Effects and Properties of SO₂

SO₂ can be produced or emitted naturally from the decay of vegetation and volcanic emissions and also by product from metal smelting, processing and combustion of coal or oil, manufacture of sulfuric acid, fertilizer plants, petrochemical industry, food preservation, wine making, bleaching, fumigation, refrigeration, biochemical and biomedical analysis and climate engineering (S Das *et al.*, 2008; Liu *et al.*, 2017). SO₂ is one of the most hazardous atmospheric pollutants because it directly contributes to acid rain. One of the main characteristics of this gas is its human, animal, flora and fauna toxicity, sturdy damage and historical monuments. (S Das *et al.*, 2008).

Life threatening can be short-term exposure to small SO₂ concentrations. In the meantime, long-term exposure can cause lung function changes and can even be fatal at

high SO₂ levels. SO₂ gas has a long and short exposure limit of 2 ppm and 5 ppm, respectively (S Das *et al.*, 2008; Kumar, Avasthi and Kaur, 2017), through the acceptable limit of SO₂ in ambient air is much less. According to Rahman Khan and Siddiqui, bronchoconstruction occur at 1.6 ppm of SO₂ and throat disturbance at 8 ppm to 12 ppm (Rahman Khan and Siddiqui, 2014). At 20 ppm, cough and irritation of the eye results immediately. Even SO₂ exposure at 400-500 ppm is life-threatening. The effect on human health due to SO₂ is shown in Table 1.6 below.

Table 1.6 Effects of SO₂ on human health

SO ₂ (ppm)	Duration of Exposure	Effects
0.037 – 0.092	Annual average	With 185 µg ^{m-3} smoke concentration, increase in lung disease and respiratory tract problem
0.007	Annual average	With high concentration of particulate matter, progression in the respiratory track and disease in children.
0.11 – 0.19	24 hours	In low concentration of particle, increase in the respiratory tract disease in the elderly
0.19	24 hours	Progression in severe respiratory tract diseases in the grown-ups
0.19	24 hours	In low concentration of particle, an increase can be observed in mortality
0.25	24 hours	With 750 µg ^{m-3} smoke concentration, an increase in daily mortality rates may be observed and sudden increase in morbidity
0.5	10 mins	In asthma patients, increase in breathing resistance during exercise (mobility)
5	24 hours	In healthy people, increase in breathing resistance
10	10 mins	Bronchospasm
20	n/a	Coughing, eye irritation

Source: Rahman Khan and Siddiqui, (2014)

An exposure to SO₂ repeatedly can cause burning sensation and has adverse effect on the health of humans and it causes respiratory illness, breathing problems, cardiovascular diseases, irritation to the eyes and skin (Tyagi *et al.*, 2016a). When the concentration of SO₂ is higher than the prescribed standards of World Health Organization (WHO), it effects especially those suffering from asthma, bronchitis, lung and cardiac problems. Asthamatic and heart patients are the most sensitive to the presence

of SO₂ in the environment (Tyagi *et al.*, 2016a). SO₂ harms human health by responding with the dampness in the nose, nasal cavity, throat and this is the way in which it decimates the nerves in the respiratory system. Respiratory tract inflammation causes coughing, mucus secretion, chronic bronchitis and aggravation of asthma it makes people more and more prone to respiratory tract infection. The study made by Vahedian *et al.* and Dastoorpoor *et al.* indicated that there was a critical increment in hospital admission for cardiovascular illness related with SO₂ (Vahedian *et al.*, 2017; Dastoorpoor *et al.*, 2019). It is thus important to control the SO₂ leakage at the source, not only to reduce accidental exposure at the source but also the environmental pollution as a whole. In order to make sure that this hazardous gas is treated safely during the SO₂ process, it is important to know the specific function of SO₂. Table 1.7 show the physical and properties of SO₂.

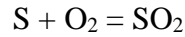
Table 1.7 Physical and Chemical Properties of SO₂

Physical and Chemical Properties
1. Gas density 2.927 g/L at 20 °C
2. Vapor density 2.263 (air=1)
3. Condenses to a colorless liquid at -10 °C
4. Density of liquid SO ₂ 1.434 g/mL
5. Critical temperature 157.65 °C
6. Critical pressure 77.78 atm
7. Critical volume 122 cc/g
8. Dielectric constant 17.27 at -16.5 °C
9. Boiling point -10 °C
10. Melting point -72 °C
11. Molecular weight 64.065

Source: SO₂ Material Safety Data Sheet, n.d; Simmons, n.d

1.6.2 Production and Uses of SO₂

Generally, SO₂ obtained from the combustion of sulfur along with air or oxygen as shown in Equation 1.1 (Balaram Sahoo, Nimai Charan Nayak, Asutosh Samantaray, 2012). SO₂ mostly produce by power plant that burn coal, automotive vehicles, petroleum industry, cement and paper pulp manufacturing meanwhile in nature cycle, SO₂ emission is cause by volcanic eruption and organism decay (Wesely and Hicks, 1977; Alì, Alì and Speight, 2005; Wang *et al.*, 2011; Balaram Sahoo, Nimai Charan Nayak, Asutosh Samantaray, 2012).



1.1

Acid rain is one of the most important effects of SO_2 on the atmosphere. A reference to the sulfur cycle as shown in Figure 1.10 will explain the process of SO_2 production.

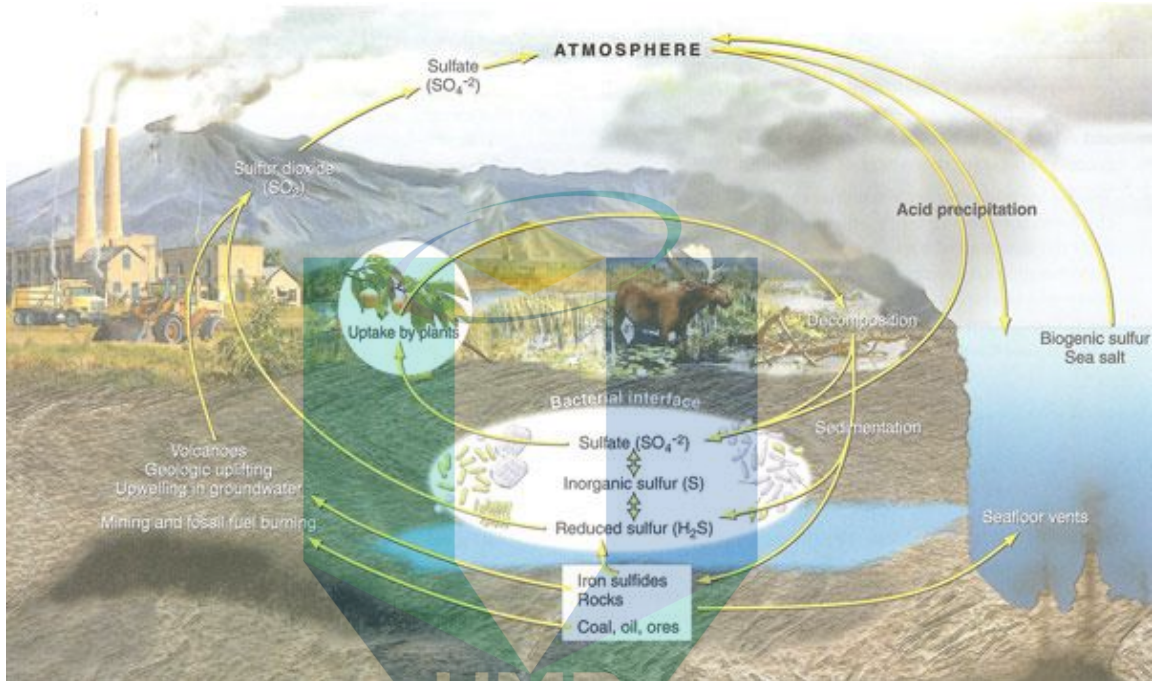


Figure 1.10 SO_2 Cycle

Source: Curtis, (2007)

Historically SO_2 was first used by Romanians in winemaking when they discovered a way to keep the wine fresh and prevent it from vinegar smell by burning candles made of sulfur in empty vessels (*Sulfur Dioxide: Science behind this anti-microbial, anti-oxidant, wine additive* | *Practical Winery & Vineyard Journal*, no date; Divol, Du Toit and Duckitt, 2012). Until now, it was used as preservatives or additives and bleaching agent in food and beverages industries (Green, 1976; Wedzicha, 1991; Adams, 1997; Salaha *et al.*, 2008; Izquierdo-Ca??as *et al.*, 2012). Moreover it also being used in manufacturing of sulfuric acid industries (Davenport *et al.*, 2006; Taieb and Ben Brahim, 2013), paper pulp industries, oil industries and etc..

1.7 Problem Statement

Over past few decades, due to public awareness about the dangerous of SO₂ gas and cases related SO₂ poisoning promoted to a development of a SO₂ sensor by many researches and scientist to detect the presence of SO₂ gas. They are being used in many industries that have presence of SO₂ as example in coal combustion, metal smelters, food, petroleum, power plant, cement, paper pulp and automotive industries. Even though SO₂ emission in Europe and the biggest SO₂ emitter's country before have shown progressive declining, some hotspots in India, China, Russia or even in Europe are not have any changes, instead it shows an increment in SO₂ emission. Moreover, cases regarding SO₂ poisoning keep happen either in industrial area or in enclosed building.

Other than that, over the past decade, most research in SO₂ sensor has emphasised there are many sensors already in the market specifically for SO₂ detection which has been developed with different technology and has their own drawbacks. The conventional sensor used for this type detection is based on microfluidic (Martini *et al.*, 2012; Kim *et al.*, 2013), colorimetric (Bartlett and Skoog, 1954; Liu *et al.*, 2012; Chatterjee and Sen, 2015), semi-conductor (Berger *et al.*, 1997; Girardin *et al.*, 1997; Tomchenko *et al.*, 2003; Wetchakun *et al.*, 2011; Singh *et al.*, 2012) and electrochemical (Worrell and Liu, 1984; Currie, Essalik and Marusic, 1999; Fergus, 2008; Toniolo *et al.*, 2010; Uneme, Tamura and Imanaka, 2013) sensor. As this SO₂ sensor has been explored decade ago, there are various weakness of it such as slower response reversibility, harder to reset the detector quickly and cannot measure instantaneous SO₂ levels (Richard, 2000). In addition it also has several weaknesses such as higher temperature and humidity dependence, difficult to achieve sensitivity, selectivity and specificity in presence of mixture gases (Richard, 2000; Misra, Mathur and Srivastava, 2004).

On the other hand, the problem faced by the conventional sensor can be solved by using the optical fiber sensor as it offer more advantages. The advantages such as the ability to transmit optical signals over longer distance without significant loss of the signal intensity, high sensitivity, high temperature performance, high selectivity and sensitivity in cross-contamination of mixture gases (Shivang Ghetia, Ruchi Gajjar and P Trivedi, 2013b; Saleh, A Mustafa and Osman, 2015; Yin *et al.*, 2018). Hence, the demand of a new sensor that capable of performing continuous measurement is crucial. Present study propose the use optical fiber that is well known has a great transmission for quick

response for the measurement. The advantage of open-path method is used together with the optical fiber to determine the best wavelength for an optimum absorption.

1.8 Objectives of the Research

The main objective of this research are:

1. Design and fabricate SO₂ gas detection cell using an open-path method.
2. Investigate and determine the best wavelength for an optimum absorption.
3. Analyse cross sensitivity with atmosphere gases.

1.9 Scope and Limitations of the Research

The limitations of this research are list as below:

1. Conducted in room temperature and in fume hood.
2. Experiment of SO₂ will be tested in fix wavelength range of UV region at 200 nm to 235 nm.
3. Limit the cross sensitivity testing to CO₂ and O₂ only.

1.10 Thesis Outline

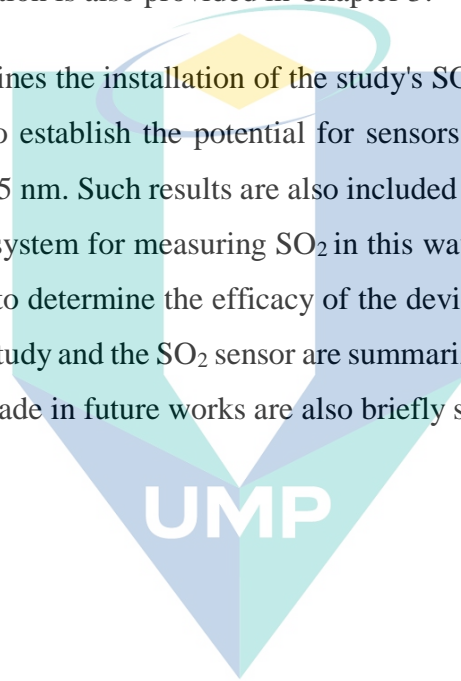
This thesis includes five chapters focusing on SO₂ gas measurement and the creation of a sensor for gas detection. In Chapter 1, a brief introduction was made to the issue of SO₂ and the value of sulfur calculation in various industries. Chapter 1 also addresses the problem regarding the SO₂ sensor and the research objectives together with limitations and scopes.

In Chapter 2, the analysis will deal with the use of fiber optic gas sensors in many newspapers and applications. A preliminary study of the optical fiber sensors was carried out. Once, different sensor configurations have been requested and the technologies used have been examined and addressed. In the visible and infrared electromagnetic spectrum area, the majority of fiber-optic sensors discussed in this segment work due to increased product supply and relatively cheap equipment. Chapter 3 justifies the choice of UV region as a light source for the development of this sensor. All tests of each type and design of fibre optical sensors are tested in order to identify the advantages and

disadvantages of SO₂ gas sensors. This evaluation examines the sensor's ability and suitability to detect SO₂ gas.

Chapter 3 provides an overview of the electromagnetic spectrum that forms the base of the study's absorption sensor. A brief overview of its operating theory and the available components of the SO₂ optical fiber sensor are presented. In relation to the elements, Beer Lambert's law describes the absorption concept as it is used to determine the concentration of SO₂ gas. A brief overview of the software used to identify and track the SO₂ gas concentration is also provided in Chapter 3.

Chapter 4 outlines the installation of the study's SO₂ gas fiber optic sensor along with measured data to establish the potential for sensors to detect SO₂ in the spectral range of 200 nm to 235 nm. Such results are also included in the report. The analysis has optimized the sensor system for measuring SO₂ in this wavelength. Further experiments have been conducted to determine the efficacy of the device in cross-sensitivity studies. All the results of this study and the SO₂ sensor are summarized in Chapter 5. Furthermore, some changes to be made in future works are also briefly suggested.



اونيورسيتي ملايسيا قهغ

UNIVERSITI MALAYSIA PAHANG

CHAPTER 2

LITERATURE REVIEW

2.1 Introduction

There are many technologies or methods available that claim to be able to detect SO₂. Fundamentally, SO₂ can be sensed using human nose because its presence is indicated by the characteristic of its own smells. However, human nose fails to quantify the exact amount of SO₂ released. This deficiency has led so many researchers to design a sensor in order to help a human quantify the gas. In this chapter, a review on a few types of SO₂ sensors and their working principle which are the ones considered to be the most relevant to this application will be described. Before that, the interactions between light and matter also will be discussed in order to have the better understanding of absorption principles of gas molecules.

2.2 Light

Light is also known as electromagnetic radiation. Light radiation strikes the optic nerves of the eyes and is sensed as color; different wavelengths of the light register in the brain as different colors (Houck, Crispino and McAdam, 2018). Light consists of photons, little packets of energy that have properties of both particles (electron, proton and neutron) and waves (Carson, 2000). All waves have a wavelength, the length of one complete cycle of the vibration. For light, the range of possible wavelengths is enormous. Different kinds of matter react with different waves of light. It's the wave characteristics which limit our ability to use light to see.

When the light is visible and wavelengths are between 4×10^{-7} m and 7×10^{-7} m, pictures of atoms that are in a range of 10^{-9} m cannot be formed. The electromagnetic spectrum diagram shows in Figure 2.1 below. The most minor things can be seen by forming an image are large molecular assemblies such as chromosomes or cells.. Chemists, biochemists and microbiologists face the problem of gaining an understanding

of what is happening at the atom and molecular level, without actually seeing atoms or molecules.

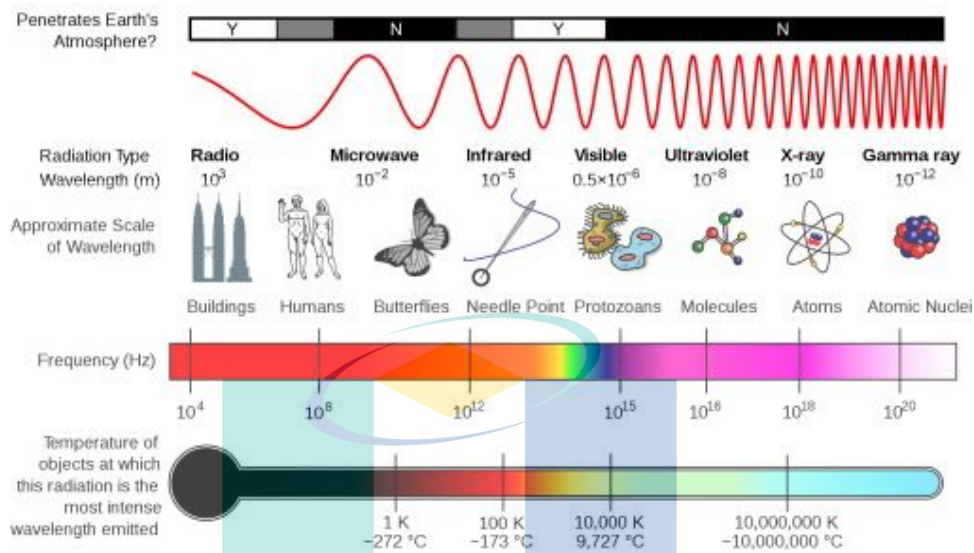


Figure 2.1 Electromagnetic spectrum diagram show different properties throughout the frequency and wavelength range

Source: Houck, Crispino and McAdam, (2018)

Even though the images of atoms and molecules cannot be made, light can be used to learn about the structures of atoms and molecules. This is because atoms and molecules can absorb or emit light (Björn, 2008; Saldanha and Monken, 2011). By looking at the light that is absorbed or emitted, the species involved can be learned. The technique for looking at such light is referred to as spectroscopy (Sharma, 2017). The spectroscopic techniques developed to study various effects in respective regions of radiation. It is the only tool available to astronomers to collect information about the cosmos. It is the most powerful tool available to scientists to study atoms and molecules, a technique that is universally used in science and engineering disciplines.

2.2.1 Types of Spectroscopy Techniques

The study of light and matter interactions is called spectroscopy (Saldanha and Monken, 2011; Sharma, 2017). Two different aspects of this relationship can be used to think about atoms and molecules. One is the detection of light wavelengths associated with atoms and molecules. The other is to calculate the light amount consumed or released at a certain wavelength. All determinations need to divide a light source into its

wavelengths of the variable. The breaking of light into a continuum is thus a critical component of any spectroscopic analysis. The energy is consumed or released in two ways by atoms and molecules. This generates four spectroscopy types called qualitative, quantitative, emission and absorption.

One of the useful aspects of spectroscopy is that a chemical species spectrum is unique to that species. The same spectrum will always be present in identical atoms and molecules. Various species will have various spectrums (Sharma, 2017). The spectrum of a species can therefore be considered as a fingerprint for the species. Qualitative spectroscopy is used for the identification of chemicals by producing a spectrum and comparing it to known spectrum to match (Ghidini, Varrà and Zanardi, 2019). As an example, consider the discovery of the element Helium (Bent, 2004). It was first observed, not on the earth, but in the sun. In 1868 the French astronomer, Pierre-Jules-Cesar Janssen, was in India to observe a solar eclipse when he detected new lines in the solar spectrum (Butt, Gole and Dyck, 2000). At that time no element known would produce these lines, and therefore he concluded that the sun contained a new element. The quest for the new element on planet Earth was started. The new element in uranium ores was identified by the end of this century and named Helium according to the Greek word for sun (Helios). Spectroscopy is now widely used in the identification of chemical species.

Quantitative spectroscopy is one of the fastest and simplest ways to assess how many atoms or molecules a sample contains (Smith, 2002). This is because the interaction between light and matter is stoichiometric. At a given temperature, in a certain period of time the same number of photons is absorbed or released with the same number of atoms or molecules. Spectroscopy is therefore one of the few methods that can directly measure the number of atoms or molecules present in a sample (Flaud *et al.*, 2005). Quantitative emission spectroscopy involves heating of samples to allow electrons to emit light. (Flaud *et al.*, 2005). This is done most often by feeding the sample in a flaming burner. As a result, use with most molecular compounds is not practical. It is often used for basic analysis. A quantitative emission technique, flame photometry, is used in clinical laboratories to assess blood plasma and urine levels of sodium and potassium. (Buzanovskii, 2018).

The opposite of the absorption spectroscopy is emission spectroscopy. Sampled electrons are stimulated by any one of a number of methods to extremely high energy levels (e.g. electric discharge, heat, laser light, etc.). (Devia, Rodriguez-Restrepo and Restrepo-Parra, 2015). When these electrons come back to lower rates, they emit light. It is divided into a spectrum by gathering this light and passing it through a prism (Demtröder, 1999). Nevertheless, this time only a dark field with colored lines that fit the electron transitions. Remember that the spectrum absorption and emission of the same material has the same wavelength values (Kang and Donnelly, 2007). These values appear as black lines on a colored field in the absorption spectrum, while the emission spectrum shows colored lines on a black field.

Absorption spectroscopy is the study of molecular absorption of light (Lagalante, 1999). White light is caused by a sample and then by a device (such as a prism), which breaks the light into a range. White light is a combination of all visible light wavelengths (Bharadwaj, 2014). If the light passes through a sample, the sample electrons will absorb certain wavelengths of light that can shift them to other levels under appropriate conditions. (Kang and Donnelly, 2007; Eastham, 2012). The light from the prism therefore lacks certain wavelengths that correspond to the permissible energy levels of the electrons in the sample. A black-line spectrum is shown where the absorbed light would have been if the sample had not been deleted.

2.2.2 Absorption Spectroscopy of UV

Absorption spectroscopy is commonly used in the field of gas detection based on the molecular absorption nature, due to its unique advantages of high selectivity, solid stability and continuous on-line monitoring in real time. (Lin et al., 2019). Gonzalez *et al* also stated (Gonzalez, Gonzalo Abad Amir *et al.*, 2019) Atmospheric gas is being monitored for nearly five decades and traces, using UV, therefore different atmospheric gas molecules absorb UV light and each of them absorbs wavelength radiation. This is a process in which the interaction between a molecule and a photon causes the atoms of a molecule to change from one energy condition to another. (Eastham, 2012). There should

be a mechanism for interaction between the molecule and the electromagnetic radiation in order to be absorbed.

UV absorption in the atmosphere arises mainly from electronic transitions of atomic and molecular O₂ and N₂ (Kali Charan Sahu, 2007). Because of UV absorption, some O₂ and N₂ molecules are photochemically dissociated in the upper atmosphere into atomic O₂ and N₂. Electron transitions take place when valence electrons are excited from a level of energy to a higher level of energy (Zhang and Hoshino, 2019). The transitional energy change provides information on the molecular properties such as their powerful states and spatial structure as well as allows the molecule to conclude whether it is in the ground or excited states.

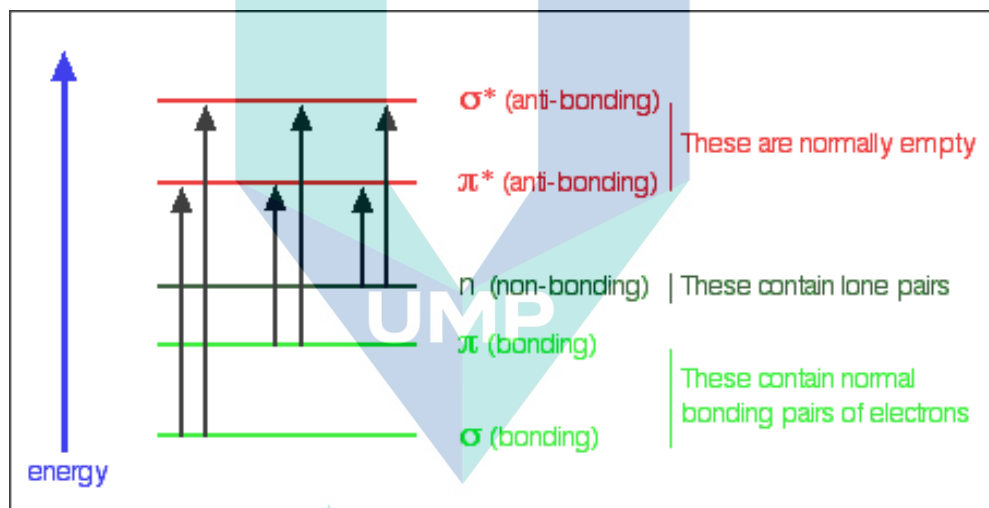


Figure 2.2 Bonding and anti-bonding energy transition

Source: *UV-visible absorption spectra*

In every possible case an electron is excited to a vacuum anti-bonding orbital from a full orbital. Each jump takes light energy, and a big jump requires more energy than a small jump. Every wavelength of light has a certain energy. If this particular amount of energy is suitable for one of the energy transitions, then the wavelength is absorbed. This explains the different absorption levels at various wavelengths. It also explains why another gas has a different absorption curve or pattern because another gas electron needs a different energy amount before it can jump. This transition or jumping electron and its energy are well explained by Kalsi (P.S. Kalsi, 2004).

According to the theory illustrated in Figure 2.2, a jump from π to a π antibonding orbital should have a fixed energy and should therefore absorb only one wavelength. Nonetheless, the fact that the molecule absorbs a vast spectrum of wavelengths indicates a variety of energy leaps. (P.S. Kalsi, 2004). Rotations and vibrations of the molecule that constantly change the gaps between the orbital electrons are responsible for this (Stewart, 2019). The energy gaps between them are therefore constantly changing. In short, the absorption occurs in a range of wavelengths instead of a fixed wavelength.

A recent development is the understanding of the existence of light. The electron leaps refer not only to the absorbed wavelength, but also to the energy gap. The greater the energy gap, the higher the energy required. (Morris, 2009). The various forms of electromagnetic radiation have long been considered as different phenomena. The list of common names for the different wavelength ranges -wave and -ray. This is because a photon's energy is (inverse) correlated with its wavelength. This means light has a greater frequency with a lower wavelength, and so it carries more energy. (Pirronello and Manicó, 1998). We can thus conclude that the bigger the energy gap, the lower the wavelength of light is absorbed.

$$E = \frac{hc}{\lambda} \quad 3.1$$

Equation 3.1 above, where E is energy of the photon in joules, λ is wavelength in nanometres, h is constant of Plank, and c is a speed of light. (Percuoco, 2013). The shorter the wavelength, the higher the photon energy. (Barrett, 2002). As the wavelength range of known electromagnetic radiation is enormous, it is also the energy difference of photons which determines the effects of the photon when interacting with matter. The radio frequency photons have very little energy, so we can saturate our environment with them without disturbing our surroundings. Olive's theoretical cross-section absorption (Olive, 2007) shows that SO₂ gas absorbs light on many wavelengths of UV field. The peaks vary from 150 nm to 450 nm at different wavelengths, as shown in Figure 2.3. Each peak has a wide absorption range instead of a single line.

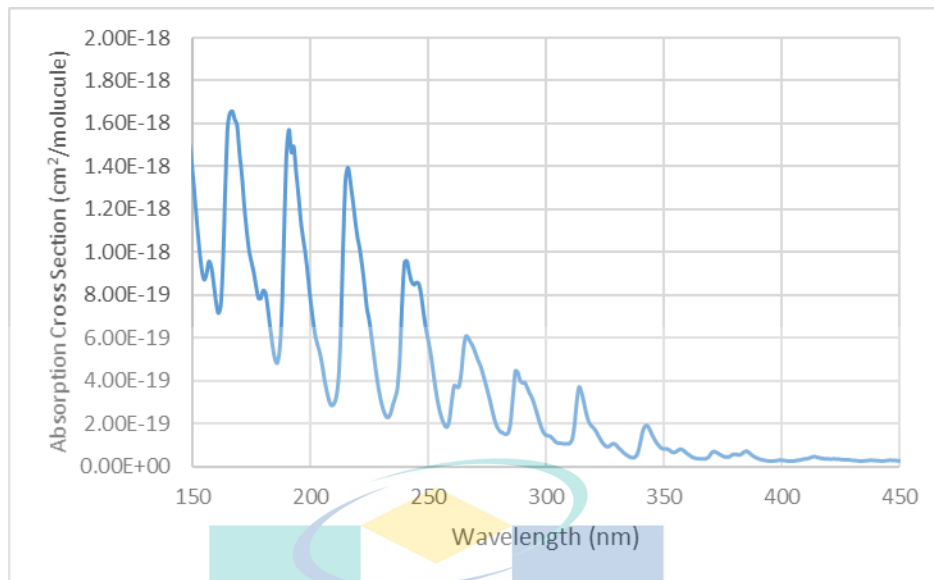


Figure 2.3 Absorption cross section for SO₂ in the UV region

Source: Olive, (2007)

2.3 Beer Lambert Law

The basic principles of Beer-Lambert Law are widely used in many fields areas of study such as pharmaceutical sciences, chemistry and even related fields of quantum testing related to absorption spectroscopy (Hardesty and Attili, 2010). In optical measurement, the Beer-Lambert law is utilized to relates the absorption of light to the properties of the material where light is travelling (Dooly *et al.*, 2011). Figure 2.4 shows that the light intensity via a medium is decreased in relation to the length of the path exponentially. As explained by Dooly et al, in Equation 3.2, the ratio of the transmitted, I and incident intensity, I_0 can determine the transmittance, T of the travelling light (Dooly, Fitzpatrick and Lewis, 2008).

$$\text{Transmittance, } T = I/I_0 \tag{3.2}$$

$$\text{Absorbance, } A = -\ln(T) \tag{3.3}$$

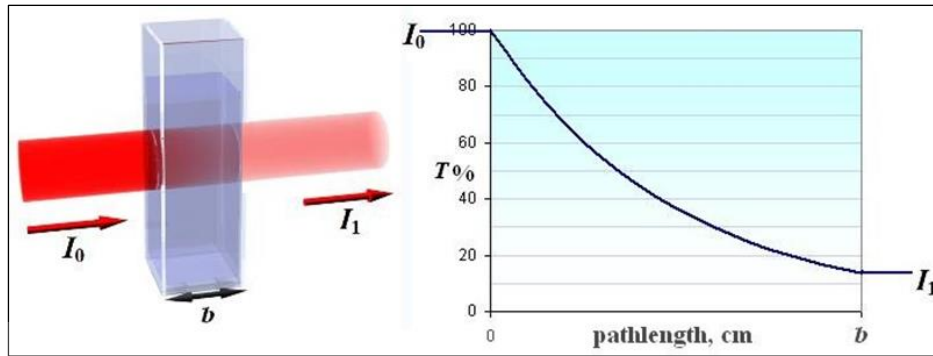


Figure 2.4 Light absorption intensity over path-length.

Source: Dooly *et al.*, (2011)

Absorbance, A has no unit as shown in Equation 3.3. If the absorption versus the path-length is shown in a graph, a straight line is established. The law can therefore also be characterized as a linear relation between light absorbance and the absorbing medium concentration. In the equation 3.4 below, it has featured the general equation of the Beer Lambert Law as also describes by Norazmi *et al.* It demonstrates the relation related absorption and absorbing species concentration (Norazmi *et al.*, 2018).

$$\frac{I}{I_0} = e^{(-\sigma.N.l)} \quad 3.4$$

Where I is transmitted intensity, I_0 is the intensity of the incident, l (cm) is the distance the light is passing through the gas, σ ($\text{cm}^2/\text{molecule}$) is the cross-section of absorption, and N ($\text{molecules}/\text{cm}^3$) is the number of molecules in unit volume. This concentration N has to be adjusted in unit $\text{molecules}/\text{cm}^3$ to ppm because the concentration of emission gas is normally read in this unit. The Beer Lambert Law as explained and derive by O'keeffe *et al.*, Hadi and Salim *et al.*, (O'Keeffe *et al.*, 2010; Hadi, 2011; Salim *et al.*, 2018) after rearranging the general equation 3.4 above, the absorption cross section can be calculated using Equation 3.5..

$$\sigma = \frac{-[\ln \frac{I}{I_0}][T \times 22.4]}{\text{ppm} \times N_A \times l \times 273 \times P \times 10^{-9}} \quad 3.5$$

Where T (K) is the measured gas temperature, the unit gas concentration is part per million (ppm), N_A is the constant of Avogadro and P (atm) is the measured pressure.

2.4 Review on SO₂ Sensor

In a control system, sensors are the most critical unit. Sensors are used to detect the physical and chemical characteristics of a device through control and display of various parameters. Many available methods and technologies claim that SO₂ can be detected. In essence, the human nose can very effectively sensitive SO₂, because its presence is characterized by the pungent and irritating smell of a just match. It can be measured by the taste at 0.35-1.05 ppm and has a pungent, irritated odor of 0.67-4.75 ppm with an odor threshold. (Cheryl B. Bast; George M. Woodall; Lorren Koller, 2010). The human nose does not, however, quantify the SO₂ level and detect the gas at lower concentrations.

For reasons of health and safety, SO₂ concentration in ambient air must in many cases be known. Certain sectors that need the quantification of SO₂ include food and beverage industries, fertilizers, bio-medical industries, leather tanning, brewing and preservation industries and SC Gad describes the reasons. (S.C.Gad, 2014). SO₂ gas detector sensors were therefore designed to determine the concentration of SO₂, some of which can detect very low concentrations up to the ppb level. (Ghimbeu *et al.*, 2010; Betty, Choudhury and Arora, 2015; Kumar, Avasthi and Kaur, 2017).

Therefore, several new analytical methods and technologies have been introduced in recent years for the analysis of SO₂. A summary of some types of current SO₂ sensors will be listed in this section. They are divided into four main types and take into account their advantages and disadvantages. The technologies for sensor SO₂ are investigated as follows:

- a) Microfluidic sensor
- b) Metal oxide semiconductor sensors
- c) Electrochemical sensor
- d) Fiber Optic Sensor

2.4.1 Microfluidic sensor

The first SO₂ sensor will be discussed is microfluidic based sensor. Antony et al. explains in his study that microfluidics are the technology sector that processes fluid's micro volumes. The requirements in several areas such as molecular analysis, biodefense, molecular biology and microelectronics have provided an opportunity for the advancement of microfluidics technology. Sensors for microfluidic systems could be referred to as "microfluidic sensors", which have emerged as a distinct new field by controlling fluids in channels spanning ten micrometers. The development of sensors for the measuring on a micro scale is a hot stream in current research when scaling decreases, as well as the sensor sensitivity, selectivity and stability also take into account the risks in design and development. (Antony *et al.*, 2014).

Antony et al. also classified two types of microfluidic sensor as physical sensors and bio-chemical sensors (Antony *et al.*, 2014). Among physical sensors as explored by Antony et al. are microfluidic flow sensor (Rasmussen *et al.*, 2001; Kim *et al.*, 2019), temperature sensor (Kim *et al.*, 2013; Mohaghegh Montazeri, O'Brien and Hoorfar, 2019) and pressure sensor (Shi *et al.*, 2016; Hoera *et al.*, 2018). Meanwhile, among bio-chemical sensor that have been investigated by Anthony et al. are gas sensor, ATP bioluminescence, DNA bio-sensor, cancer cell detection, cell flow detection, cholesterol detection, cocaine detection, glucose sensor, pH measurement and bacterial bio-sensor (Antony *et al.*, 2014).

Many microfluidic sensors are electrochemical devices, containing multidisciplinary sensing theorems. As an example, Cleary et al. in describing detection principle of phosphate sensor in his paper mention that by using optical detection method and the colorimetric technique, it involving the formation of vanadomolybdophosphoric acid when a phosphate-containing sample is mixed with an acidic reagent containing ammonium molybdate and ammonium metavanadate in a T microchannel reactor (Cleary, Slater and Diamond, 2007). In developing his force sensor, Ponce Wong et al. has recently reported that it transforms mechanical deformations into electrical output by detecting the capacitance transition of the dielectric medium inside the tube. (Ponce Wong, Posner and Santos, 2012).

To date there are many types of gas microfluidic sensor have been reported such as chlorine gas sensor (Gao *et al.*, 2008), ammonia gas sensor (Martini *et al.*, 2012), O₂ gas sensor (Bunge *et al.*, 2019) and others. In a study investigating SO₂ sensor, Montazeri et al. found that one of the technology to detect SO₂ is microfluidic paper-based analytical devices (μ PADs) (Mohaghegh Montazeri, O'Brien and Hoorfar, 2019).

According to Montazeri et al., Busa et al. and Ramdzan et al., μ PADs have many great advantages over conventional equipment, including very small volumes of reagents and sample, rapid response times, low cost, excellent portability, energy-free fluid transportation through capillaries, high volume area to volume ratio and the ability to store reactions within the fiber network (Busa *et al.*, 2016; Ramdzan *et al.*, 2016; Mohaghegh Montazeri, O'Brien and Hoorfar, 2019). μ PADs thus provide a promising approach to a wide array of chemical, biomedical, biological, environmental and clinical applications, including food additive or derivative assessment, bacterial monitoring, beverage detection and cell culture.

Nevertheless, traditional techniques and equipment such as colorimetry, electrochemical analysis, chemiluminescence, and others continue to be used in the last detection phase. Furthermore, calibration (i.e., training) across a broad spectrum of parameters is a major challenge in microfluid gas detectors including gas types, variable concentrations, temperature, strain, moisture, etc. (Mohaghegh Montazeri, O'Brien and Hoorfar, 2019). It involves multiple detectors and detailed tests, both time consuming and expensive.

2.4.2 Metal Oxide Semiconductor Sensor (MOS)

Metal oxide semiconductor sensor also known as MOS is one of another type of SO₂ sensor. MOS gas sensors are the most commonly investigated gas sensor community because of their excellent sensing capabilities, high electrical stability, rapid response and recovery (Barsan, Koziej and Weimar, 2007; Lupan, Chow and Chai, 2009; Chaudhary and Kaur, 2015). Semiconductor gas sensors rely on a gas in contact with a metal oxide surface which is then oxidized or decreased. This works on the principle of absorption or desorption of the metal oxide gas, which changes the conductivity or resistivity of the base value. The conductivity or resistivity transition can be tested with electronic circuits.

The change in conductivity or resistivity is typically a linear and proportional relation to the gas concentration.

The metal oxide semiconductors used for the detection of SO₂ are usually tin oxide (SnO₂). Tyagi et al. suggest that SnO₂ is the favored one for its natural non-stoichiometry, which allows O₂ to be adsorbed by the atmosphere on its surface and makes it immune to many harmful and toxic gasses (Tyagi *et al.*, 2016b). SO₂ sensing responses were contrasted by Tyagi et al. with SnO₂ thin films combined with various metal oxide catalysts such as PdO, CuO, NiO, MgO and V₂O₅ (Tyagi *et al.*, 2016b, 2017).

At 220 °C, a gas response of 1.3 was shown by the bare SnO₂ thin film sensor while a NiO/ SnO₂ composite sensor had a gas response of 56 to 500 ppm SO₂ gas with a low 80 s and 70 s recovery time at 180 °C respectively. Das et al. investigate the highly selective gas sensing characteristics of nanostructured vanadium-doped SnO₂ sensors that can detect SO₂ gas down to 5 ppm in the presence of CO, CH₄ and butane gases (S. Das *et al.*, 2008). It proposes that SO₂ to SO₃ surface oxidation occurs in redox cycles involving species of vanadium-sulfur- O₂ adsorbed.

Although SnO₂, showing great capability in detecting SO₂, there are few research on ZnO and WO₃ are also studied. For instance, Zhou et al. developed the hierarchical ZnO gas sensor based on the nanoflower and investigated its gas sensitive properties for SO₂ gas. (Zhou *et al.*, 2016). 16.72 and 26.14 gas responses respectively were observed for 30 and 60 ppm of SO₂ gas at 260 °C. The response time was 7 s for 80 ppm gas concentration, while 8 s recovery time was observed.

Shimizu et al. studied extensively the SO₂ sensing properties of several semiconductor metal oxides (WO₃, SnO₂, ZnO, TiO₂, In₂O₃, and In₂O₃-5.0 mol % MgO) and reported that the SO₂ sensor response was the highest at 400 °C. (Shimizu *et al.*, 2001). The researchers also tested the effect of noble metal add-ons on WO₃ in an attempt to improve the SO₂ sensor response, and found that adding 1.0 wt% Ag improved the most the efficiency of WO₃, which showed significantly increased resistance to 450 °C.

The mechanism for the increased resistance of WO₃ was the formation of SO⁻² and the forming of SO⁻⁴ of 1.0 wt percent Ag/WO₃ at 450 °C, according to Shimizu et al. (Shimizu *et al.*, 2001). Surface chemistry plays an important role in the gas sensing of semiconductor metal oxides, but the further development and improvement of sensor

materials can be supported by understanding the effects of the addition of noble metals in the phase balance in the presence of SO_2 species. While thermodynamic phase stability of SO_2 gas sensing semiconductor oxide materials may give an insight into working principles, thus selectivity, sensor response and stability, they are scarcely taken into account.

There have been extensive research on these metal oxide semiconductor sensors and promising performance, with robust and inexpensive sensors (Clifford and Tuma, 1982; Srivastava *et al.*, 1994; Sberveglieri, 1995). Nevertheless, the sensors of metal oxides semiconductor have their own disadvantages. One of the key drawbacks is that SO_2 gas alone is not selective (Ampuero and Bosset, 2003) especially in the presence of water vapor when gas is detected (Wang *et al.*, 2010).

According to Wang *et al.* (Wang *et al.*, 2010), the absorption of water molecules results in less chemical absorption of SnO_2 surface O_2 species due to the decreasing of the sensor response surface area. On the other side, water molecules also act as a barrier to absorption of C_2H_2 . The superficial C_2H_2 migration on the SnO_2 surface is difficult, which reduces the sensitivity. Therefore, a new method is necessary to solve this question of selectivity.

This selectivity problem was reduced or solved by different methods, like the neural network system (Mondal *et al.*, 2015; Krivetskiy *et al.*, 2018), numerical modelling (Kumar *et al.*, 2019) or through the use of metals or additives that boost chemical supply of different gases (S Das *et al.*, 2008; Betty, Choudhury and Arora, 2015; Zhou *et al.*, 2019). Specific approaches used to boost the sensor selectivity include the use of masks and filters, or temperature controls, so that the sensor detects only a single gas with a high sensitivity (C. Zhang *et al.*, 2019). MOS sensors also face other issues, such as electromagnetic interference sensitivity. It can also be affected by moisture and have a short service life due to the weakness of the filter. The difficulty of rising MOS sensor technology can also increase production costs.

2.4.3 Electrochemical Sensor

Due to its attractive features, including reduced power consumption, portability and efficient production, high sensitivity and fairly perfect selectivity, this system for gas sensors has been employed. (Xiong and Compton, 2014). A standard electrochemical gas sensor typically comprises a sensory electrode (or work electrode), a counterelectrode, a reference electrode, electrolyte and a hydrophobic gas permeable membrane (usually PTFE or Teflon) (Wang, 2006; Giddey, Badwal and Kulkarni, 2013). R. Sathiyamoorthi et al developed a fluoride and chlorine electrochemical sensor (Sathiyamoorthi *et al.*, 2004). Lu et al and Gan et al. in their review study on electrochemical sensors based on graphene materials indicated the fact that nanoscale materials are good candidates for gas sensing elements due to their high surface-to-volume ratio, reduce size and power consumption and have been used to detect multiple sensors (Lu, Ocola and Chen, 2009; Gan and Hu, 2011).

For the most part, in this category of sensors, the sensors are organized as kinds of electrolyte which use the most solid and liquid electrolytes. More specifically, amperometric and potentiometric methods typically utilize solid-state electrolyte-based sensors. On the other hand, voltammetric and potential step chronoamperometric methods are commonly used in liquid state electrolyte sensors (Rogers *et al.*, 2010). Silvester et al. investigated that amperometric and potentialometric sensors are mostly used to detect gasses, while coulometric and conductometric sensors are rarely used for sensing gasses. (Silvester, 2011). To identify specific gases by adjusting the electrolyte form, amperometric sensors have been used.

As an example, Kuo-Chuan Ho and Wen-Tung Hung (Ho and Hung, 2001) developed an amperometric NO₂ gas sensor based on Pt/Nafion electrode, NO₂ concentrations in the range of 0 to 485 ppm were detected. Lu et al. also developed an amperometric hydrogen sensor based on the Nafion membrane polymer electrolyte membrane as a conductive polymer. (Lu *et al.*, 2005). The response to the concentration of hydrogen was between 260 and 11,500 ppm. Yente Chao et al. have developed an amperometric sensor using three different hydrogen and carbon monoxide sensing sensor designs (Chao *et al.*, 2005). In H₂ and CO concentration, the three main systems were tested, while devices II and III had slower response times as opposed to system I. The

sensor selectivity in hydrogen concentrations was significantly improved by switching Pt-air RE with updated Ag / AgCl RE and incorporating semi-permeable membrane.

Gas detection users have traditionally learned the disadvantages of the electrochemical gas detection system from the chemical reaction factors. For instance, the reaction speed decreases with decreasing temperature. As the function, the electrochemical cell temperature range appears to be narrower than other sensor types. Electrochemical instruments have traditionally been unable to function in extreme, cold weather. A low ambient temperature limit of $-10\text{ }^{\circ}\text{C}$ is not uncommon in certain commercial models. These sensors are also adversely affected by alkaline metals, which cause sensor drift, and by silicone vapors, which may coat the sensor surface and irreversibly inhibit sensitivity. Operation in low O_2 environments also alters sensor performance in sensors in which oxidation of the target gas takes place at the sensing electrode. Examples are certain ammonia, carbon monoxide, and hydrogen sulphide electrochemical cells.

2.4.4 Optical Fiber Sensor

Optical fiber sensor (OFS) technology has been used in variety of application for more than four decades since the very first sensor reported in the literature. In the late 1970s, the optical fiber sensor development becomes crucial. Since the optical fiber has many advantages as it has been widely used in many areas such as telecommunication (Landsbergen, Shiang and Byrnes, 1994; Carlier, Li and Lutton, 1997), medical (Gauthier, 1993; Arata, Terakawa and Fujimoto, 2013; Sanders *et al.*, 2014), environment (Gangaiya and Mahendra, 2008; Jiang *et al.*, 2013), military (Jamieson, 1982; Li *et al.*, 2012), space (Taylor and Thacker, 1982; Rößner *et al.*, 2012), oil and gas industry (Fu, Wan and Qiu, 2010; Yan and Chyan, 2010; Mirzaei *et al.*, 2013) and etc..

2.5 Optical Fiber Review

There many examples of the early development and application of fiber optic sensor reviewed by Culshaw and Kursey (Culshaw and Kursey, 2008). 'Basically, fiber optic has three important parts which is core, cladding and coating or buffer as shown in Figure 2.5 (*General Fiber Information*, n.d).

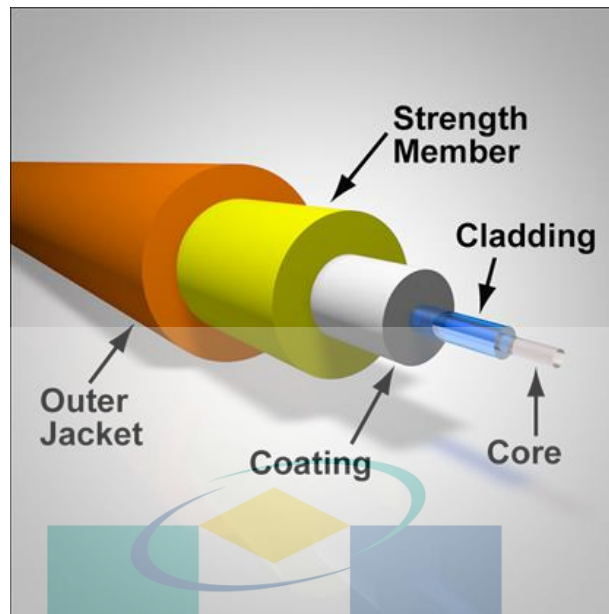


Figure 2.5 Optical Fiber Basic Structure
 Source: *Custom Fiber Optic Patch Cables*, n.d

Core is the centered layer of optical fiber usually made of silica where the light is transmitting through it. Cladding is the coating around the center reflecting the light in the middle, often made from silica with a different composition. Meanwhile coating is the first layer that protect the silica structure; core-cladding from physical or environmental damage. Usually the optical fiber has at least four to five layer which is will protect more the important part from breaking during installation.

2.5.1 Advantages of Optical Fiber

The conventional electrical sensors have more disadvantages than the optical fiber such as heavy shielding, significantly increasing cost, size and weight. On the other hand, optical fibers which is have more advantages such as the ability to transmit optical signals over longer distance without significant loss of the signal intensity. Optical fibers also have many other benefits as shown in Table 2.1 below and apply to optical fibers.

Table 2.1 Optical Fiber Advantages

Optical Fiber Advantages
Passive (all-dielectric)
Light weight
Small size
Immunity to electromagnetic interference
High temperature performance
Large bandwidth
Environmental ruggedness to vibration and shock
High sensitivity
Electrical and optical multiplexing
Component cost driven by large commercial telecommunication and optoelectronic market

Source: Zanger and Zanger, (1991) ; Saleh, A Mustafa and Osman, (2015)

2.6 Classification of Optical Fiber Sensor

There are various types of fiber optic sensor has been developed today. Basically the principle of fiber optic sensor is shown in Figure 2.6 below. It consists of light source, modulator element and detector. The light source will feed the light signal that propagates through the fiber optic and in the modulation region; the measurand will modulated the light signal. Then the light detector will sense the light signal before it will be analyzed. Previous research has shown that there are few types on how the fiber optic sensor is classified; location of modulation region, the operation principle, its application and response to their measurement point (Fidanboylu and Efendioglu, 2009; Thakral and Manhas, 2011; Ghetia, Gajjar and Trivedi, 2013). In summary, the categories that classified the FOS into which types are presented in the Table 2.2 below (Yio *et al.*, 2008; Scholar, 2012) and the types of FOS will be further explained in the next sub-chapter.



Figure 2.6 Block Diagram of Basic Optical fiber Principle

Table 2.2 Classification of Fiber Optic Sensor System

Classification of Fiber Optic	Classification of Sensor
Location of Modulation Region	1. Intrinsic 2. Extrinsic
Operation Principle	1. Intensity 2. Phase 3. Frequency wavelength 4. Polarization
Based on application	1. Physical 2. Chemical 3. Bio-medical
Response to measurement point	1. Point to point 2. Multiplexed 3. Distributed

Source: Bahareh and Hooman, (2008); Scholar, (2012)

2.6.1 Location of Modulation Principle

The characteristic that sensing takes place in the area outside of the fiber itself can be distinguished by the extrinsic sensor or also the hybrid sensor. It is a measurement tool with an open air optical system, such as a Laser Doppler anemometer for measuring flow velocity.

The principal advantage of the external sensor is its ability to reach places which other sensors can not reach, for example, when measuring a high-temperature spot of a gas turbine blade. (SCHENK and RAAKE, 1999; Sebastián, Armiens and Gómez-Elvira, 2010). The optical fiber is used to relay radiation to the gas turbine and a pyrometer measures thermal radiation. Extrinsic sensors can also be used for measuring the interior temperature of electrical transformers where intense electromagnetic fields prohibit the use of external measurement techniques. (Deng *et al.*, 2001). The diagram of the extrinsic and intrinsic fiber optic sensor concept is shown in Figure 2.7 below.

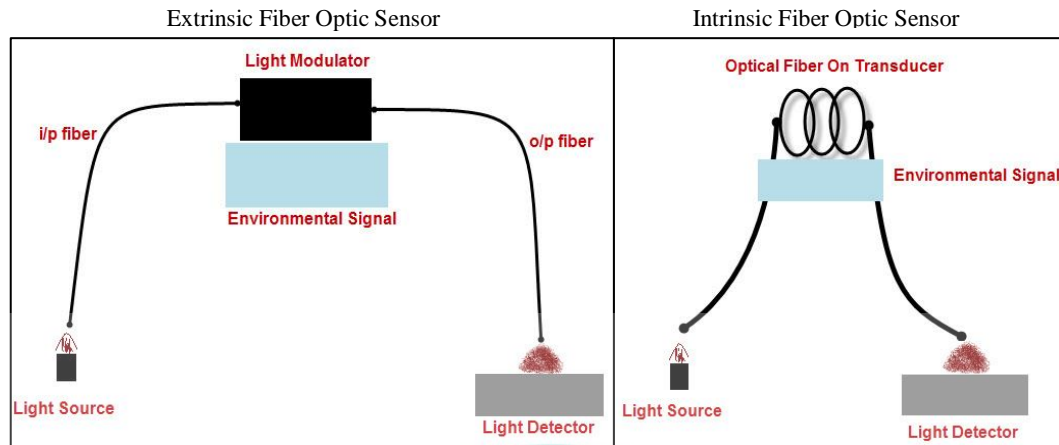


Figure 2.7 Extrinsic and intrinsic fiber optic sensor

Source: Shivang Ghetia, Ruchi Gajjar and P Trivedi, (2013a)

Intrinsic or all-fiber sensors imply that the sensor parameters, for instance intensity and wavelength, modulate the sensing properties in the fiber itself. It is being categorized into two types which are direct sensor which is the measurands act on the fiber itself and indirect sensor which is the measurands act on another medium transduced through the fiber optic (Nguyen *et al.*, 2014; Pospíšilová, Kuncová and Trögl, 2015). Fiber Optic Gyroscope (FOG) (Merlo, Norgia and Donati, 2002; Shamir, 2006; Fidanboylu and Efendioglu, 2009; Juang and Radharamanan, 2009; Lecler and Meyrueis, 2012) and interferometric sensor (Vukmirica, 2008) are an example of direct sensor and indirect sensor such as coated optical fiber sensor (James and Tatam, no date; Wysokiński *et al.*, 2015).

2.7 Open-path Optical Technique

Open-path technique is amongst the most common gas detection methods that use the spectroscopic concept. (Briz *et al.*, 2007; Trottier *et al.*, 2009; Detto *et al.*, 2011; Schütze *et al.*, 2013; Sung and Lu, 2014). The advantage of the open path technique is that the detector interacts with the test gas for a substantial proportion of the light. The advantage of this approach is that multiple gas species can be simultaneously detected in unique blend and in real time. (Gibbs *et al.*, 1994).

Ohtsu *et al* exhibit the open path technique for the measurement of spectral absorption patterns with a laser light for NH_3 and H_2O (Ohtsu, Kotani and Tagawa, 1983). This open path technique used an absorption cell with a length of 0.55 meters. During the

first half of the experiment, the spectral absorption lines were measured at 1.5 μm without optical fiber, which resulted in 21 emission spectra for NH_3 and another for H_2O , as highlighted in Figure 2.8. A multimode fiber with a diameter of 30 μm was connected in the second half of the experiment to one early part of the absorption chamber. The tests of the second period of the test reveal that when an optical fiber is being used the signal to noise ratio is reduced by about 10 times.

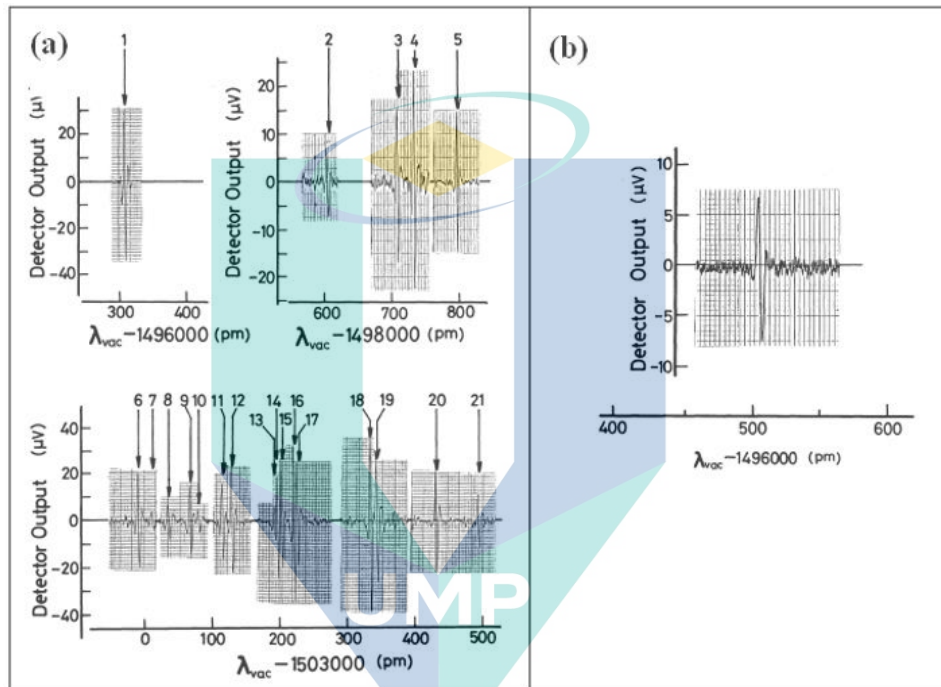


Figure 2.8 Third derivatives of (a) NH_3 spectral lines (b) H_2O spectral line
Source: Ohtsu, Kotani and Tagawa, (1983)

The sensor system using the equivalent approach is the DOAS system. Al-Jalal et al. define DOAS as a modification of an open path sensor system, which can be used to measure various gases at the same time (Al-Jalal *et al.*, 2019). The underlying method is identical to the open path technique and DOAS system. Moreover, as stated by Zheng et al., the DOAS system needs radiation intensity measurement at two or more wavelengths (Zheng *et al.*, 2018). A standard DOAS instrument consists of a continuous source of light as shown in Figure 2.9, a receiver and an analyzer.

The major advantage of this method is that in real time a variety of applications with various trace gas species are measured (Kim and Kim, 2001). Nonetheless, DOAS sensors need to have a high-energy source of light, which is not economic and

environmentally acceptable to long-range measurements. The path from the transmitter to the receiver can be up to 20 km for a functioning DOAS (Platt, 2017).

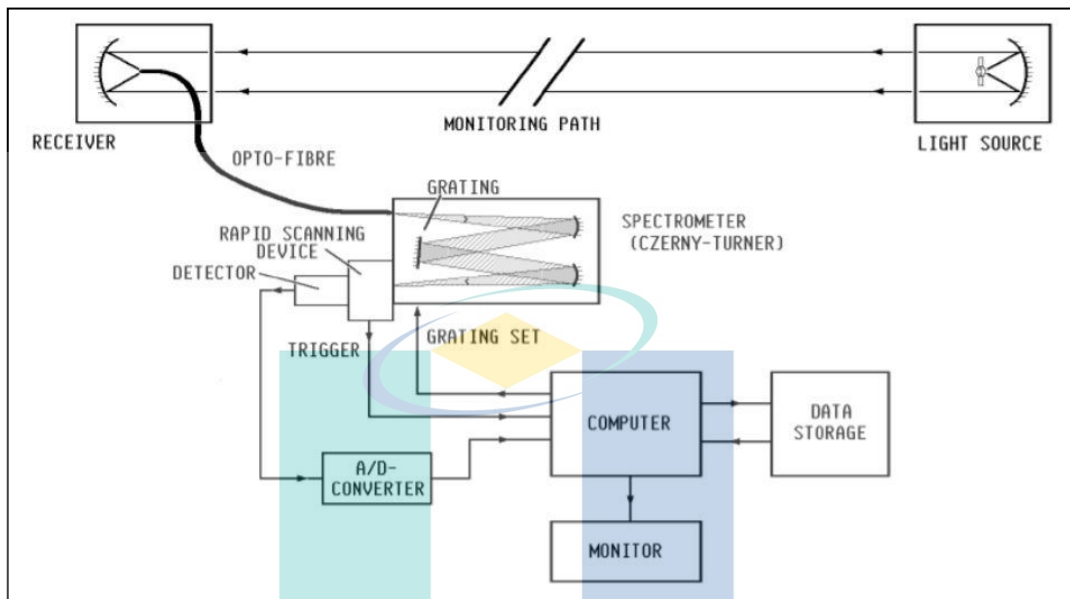


Figure 2.9 Schematic diagram of DOAS sensor system

Source: Wang, Zhu and Niu, (2008)

As shown by Wang et al, DOAS system has the same configuration as the detection system in this research (Wang, Zhu and Niu, 2008). Nevertheless, a cylinder rod is used as a testing gas cell for this optical fiber SO_2 sensor. The benefit of using the gas test cell is that before the measurement has taken place especially in the initial phase of sensor growth or during the calibration process it is easier to draw and cleanse the necessary quantity of the test gas into the system.

Extensive method in open path technique is Differential Absorption Lidar (DIAL) system. DIAL is widely used in the measurement of various kinds of gases, including O_3 , CO_2 , and CH_4 (Burlakov *et al.*, 2010). In order to measure the atmospheric concentrations of gases such as water vapor and ozone, it uses the atmospheric backscatter technique (Grant, Kagann and McClenny, 1992). DIAL consists of four components: the laser unit, the telescope unit, the detection unit, the system acquisition and control unit. The DIAL system shown in Figure 2.10 below.

The laser transmitter consists of a teint laser, an oscillator, a preamplifier and an end amplifier. Only the oscillator stage is shown in Figure 2.10. For coarse-wavelength

tuning, a stepper motor rotates the tuning mirror of the color laser while the tuning mirror angle is controlled by a piezoelectric transducer (PZT) for fine tuning. It combination requires fast switching at speeds up to 50 Hz between on and off wave lengths. This is faster than the pulse repeater frequency (20 Hz), which allows the space between one pulse and the next to be moved from wavelength.

According to Grant et al., there are several likely reasons why the DIAL laser system has not been used more widely. Next, it is quite difficult to use the laser DIAL system, including tunable lasers, cooled detectors, and local oscillators for heterodynamic detection for long-range application, or efficient pulsated lasers for direct detection. Second, the operation of the DIAL laser system depends only on the presence of sufficient aerosol atmospheric loading to provide useful backscatter signals. This condition for aerosols contrasts with UV and visible wavelength lidar structures that can cope with only molecular backscatter.

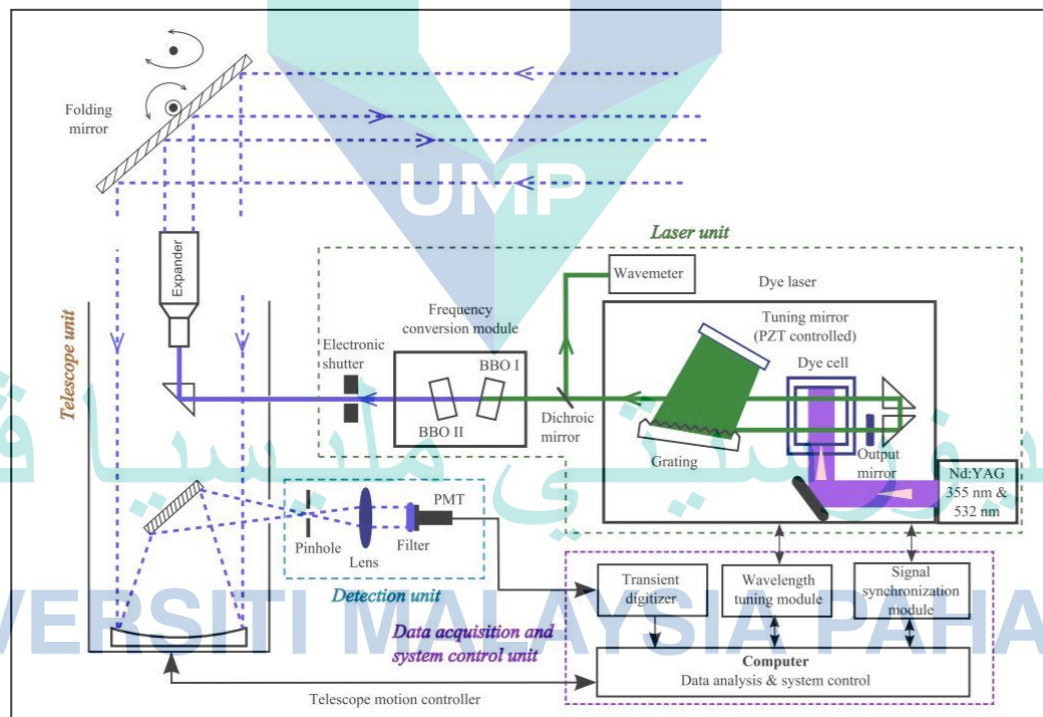


Figure 2.10 Scheme of the differential absorption lidar (DIAL) system.

Source: Mei, Zhao and Svanberg, (2014)

2.8 Summary

In this chapter, several types of spectroscopy and the open-path optical method techniques had been discussed. Their characteristics, working principle, advantages and disadvantages were examined. Types of spectroscopy included qualitative spectroscopy, quantitative spectroscopy, emission spectroscopy and absorption spectroscopy. Among all the types of spectroscopy, absorption spectroscopy is commonly used in the field of gas detection based on the molecular absorption nature, due to its unique advantages of high selectivity, solid stability and continuous on-line monitoring in real time. In addition, the Beer–Lambert law is also been discussed as it is been used in the optical measurement.

This chapter also will not be complete without reviewing on types of SO₂ sensor. Therefore four types of sensor has been discussed thoroughly which is microfluidic sensor, metal oxide semiconductor sensor, electrochemical sensor and optical fiber sensor. Futhermore, there are many techniques in optical fiber sensor which is Open-path Technique, Differential Optical Absorption Spectroscopy (DOAS) and Differential Absorption Lidar (DIAL) systems. All these methods were reviewed in this chapter. The techniques are capable in making a long path measurement to measure visibility and each of them has their own advantages.

اونيورسيتي ملايسيا قهغ

UNIVERSITI MALAYSIA PAHANG

CHAPTER 3

METHODOLOGY

3.1 Introduction

Chapter 2 dealt with different types of SO₂ gas sensing designs and the suitability of each sensor to use as a possible SO₂ gas sensor. Chapter 2 reveals that open path configuration provides the most advantages. The designs of optical sensors differ according to light source, modulation method and detector types. The result is a number of differences, such as gas range detection and its detection limits, durability, sensitivity susceptibility and development costs. The open path absorption sensor was chosen for the new sensor development in this project. The part used, including related software, is discussed in this chapter. This chapter also involves testing and development of this device into a functioning gas sensor.

3.2 Development of Sensor System

3.2.1 UV Light Source

The absorption wavelength of SO₂ gas is most appropriate for the UV electromagnetic light area, as described in Section 2.2.2 in Figure 2.3. UV light is part of electromagnetic radiation (Diffey, 2002) (Canadian Centre for Occupational Health and Safety (CCOHS), 2016) generally in the range of 100 nm to 400 nm, has higher frequencies (shorter wavelength) than visible light but have lower frequencies (longer wavelength) compared to x-rays. The light that enables human to see is composed to the colours in a rainbow and the UV region is started after the violet end of the rainbow which is invisible to human eyes but visible to some species of birds, insects and certain fish. Some UV exposure is essential for good health but excessive exposure can bring damage to human health as painful as sunburn. As shown in Figure 3.1, UV light can be separated into three groups of the electromagnetic spectrum. Nevertheless, according to ISO Standard (ISO International Standard 21348, 2007) UV radiation classified with a wavelength of between 10 nm and 400 nm is listed as Table 3.1.

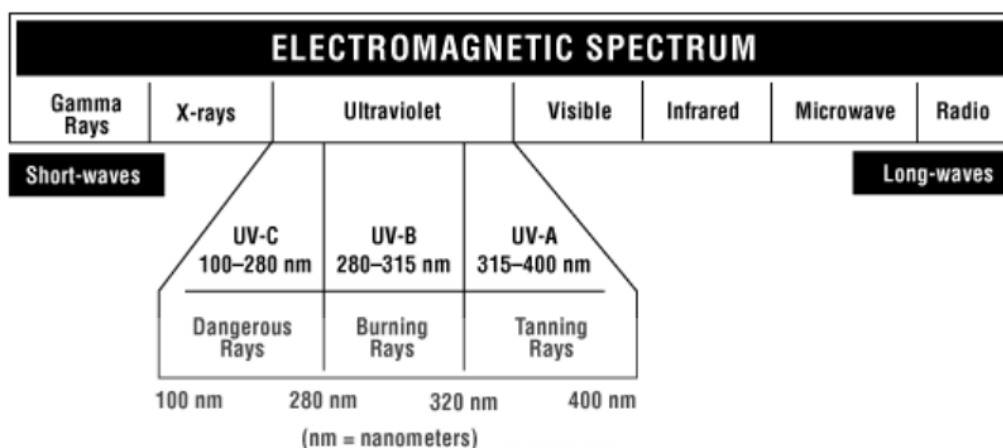


Figure 3.1 Electromagnetic Spectrum

Source: Canadian Centre for Occupational Health and Safety (CCOHS), (2016)

Table 3.1 Subdivided of UV Radiation

Name	Abbreviation	Wavelength Range
Vacuum	VUV	200 nm – 10 nm
Extreme	EUV	121 nm – 10 nm
Hydrogen Lyman-alpha	H Lyman- α	122 nm – 121 nm
Far	FUV	200 nm – 122 nm
Ultraviolet C	UVC	280 nm – 100 nm
Middle	MUV	300 nm – 200 nm
Ultraviolet B	UVB	315 nm – 280 nm
Near	NUV	400 nm – 300 nm
Ultraviolet A	UVA	400 nm – 315 nm

Source: ISO International Standard 21348, (2007)

In addition to sun, as the natural source of UV radiation, different types of artificial UV sources emit UV light at different wavelengths such as UV light emitting diode (LED) (Muramoto, Kimura and Nouda, 2015), UV laser (Delmdahl and Pätzelt, 2008), halogen lamp (Yubero, García and Calzada, 2008), deuterium lamp (Finkenzeller and Labs, 1979), xenon arc lamp (Diffey, 2002). With the technological development in UV light source, many manufacturer has offered UV light source with different use and specific wavelength as shown in table 3.2 below.

Table 3.2 Commercially Available Light Source

Light Source	Wavelength Range	Manufacturer
Halogen	360 nm – 3800 nm	Thorlabs
Deuterium	190 nm – 400 nm	Ocean Optics
Xenon Arc	240 nm – 2400 nm	Thorlabs
LED	240 nm – 627 nm	Ocean Optics
Laser Diode	450 nm – 2400 nm	NKT Photonics

The LED is a compact and inexpensive tool which can be used as a source of UV light. Though some researchers have already manufactured deep-UV LEDs of 232 nm wavelength, they are not commercially available (Hirayama, 2018). Ocean Optics currently has the shortest commercially available wavelength of 240 nm, as indicated above in Table 3.1. The absorption of SO₂ gas in the UV region is therefore too strong to detect, as it does not exceed 200 nm in wavelength. It is therefore not appropriate for use in this analysis. Nonetheless, LEDs are increasingly extended to become a viable option for future versions, because they are relatively inexpensive and compact, as research contributed to the range of the LED wavelength. (Taniyasu, Kasu and Makimoto, 2006).

Another kind of UV source is laser diode and is currently the cheapest and most effective. However, they are not also available in the needed UV range but the new hurdle has been solved recently. A 340 nm long laser diode was produced by Yamashita et al. (Yamashita *et al.*, 2013). To date, recent research has been conducted by Z to develop a laser diode with a shorter wavelength of 271 nm. (Z. Zhang *et al.*, 2019). Later, the use of comparative manufacturing strategies will make LED and laser diode with shorter wavelengths conceivable. As all currently available commercial LEDs and laser diodes emit wavelengths over 240 nm, deuterium light is the best light source choice in this study.

Currently, Ocean Optics Inc. is one of the largest producers of existing UV sources. (Ocean Optics, 2019). They provide a unit of light sources comprising of a deuterium and halogen lamp as described in Figure 3.2, called the DH2000-BAL. A combination of light sources produces continuous light between 190 nm and 2000 nm and is easy to connect to an optical fiber. The optical intensity of the light can be adjusted by putting a potentiometer on the back of each panel. DH2000-BAL information is provided in Appendix B.



Figure 3.2 DH2000-BAL Light Source

Ocean Optics also supplies the Xenon lamp branded as HPX2000 with UV-NIR. It is a strong source providing 35-watt xenonarc lamps of continuous spectrum from the UV to NIR (185-2200 nm). This region of the wavelength indicates that HPX2000 can also be better used in this analysis. Nonetheless, as shown in Figure 3.3, HPX2000 is less than DH2000-BAL in power. This was tested by Dooly et al (Dooly, Lewis and Fitzpatrick, 2007) experimentally.

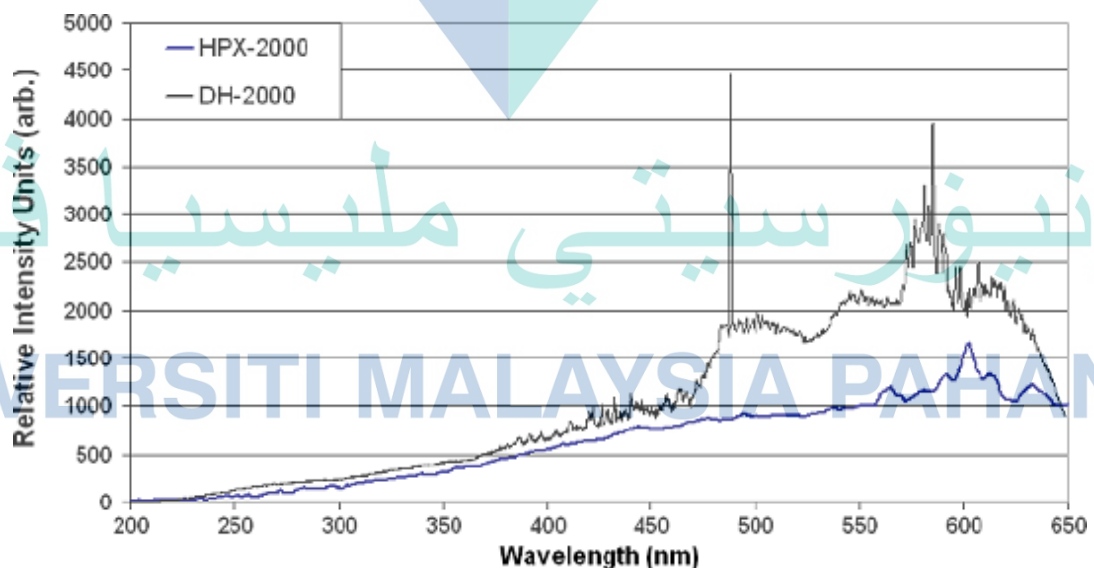


Figure 3.3 Comparison of Ultra Violet light source intensity performance
Source: Dooly, Lewis and Fitzpatrick, (2007)

3.2.2 Optical UV Detector

The human eye is an innate powerful optical detector. In some ways, the eye has been regarded as a detector device advanced, with characteristics comparable to the commercially available artificial detectors. The eye has a spectral response that extends from about 400 to 700 nm, the range known as the visible spectrum. (Orna, 2013). The retina is unable to detect light energy events at longer and shorter wavelengths. At this point, the artificial detector needed to overcome the human eye weakness to accurately measured the intensity of light. Most applications in photonics require detectors of optical rays. Applications include optical radar, laser power rates control for raw materials and laser metrology (Molebny *et al.*, 2016).

To date, various types of optical sensors covering the electromagnetic spectrum's UV, visible and infrared portions are available. The optical detector transforms the received optical signal into an electrical impulse that can be extended and processed as appropriate. (Dasan *et al.*, 2019). There are a few detectors accessible for detection of various sort of light, for example, photomultiplier tube (PMT), photoresistor, photodiode, photodiode array (PDA), charge-couple device (CCD) and spectrometer (Goushcha and Tabbert, 2007). For instance, PMT is a photoemissive device that suitable for light detection of poor signals that can operate at high speed and high sensitivity with high linearity. Their general principle of operation is to convert incident photons into electrons by means of a photocathode (Rouse, 2018). It has other advantages like fast response, high gain, high signal-to-noise ratio and is suitable for use in a large area for UV detection (Pendse and Chin, 2001). However, they also have a range of drawbacks, such as large sizes, high voltage, and are typically expensive compared to photodiodes. All these factors make photomultipliers less common in particular for use as field detectors (Tao, Chan and Van Der Graaf, 2016).

The other type of UV detection device is photoresistor. It is less expensive than photodiodes however has a couple of disadvantages, for example, slow response time and strongly nonlinear response (Mörmann *et al.*, 2003). The scope of detection is also limited to close to UV (320-400 nm) (De Sanctis *et al.*, 2018). However, little research has been found on these photoresistors since they are rarely used in such a way that they are less

ideal than a UV detector decision in contrast with photodiodes. Photodiode generally made from single crystal silicon wafers, but the material used depends distinctly on the photodiode detection range. (Iftiqar *et al.*, 2012). It is economical, robust, compact in size and creates low noise relative to other detectors. (Oliveira, Khoury and Santos, 2016). In any case, this photodiode has poor temperature stability and effectively harmed by light of excessive intensity.

PDA or photodiode array is a linear array on a discrete and built-in circuit chip of photodiodes. PDA usually provides a one-dimensional photodiode arrangement providing one-dimensional spatial intensity information (Martono, Febriani and Rohman, 2018). The spectral distribution depends on its size of physical array. PDA has faster spectral acquisition, higher NIR sensitivity and higher SNR relative to photomultiplier tube (PMT) (Kenneth Hopkins *et al.*, 2018). On the other hand, PDA is better suited for applications where the photon saturation charge is relatively high, which makes the detection range of PDA larger than CCD. (Eshaghi, 2011). In addition, PDA produces less noise than CCD, which recommends PDA for applications where higher output precision is required. (Eshaghi, 2011). The advantage of a PDA-detector spectrometer is that it is typically cheaper than the CCD spectrometer. Nonetheless, PDA have certain drawbacks, such as small pixels and no UV response (Kenneth Hopkins *et al.*, 2018).

Other than PDA, charge-coupled device or CCD have been the most widely recognized visible and near UV sensors in cosmology since the 1970s (Amelio, Tompsett and Smith, 1970). CCD is a detector that provides two-axis intensity information with a two-dimensional set of photodiodes (Fossum and Hondongwa, 2014). The benefit of the two-dimensional system is the ability to concurrently acquire many spectras side-by-side, which is ideal for multiple optical inputs (Fossum and Hondongwa, 2014). A reference signal can therefore be recorded during a simultaneous measurement to monitor various changes such as lamp fluctuations. Charge packets can also be controlled near a semiconductor insulator interface to transfer them through closely differentiated metaloxide-semiconductor (MOS) capacitors. (Coburn, Fan and Forrest, 2019).

CCD has a lower capacity, which is one pixel whereas the PDA read-up line represents hundreds of pixels (Lesser, 2015). As a result, the read-out noise of a standard

PDA is approximately two orders greater than a CCD detector. To date, CCDs were applied effectively to high-sensitivity optical imagery and have been valued for their superb signal to noise ratio, high quantum efficiency, linearity and speed (Tiffenberg *et al.*, 2017). Compared to PDA, the CCD has no read-out line, and the design is simpler because electronic switches are not necessary and driving circuits are not needed (Lesser, 2014). However, CCD requires a smaller electrical charge than PDA and also more power for conversion, making it useful for low light detection such as Raman and Luminescence (Stotts, 2019). The disadvantage of the CCD detector is that it is relatively high in comparison with PDA.

3.2.3 Spectrometer

A spectrometer is a spectroscopy which can calculate the light intensity of specific wavelengths by installing a meter (Hopkins, 2014). Therefore, a numerical measurement of the light emitted or absorbed at a certain wavelength is to be provided. It was designed to modify the wavelength and the quantity of rays absorbed or transmitted by the sample for each wavelength. (Beasley and Panayiotou, 2019). Thus it is possible to understand which wavelengths of radiation are available and in what relative concentrations. Recent developments in the innovation of miniature spectrometers and increased UV response from improved optical components allowed the use of such devices as feasible UV-detectors (Lesser, 2015).

In this study, a CCD spectrometer is chosen as a detector because, as discussed above in section 3.2.2, it provides most advantages. Maya 2000Pro from Ocean Optics was the spectrometer used in the project and the exoskeleton of a miniature spectrometer includes many parts, as shown in Figure 3.4 below (Ocean Optics, 2019). This device employs Hamamatsu S10420 FFT-CCD, which can provide a spectral resolution of up to 0.035 nm (FWHM). Anyways, as described by Dooly *et al.*, the minimum spectrometer resolution obtained in this analysis was just 0.23 nm due to the low-end grating used (Dooly *et al.*, 2011). The specifications of Maya 2000Pro are set out in Appendix C..

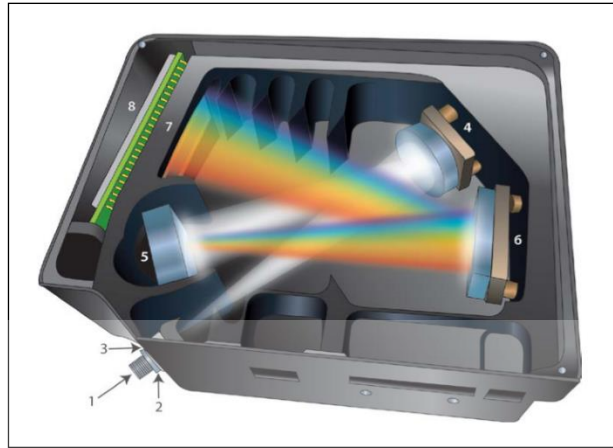


Figure 3.4 Internal structure of the miniature spectrometer

Source: Ocean Optics, (2019)

As in Figure 3.4, light passes the spectrometer through the input slit and travels over several areas: an objective lens, a grating, and an output slit. This set of components acts as a monochromator, the system that only selects one light of all the wavelengths/colors available at the source (actually a narrow band). A single wavelength is chosen by changing the angle of the grating by using the wavelength function. It happens as different light wavelengths mirror the grating at multiple angles. The end result is that the white light is split into a "rainbow," equivalent to the illumination reflected through a glass prism. The wavelength chosen is in the middle of the narrow band of the slit wavelengths. The light hits a detector which produces a voltage commensurate with the intensity of the light. This voltage is then used to guide a read-out device designed to provide data in a practical way, such as intensity

Photodiode Arrays (PDAs), Charge-Coupled Devices (CCDs) or Indium Gallium Arsenide (InGaAs) can be chosen as a detector, depends on the type of spectrometer. A linear CCD array spectrometer was used in this device. Although PDA and CCD are close in spectral range (200-1200 nm), there are several variations between them, as described in segment 3.2.2 above. In contrast to InGaAs, it's being used with a wider spectral range (800-2600 nm) (Kreutz *et al.*, 2001). The mounted CCD spectrometer is therefore ideal for devices where the intensity of the light source is not linear (Fossum and Hondongwa, 2014). Another justification for using a CCD spectrometer is that it is more sensitive to UV relative to a PDA spectrometer (Lesser, 2015).

3.2.3.1 Spectrasuite

Five main segments of SpectraSuite are the Top Menu, the Toolbar, the Data Source, the Data View and the Result Display as shown in Figure 3.5. The spectrometer linked to acquisition list and some other properties like serial number, total pixels and spectral bandwidth are displayed in the data source section. The data view segment reveals essential active graph details and associated database creation results. The final segment is the result display which displays five different display forms, but only three shown in the graph, strip chart and time table are used. The graph shows the width of the whole spectrum continuum, and the intensity counts of the wavelength are shown on the top of the strip chart. It can also show an average wavelength of several specified wavelengths, and display them within the same strip-chart which can be seen in Figure 3.5. The intensities of a single wavelength are a blackline in Figure 3.5; the smoother green line represents the average intensities of three adjacent wavelengths.

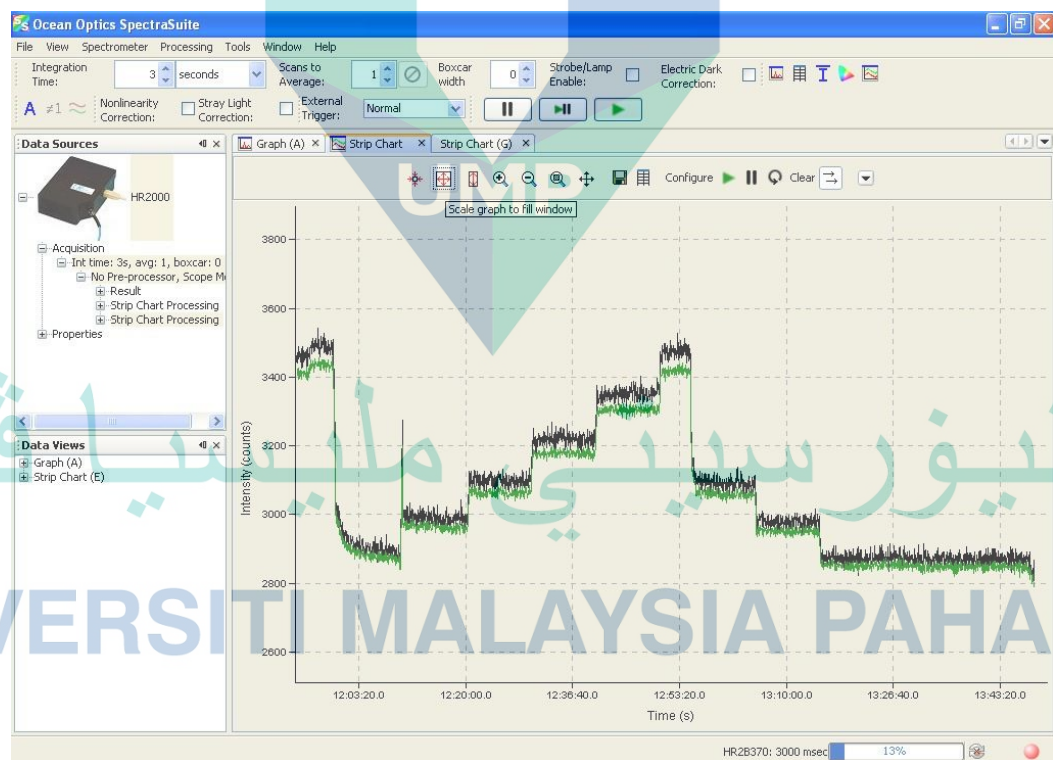


Figure 3.5 Interface of SpectraSuite

3.2.4 Gas Cell

A test gas cell was designed to determine the absorption line of SO_2 . After the sizes and shapes of test gas cells in Chapter 2, a hollow cylinder was adopted as the experimental gas cell, and this preference was based on several criteria. Next, it is easier to obtain a certain length desired for the gas cell by cutting the cylinders into sizes. Several pieces of lengths are listed in this section for comparison, even though Ouyang et al and Inagaki et al have already stated that the longer the length, the better the sensitivity for the optimum sensitivity (Ouyang and Jones, 2012; Inagaki, Watanabe and Tsuchikawa, 2017).

Secondly, it is relatively easy to make the screw string required to install UV collimating lenses on a freshly cuts ring. Even though a longer gas cell could be more resilient, it is crucial to choose the optimal length to achieve the best performance. This is because the increased length of the path reduces the detector's detected optical radiation (Kaspers, Sterenborg and Amelink, 2008; Wei *et al.*, 2018). Therefore, the optical path length of the sensor should be calculated by agreement between the transmission loss and the acquired sensitivity of each centimeter (cm) in the direction of the optical path. In addition, it also can be assumed that if the path length is too short, the sensor will face a lot of noise during the experiment.



Figure 3.6 Different Length of Gas Cells

Dooly et al found that three experimental gas cells without absorbing gas with different lengths specific Signal to Noise Ratio (SNR) (Dooly, Lewis and Fitzpatrick, 2007). Dooly et al also revealed that the finest SNR in the three gas cells examined was 60 cm long (Dooly, Lewis and Fitzpatrick, 2007). Therefore, a longer gas cell is assumed to have a higher response. In this analysis, the length of five cells as shown in Figure 3.6

and Table 3.3 has been selected in order to analyze the best-sensitive cell duration in the analysis of the absorption line SO_2 . The aim is to create a compact, durable and low-cost system. Stainless steel has been used as a hollow rod material because it is quite easy to use and extremely sturdy as it is not bendable. While plastic is lighter, the key material was not chosen for testing a corrosive product, such as SO_2 , as mentioned in Chapter 1. In fact, when exposed to UV radiation, plastic can degrade (Yousif and Haddad, 2013).

Table 3.3 Cylinder gas cells length

Cell Cylinder	Length (cm)
1	10
2	20
3	50
4	70
5	100

The stainless steel absorption cell has a hollow center diameter of 7 mm and a wall thickness of 1 mm. To suit the collimating lenses in the wrist, the input and the outlet rods were threaded on each end of the cell whereas two 1 mm diameter holes were tapped onto the top end of the cell. Eventually, the inner part of the cell was dipped in black lacquer paint to prevent any inward reflection from the cell walls which could create a complex and volatile duration of the path i.e. excessive noise on the transmitted signal.

3.2.5 UVNS Optical Fibre

Before selecting the optimum optical fiber, two main suppliers, CeramOptec and Ocean Optics, a comparison was carried out to evaluate the transmission properties of their optical UVNS fiber. Based on Dooly's study (Dooly, Lewis and Fitzpatrick, 2007), it reveals that CeramOptec's UVNS optical fiber has a great transmission of deep UV wavelength in the lower region as shown in Figure 3.7 below. In comparison, CeramOptec fibers have a lower attenuation which, based on the attenuation properties as shown in Appendix D is less than 1 dB/m in the area, as small as 160 nm. The UVNS fiber from CeramOptec was therefore selected for this study.

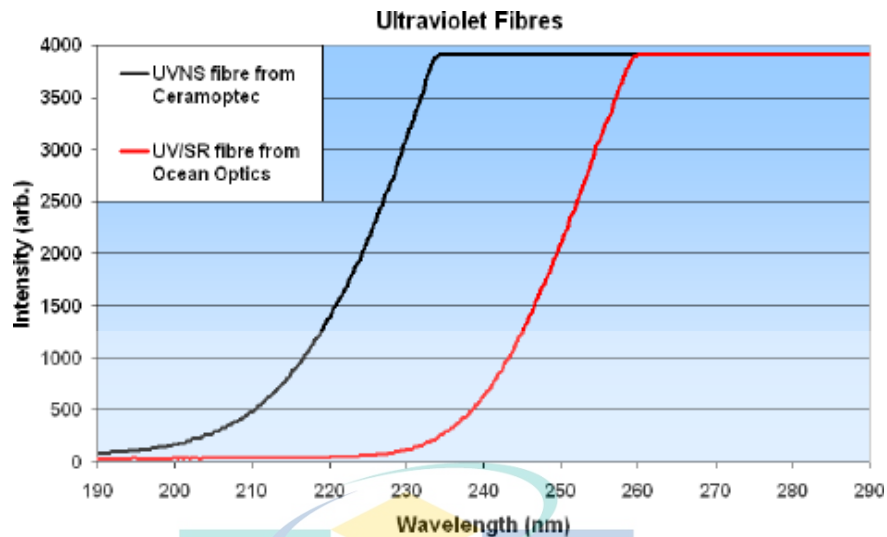


Figure 3.7 Transmission properties comparison between two UVNS fibres
 Source: Dooly, Lewis and Fitzpatrick, (2007)

CeramOptec claimed that the UVNS fiber will continue to operate for a long time for up to 40,000 hours, retaining the transmission rate at wavelengths around 160 and 1200 nm at 95% of initial output. In the experimental setup, the length of the UVNS fiber used is 1 m and the core diameter is 644.4 μm . It will emit light at wavelengths between 193 and 400 nm without major degradation in its transmitting characteristics such as solar attenuation. Figure 3.8 below displays the CeramOptec UVNS fiber coupled with the SMA connector.



Figure 3.8 UVNS Optical Fiber Cable

3.2.6 UV Lens

The definition of an UV lens is a lens for use of less than 380 nm wavelength. These are normally made of calcium fluoride (Maushake, 2008), quartz, lithium fluoride (Dauer, 2000) or another UV element since regular silica glass becomes invisible in this region (Kitamura, Pilon and Jonasz, 2007; Fischer, Tadic-Galeb and Yoder, 2008). A common material used in UV lenses is quartz fluoride (Thoeniss and Mewes, 2014).

In this experiment, a series of UV-collimating bi-convex lenses was used to handle UV fiber radiation to return fiber through the testing gas. Dynasil Corporation manufactures quartz lenses with a transmission range ranging from 200 nm to 2000 nm. The lenses are manufactured synthetically using a silicon halide vapour phase hydrolysis. They develop high-end, high-purity, non-crystalline lenses which are one of the transparent ones for UV radiation. Each lens is 10 mm long in focal length and 5 mm in diameter. The lenses could be incorporated into the sensing system in this investigation in order to boost the transmission and optimize the signal-to-noise ratio for the system. To order to acquire accurate data, the light propagating through the test gas cell needs to be properly collimated. This can be achieved by adjusting the collimating lens's focal point. If this is not implemented correctly, every photon propagating via a gas cell could endure a major number of incidents, which could lead to significant transmission losses and uncertainty over the long distance.

As shown in Figure 3.9, the lens was mounted in the gas cell of stainless steel through a black oxide finish of the screw thread called a barrel. Using the grub screw, the lens will slide through the barrel and tighten. For a robust connection to the gas cell, the barrel is threaded. The requirements for adjusting the collimating lens for optimum light propagation are clarified in Appendix E.

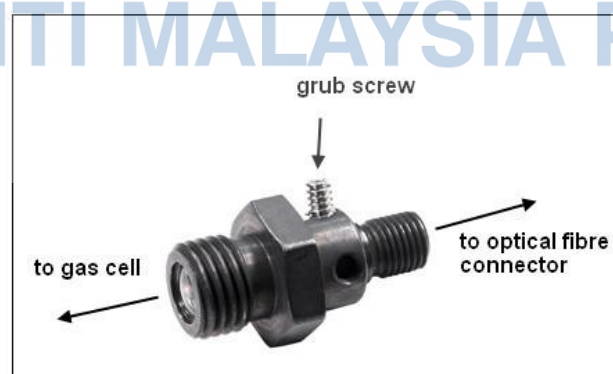


Figure 3.9 UV Lens Holder

3.3 Generic Design of Experimental Setup

In order to detect SO_2 , the OFS is characterized by light source, modulation method and type of detector. Wide transmitting ability of an optical fiber and its other benefits, including the propagation of trillions per second when the signals are multiplexed with a wavelength suit and an open path absorption sensor. Open path technique is developed to analyze the spectral SO_2 absorption lines and to determine cross-sensitivity with some other environmental gasses such as CO_2 and O_2 . This method is commonly used because it permits the detector to sensor a significant proportion of light associated with the test material, and it can track multiple gas compounds concurrently in a mixture in real-time.

The main function includes the transmission of light signals through the fiber from the optical sources and then modulation in the modulation field, before the detector is sensed. Geometrically, this is an extrinsic sensor that represents the light pulse, but the contact between the light and the measuring devices takes place outside of the fiber. The OFS is also known as the quasi-distributed sensor (multi-point or multi-plexed) because of its convergence and length averaging. A proposed generic design of an open path optical based fiber sensor for SO_2 detection as shown in Figure 3.10.

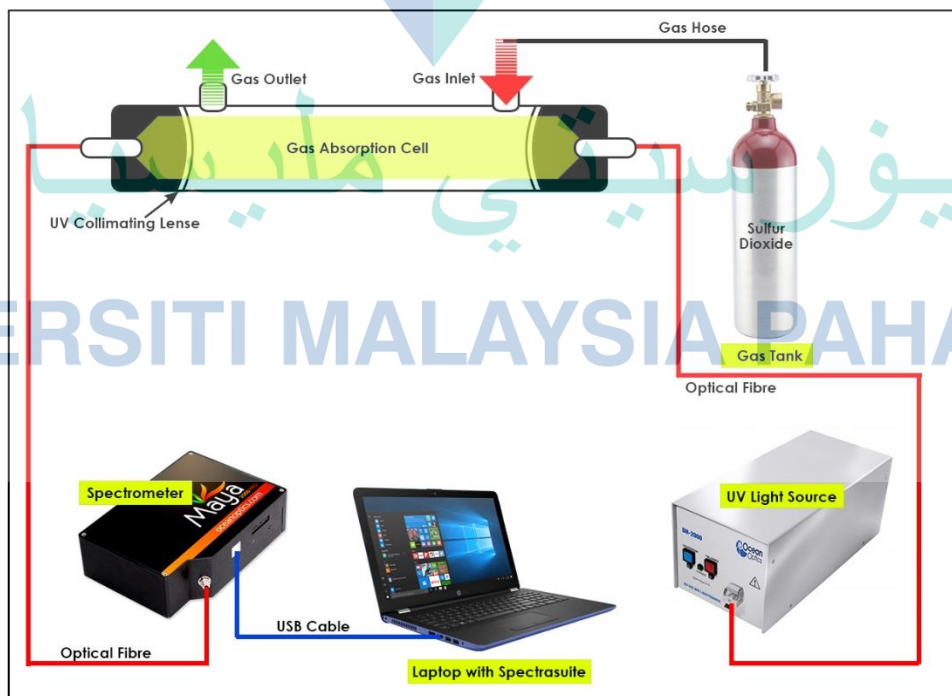
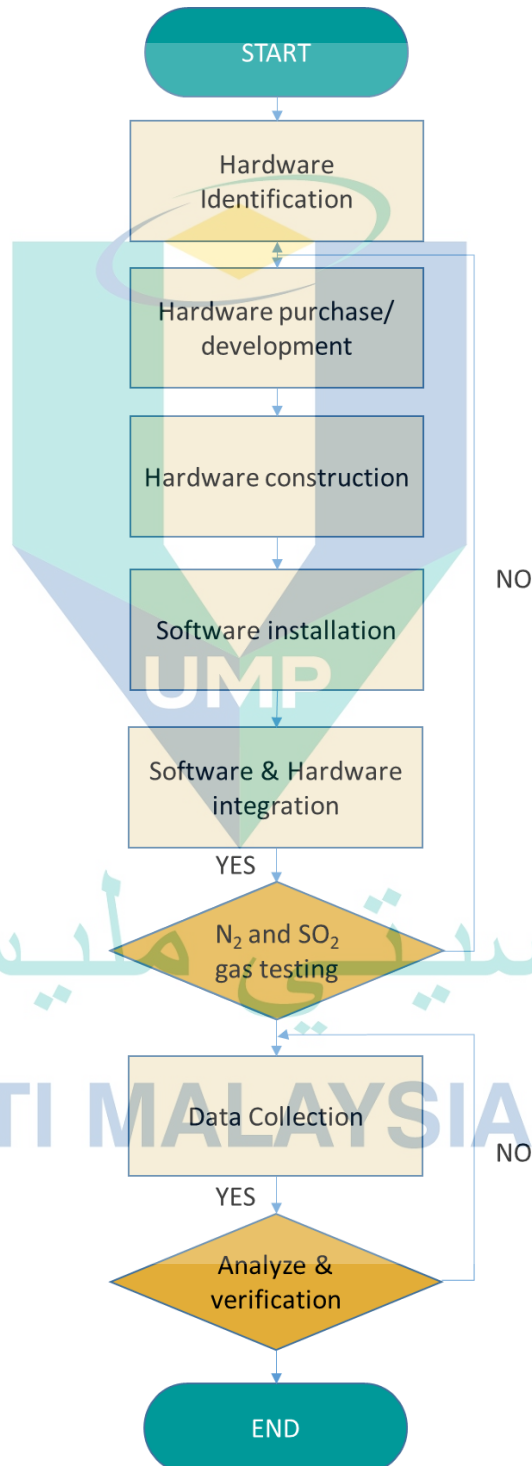


Figure 3.10 Generic Design of Experimental Setup to measure UV absorption of SO_2

3.4 Flowchart of Optical Fiber Sensor Development

All the methods that had been discussed are summarized into the following flow chart. The flowchart is a visual representation of the sequence of steps to depict a process of the UV SO₂ sensor using open-path optical fiber development.



3.5 Data Collection Process

SO₂ gas is toxic and can present a health risk to humans, as discussed in the Chapter 1. All safety measures also had to be applied equally. The first experiment was conducted in the Chemistry Laboratory at the University of Malaysia Pahang, with a fume hood and air mining system for SO₂ discharge during the trial. Certain safety equipment, such as emergency rinse shower and fire extinguishers, is also issued for the laboratory. Additional measures involved completing a brief protection training course prior to FTek installs. During the trial, a field hat, a half face mask and protective goggles had to be carried at all times.

3.5.1 Calculation of Beer-Lambert Law

The experimental calculation of the absorption cross section of SO₂ in this experiment as reported in Section 2.3 is based on the Beer Lambert Law. Equation 3.1 is a variant of the Beer Lambert Law extracted here and expressed as follows:

$$\sigma = \frac{-[ln\frac{I}{I_0}][T \times 22.4]}{ppm \times N_A \times l \times 273 \times P \times 10^{-9}} \quad (3.1)$$

The absorption cross-section, σ , based on equation (3.1) was determined if the concentration of SO₂ (ppm), gas temperature (T) and gas cell pressure (P) are specified. If it is known that the gas temperature is 20° C and the pressure is 1 atm, the equation (3.1) can be simplified.

$$\sigma = \frac{-[ln\frac{I}{I_0}][24.04]}{ppm \times N_A \times l \times 10^{-9}} \quad (3.2)$$

There were two variables to calculate in order to use equation (3.2), I_0 and I , describing the incident intensity and the transmitted intensity. I_0 is the intensity measured when the gas cell is empty or without SO₂. In this scenario, N₂ was employed to clear the gas cell prior to determining the I_0 . However, the intensity measured by releasing SO₂ into the gas cell represented by transmitted intensity, I . Once these two values are determined, the absorption cross section, σ , was calculated for SO₂ gas. After these two values were measured, an absorption cross section, σ , for SO₂ gas was calculated. The measured absorption cross-section of the SO₂ gas is shown in the 200-235 nm

wavelength and is contrasted to the Olive's combined data in Figure 3.11 below (Olive, 2007).

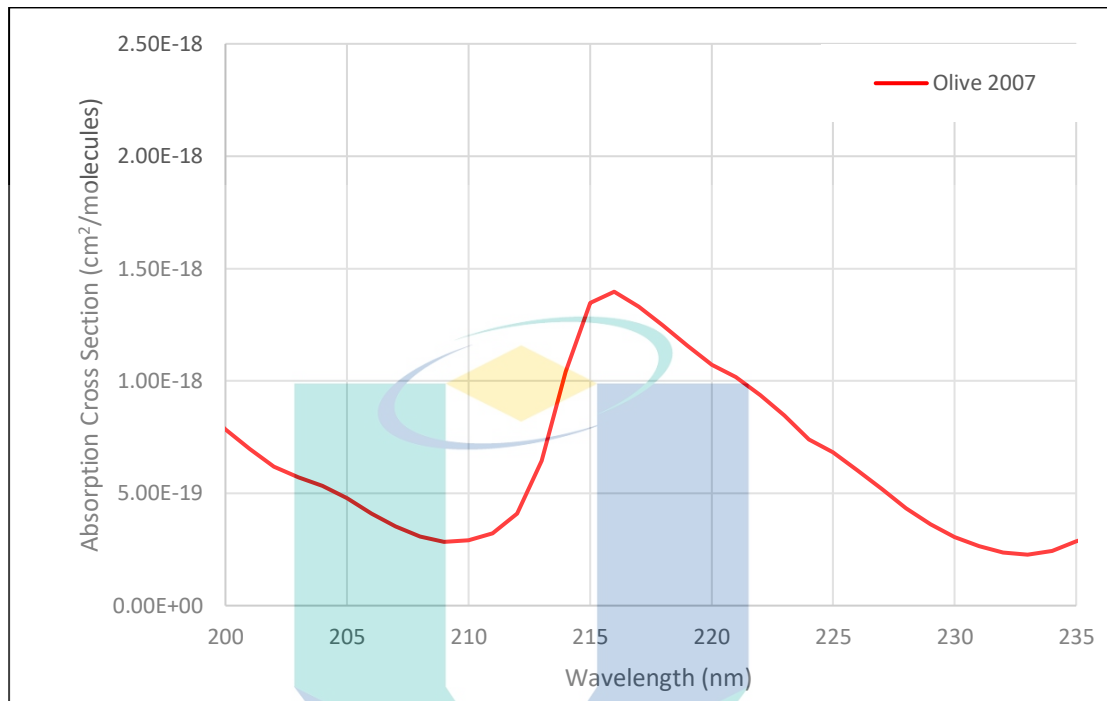


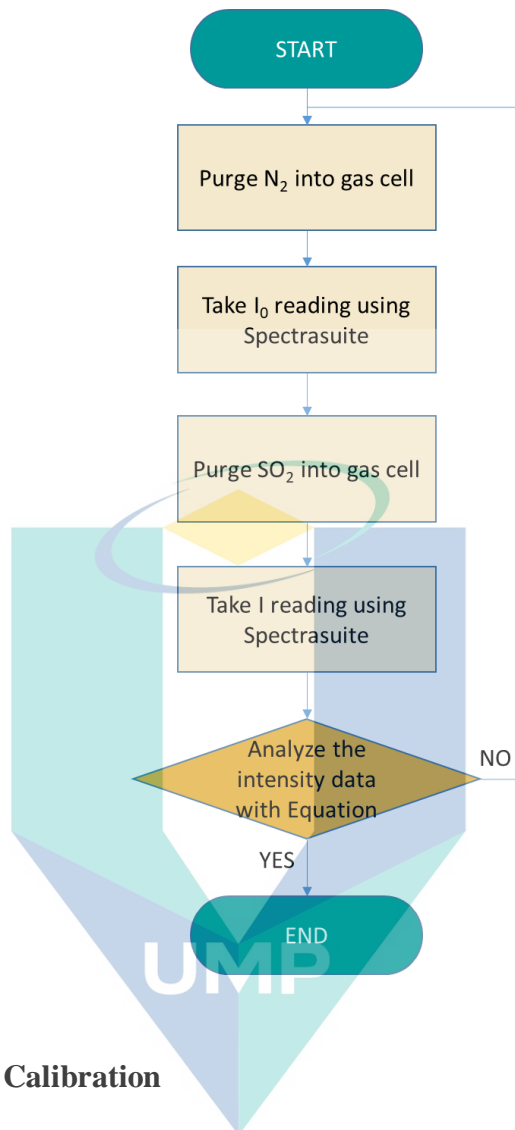
Figure 3.11 Theoretical SO₂ absorption lines

Source: Olive, (2007)

Figure 3.11 provided above shows the theoretical SO₂ absorption spectra from 200 - 235 nm with temperature of 298 K using spectral resolution of 0.08 nm (Olive, 2007). These theoretical spectra has been selected to be compared with experimental result because it falls in the same UV region. In fact, the temperature is similar to 295 K and the temperature did not influence the absorption values as reported by Bogumil et al. (Bogumil *et al.*, 2003).

3.5.2 Flowchart of Experimental Process

All the experimental process that had been discussed are summarized into the following flow chart. The flowchart shown below is a visual representation of the sequence of steps to depict a process of the SO₂ data collection process. The process been repeated three times in order to get the right data. By using the same process, the cross sensitivity testing also has been determined by adding CO₂ and O₂ gas.



3.6 Spectrometer Calibration

Instrument calibration is a must to determine a correct measurement. In this experimental setup, only Maya2000Pro spectrometer provided by Ocean optics needs to be calibrated. Even though it has been carried out before by senior researchers, it might have potential to drift slightly from the correct reading. Ocean Optics suggested that the spectrometer be calibrated once in a while because the wavelengths could be marginally moving over time due to environmental factors, including temperature and force (Ocean Optics, 2019). Ocean Optics provides its spectrometer calibration service and makes the self-calibration simultaneously, and the process is well illustrated in Appendix F. For Maya2000Pro spectrometer calibration, Ocean optics recommends a Mercury lamp, HG-1 is used as a light source. Therefore it is used in this calibration and the picture is shown in Figure 3.12.

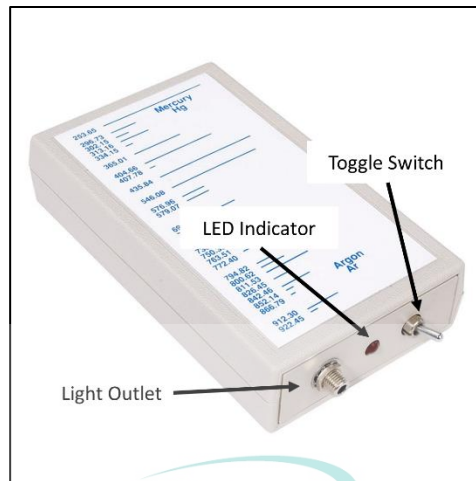


Figure 3.12 HG-1 Mercury Lamp

The Mercury lamp, HG-1 is connected to the Maya2000Pro spectrometer using a UVNS optical fiber cable. Then the spectrometer is interfaced with a laptop with a Spectrasuite software installed. Figure 3.13 below illustrated the experimental setup for spectrometer calibration. The calibration approach in Appendix F requires a database such as Microsoft Excel to run a linear regression to obtain the calibration result. The value for R squared should be very close to 1 (0.95-1.00). If the value obtained is outside this range, it might be due to one of the wavelengths is incorrectly assigned.

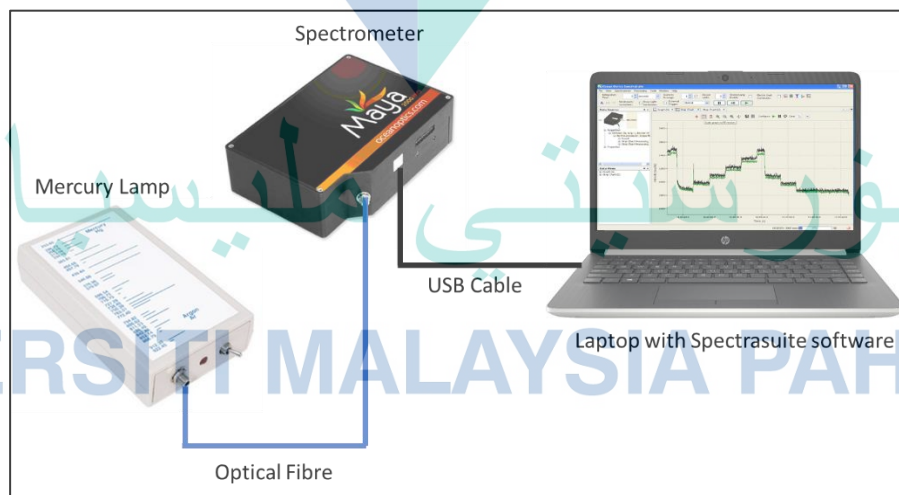
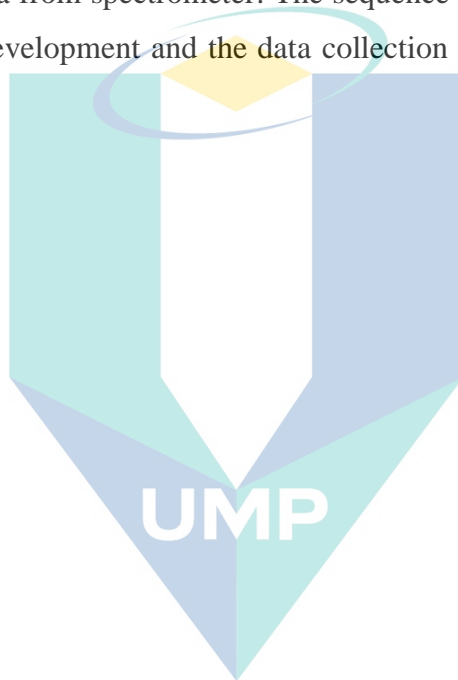


Figure 3.13 Calibration Experimental Setup

3.7 Summary

This chapter discussed about the methodology that is used in this research study. The process of hardware or equipment in developing the sensor has been discussed. Each equipment has been selected due to the advantage offered by the tools and concerning the developed sensor condition. The generic design of the experimental setup which is believe can be use to detect the SO₂ after the literature study has been proposed. Spectrasuite are used as the intensity detector software. Laptop installed with Spectrasuite is used to read the data from spectrometer. The sequence of steps to depict a process of the UV SO₂ sensor development and the data collection process has been show in the flowchart given.



اونيورسيتي ملايسيا قهغ

UNIVERSITI MALAYSIA PAHANG

CHAPTER 4

RESULTS AND DISCUSSION

4.1 Introduction

In the previous chapter, sufficient components for an optical fiber sensor for measuring SO₂ gas concentrations in the UV region were established. This chapter examines the testing and the development of this setup into an operating gas sensor. To create an appropriate and accurate sensor it must undergo tests based on different parameters such as accuracy, validation and other specifications depending on the sensing systems measurement and setting.

The sensor must, first of all, solve the issues of cross-sensitivity with other gases. The detection of all current gases is neither practicable nor appropriate, therefore a cross-sensitivity check is conducted for gasses known to exist in the sensing environment either CO₂ or O₂. Furthermore, the sensor must show a precise result in detecting the same concentration level of SO₂ after the experiment to validate the sensor error. This optical fiber sensor has been designed to precisely detect and quantify the concentration of SO₂ which can be used to efficiently track emissions of SO₂. Tests are performed under each of the conditions listed above to assess the suitability of this sensor.

4.2 Results of Spectrometer Calibration

The screenshot shows the following data:

Regression Statistics	
Multiple R	0.999999995
R Square	0.999999991
Adjusted R Square	0.999999999
Standard Error	0.019151548
Observations	34

ANOVA					
	df	SS	MS	F	Significance F
Regression	3	1176364.537	392121.5123	1069086652	1.6441E-120
Residual	30	0.011003454	0.000366782		
Total	33	1176364.548			

	Coefficients	Standard Error	t Stat	P-value	Lower 95%	Upper 95%	Lower 95.0%	Upper 95.0%
Intercept	200.5622429	0.021892472	9161.242393	2.87043E-98	200.5175325	200.6069533	200.5175325	200.6069533
X Variable 1	0.472182549	0.000104647	4512.137234	4.84286E-89	0.471968831	0.472396268	0.471968831	0.472396268
X Variable 2	-1.34103E-05	1.42146E-07	94.34195652	1.13292E-38	-1.37006E-05	-1.312E-05	-1.37006E-05	-1.312E-05
X Variable 3	-1.32044E-10	5.70179E-11	2.315840231	0.027586166	-2.4849E-10	-1.55982E-11	-2.4849E-10	-1.55982E-11

Figure 4.1 Calibration coefficients data for spectrometer

Experimental setup for spectrometer calibration has been discussed in the previous chapter and the calibration method is well explained in Appendix F. As stated in the calibration method, to obtain the regression data, an Analysis Toolpak in Microsoft Excel can be used and the calibration result is shown in Figure 4.1 above. The spectrometer wavelength is incorrectly assigned if the value of R squared is not closely in the range of 0.95 to 1. After the experiment is that, the linear regression reveals that the R squared value is below 1 which is 0.999999991 and that the correct configuration of Maya 2000Pro was preserved throughout this experiment.

4.2.1 Experimental Setup

A pictorial illustration of the laboratory set-up is shown in Figure 4.2 below for measuring SO₂. The main objective of this experiment was to check the identification of SO₂ gas provided by the sensor design and the system. Second, the SO₂ absorption spectrum was contrasted with the theoretical data from the UV region, since a particular pattern of absorption is known to exist, as described in Chapter 3. When the SO₂ absorption spectrum has the same unique pattern than the theoretical results, then SO₂ can be detected by the newly developed sensor. The process of the data collection has been explained well in the section 3.5.2.

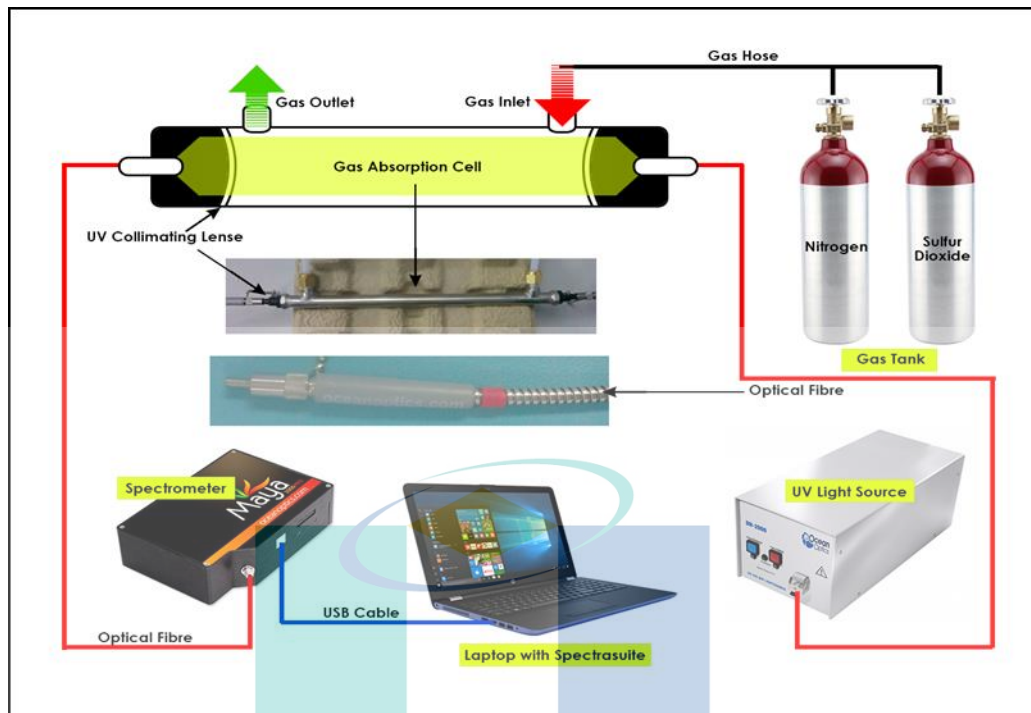


Figure 4.2 Pictorial diagram of experimental setup

All sensor components are listed in Figure 4.2, and Chapter 3 describes their specifications. The gas cylinder contains N_2 comprising 100 ppm of SO_2 . The second gas flask provides pure N_2 used to purge the gas cell until I_0 reading has been made. All SO_2 and N_2 were combined with a gas regulator to the absorption gas cell. Throughout this study, the software of SpectraSuite described in Section 3.2.3.1 has been used to capture optical signal intensity using a Ocean Optics spectrometer called MAYA HR2000Pro. The integration time was set to 3s to enable the establishment of an acceptable signal to noise ratio. The intensity of the optical signal was used with the Microsoft Excel program to produce the SO_2 absorption cross section.

4.3 Spectral Line Results and Discussions

As reported in Chapter 3, this experiment will consist of five different cell length as one of this experiment focus is to find the best cell length to be used and the best wavelength for an optimum absorption to be setup as SO_2 sensor in the future. In this test, the SO_2 absorption cross-section was analyzed and contrasted to the theoretical values of Olive (Olive, 2007) as described in section 2.2.2.

4.3.1 Result of 10 cm Cell Length

Figure 4.3 below displays the experimental spectral line on using 10 cm cell length as the light absorption chamber. The spectral line of absorption cross section in 10 cm cell length is represent by light blue colour and theoretical spectra line represent by red colour.

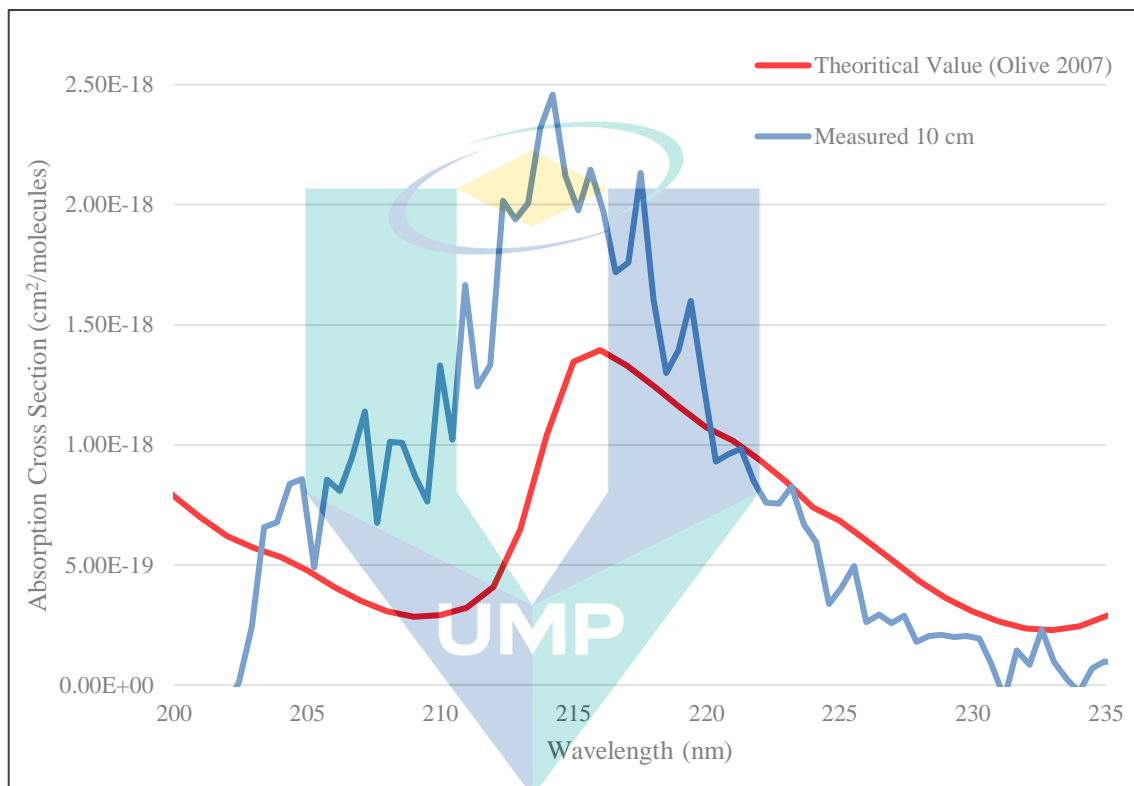


Figure 4.3 Spectral line of 10 cm cell length

It have the highest peak centered at 214.23 nm and absorption cross section of $2.46\text{E-}18 \text{ cm}^2/\text{molecules}$. The results of this experiment in Figure 4.3 clearly show there is unclear pattern between theoretical and measured spectra because of lots of fluctuation occurred. However, closer observation on the pattern shape of the measured spectra, starting from 210 nm to 230 nm, it shows the pattern shape of measured spectra have almost close to the pattern shape with theoretical spectra. Due to early calibration of spectrometer, it was assumed the spectrometer has already given a correct wavelength reading as stated in previous discussion. Therefore, it can be assumed that this sensor can detect the SO_2 gas in 10 cm cell, but still unstable.

Closer inspection of the Figure 4.3, it is also clearly show there are many fluctuations within measured spectra compared to theoretical spectra line occur through the wavelength region starting from 203 nm to 235 nm. The factor of the numerous value of fluctuation occur due to vibration and movement of cell length or fiber optic cable during the experiment. A further explanation on this due to short absorption cell length giving short space for the light and gas to interact each other as explained in section 2.2.2 and cause random noise.

4.3.2 Result of 25 cm Cell Length

Figure 4.4 below presents the measured spectral line obtained by using 25 cm cell length as the absorption cell. The spectral line of absorption cross section in 25 cm cell length is represent by black colour and theoretical spectra line represent by red colour.

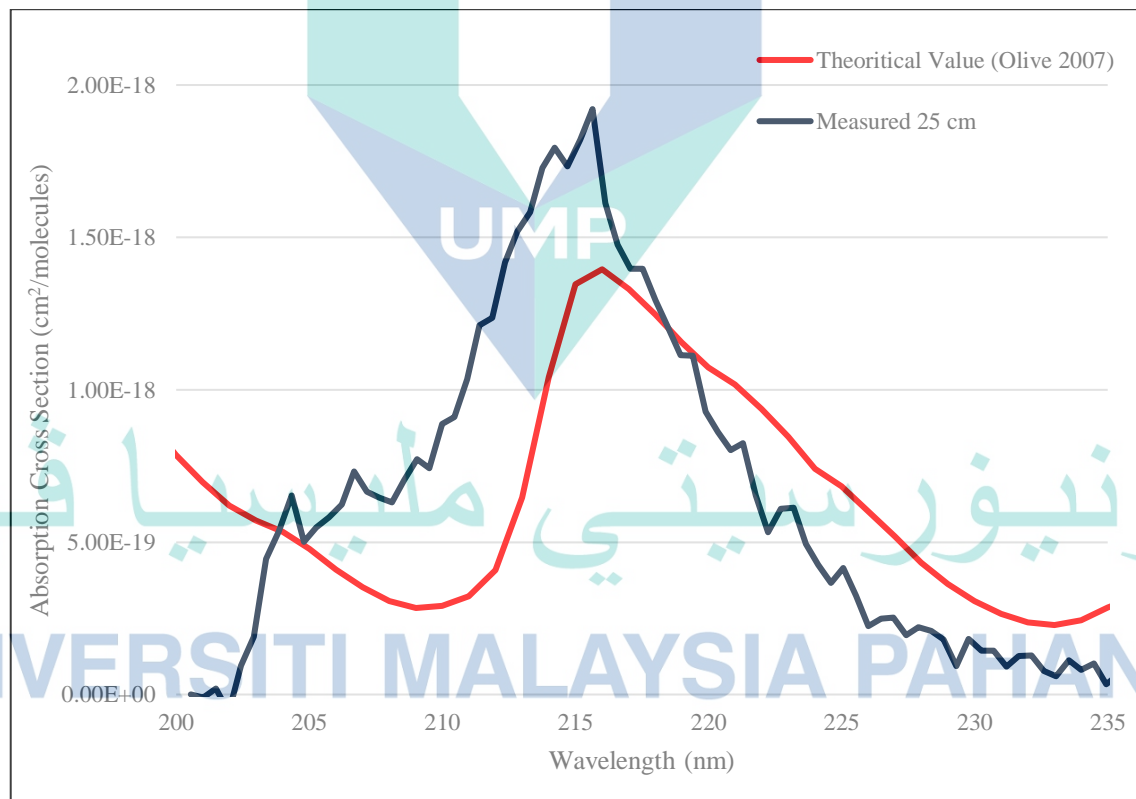


Figure 4.4 Spectral line of 25 cm cell length

As can be seen from Figure 4.4 above, it has many fluctuations as well as Figure 4.4 before, but less aggressive. The highest peak for the measured SO₂ gas centered at 215.65 nm with absorption cross section of 1.92E-18 cm²/molecules. Compared to Figure

4.3, the measured pattern present in Figure 4.4 displays less fluctuation, hence its pattern shape look almost same to the theoretical spectra pattern. From Figure 4.4, it can be assume it have less vibration and movement of the optical fiber or gas cell during the experiment. Another possible explanation is the SO₂ gas start to interact with the light and have almost enough space to absorb the light but still have random noise. In addition, it was assumed the ‘V’ curve occurs as a result of noise in term of other light penetrate the cell when running the experiment.

4.3.3 Result of 50 cm Cell Length

Figure 4.5 below compares the measured spectral line obtained by using 50 cm cell length as the absorption cell with theoretical spectra line represent by green and red colour respectively.

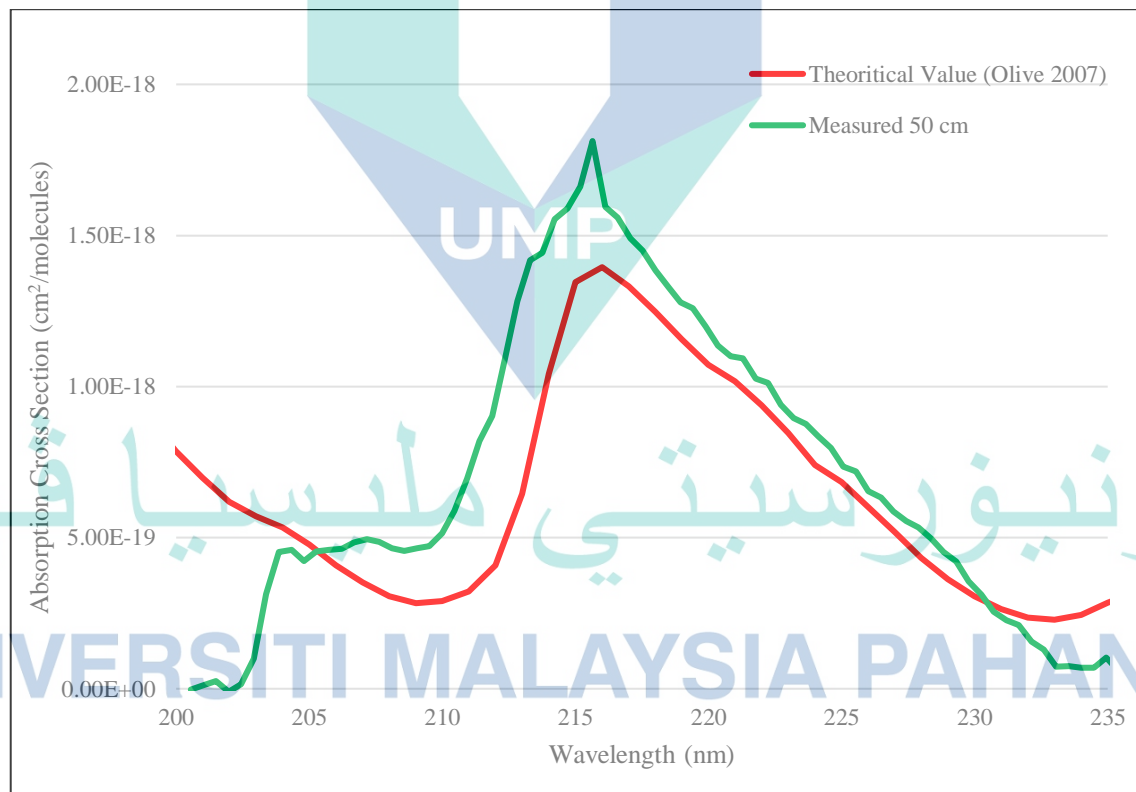


Figure 4.5 Spectral line of 50 cm cell length

What stands out in this Figure 4.5 is the pattern of the green measured line looks identical to theoretical spectra line. Interestingly, starting from 207 nm, the value climbs up smoothly until it reach its peak, centered in the wavelength region at 215.65 nm and

have the highest absorption cross section at $1.81\text{E-}18\text{ cm}^2/\text{molecules}$. The reason it have rarely fluctuation because of stability setup results in minimum vibration and movement of cell length or fiber optic cable during the experiment. Another possible explanation, is because that the gas have enough space to absorb or interact with light hence it give the nice result. However, the internal reflexion from cell walls, which may contribute to a variable and uncertain gap i.e. external noise on the obtained signal was removed well by dip-coated in a black lacquer paint inside the cell.

4.3.4 Result of 75 cm Cell Length

The graph in Figure 4.6 below show the 75 cm cell length of measured spectra line. It is represent by purple spectra line and the theoretical spectra line is represent by red colour.

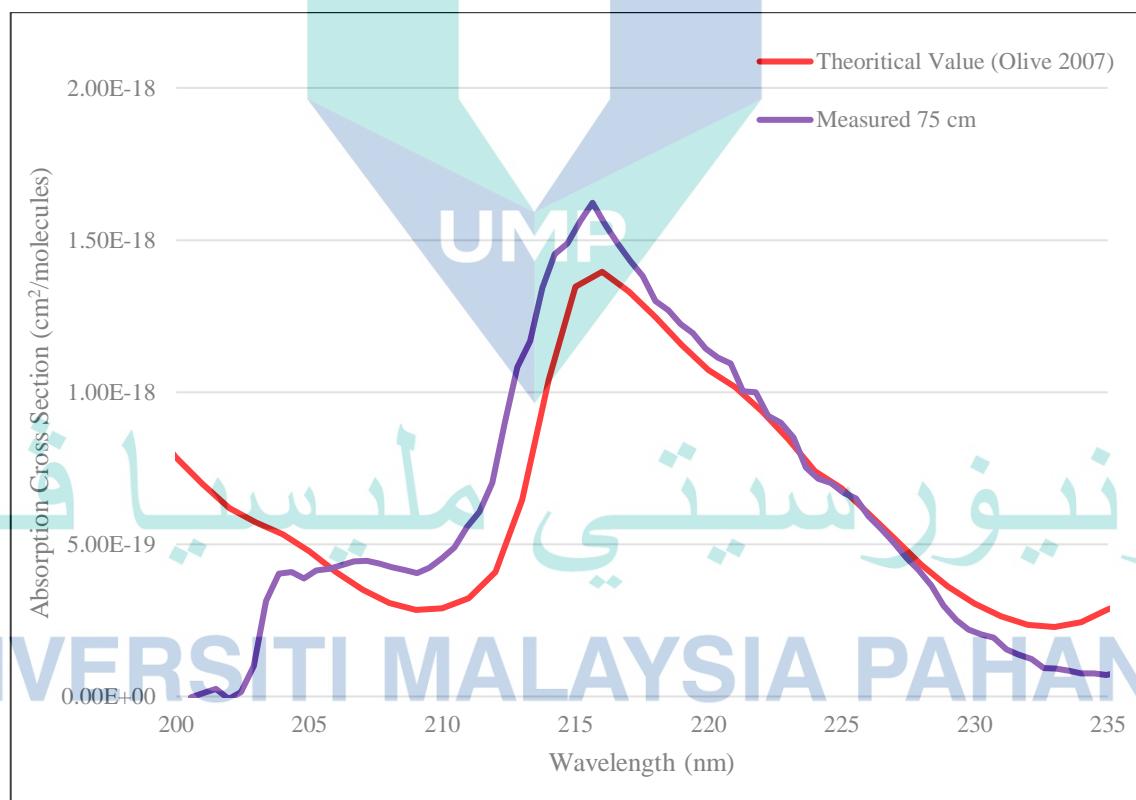


Figure 4.6 Spectral line of 75 cm cell length

As can be seen from the Figure 4.6 above, it is apparent that the longer the length of the path the better the sensitivity as mentioned by Inagaki et al. (Inagaki, Watanabe and Tsuchikawa, 2017). The measured spectra line of 75 cm has shown a result that more

close to theoretical spectra line compared to measured spectra in Figure 4.5. As mentioned previously in section 3.2.4, Dooly et al. mentioned that the longer cell length have the better SNR (Dooly, Lewis and Fitzpatrick, 2007). It have the highest peak also at 215.65 nm and absorption cross section of $1.62\text{E-}18 \text{ cm}^2/\text{molecules}$. Even though measured spectra of 75 cm is more close to theoretical spectra, its absorption cross section of 75 cm spectra line is less than the value of absorption cross section of 50 cm as shown in Figure 4.5. This result indicate that increased length of the path reduces the detector's detected optical radiation as mentioned before in section 3.2.4. However, this result just an assumption until 100 cm cell length experimental result were obtain.

4.3.5 Result of 100 cm Cell Length

Figure 4.7 below displays the theoretical spectra line represent by red line compared to measured spectra line of 100 cm cell length represent by orange line.

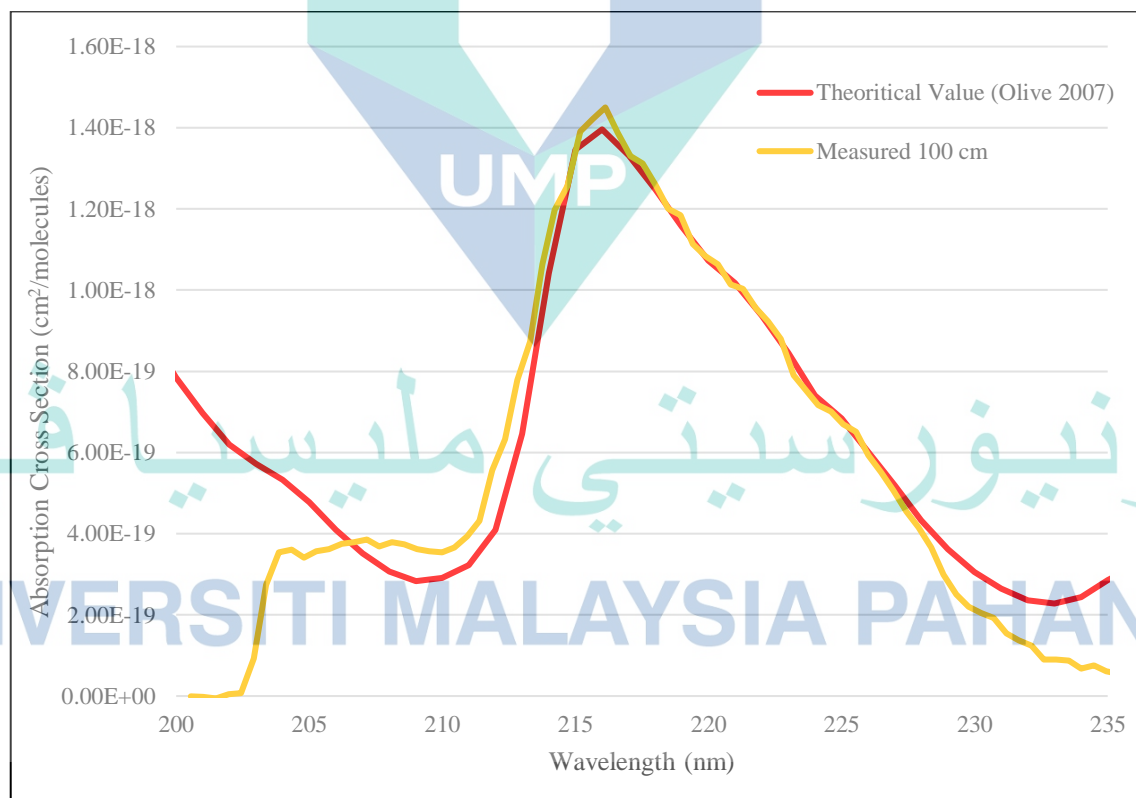


Figure 4.7 Spectral line of 100 cm cell length

What is striking about the measured spectra line in this Figure 4.7 is that it clearly identical to theoretical spectra line. Starting 209 nm, its value climb up align with theoretical spectra until it reach its peak that higher than theoretical peak at 216.12 nm and absorption cross section at $1.45E-18 \text{ cm}^2/\text{molecules}$ then started to align back until wavelength of 228.37 nm. Even though the spectra line are identical to theoretical spectra, its absorption cross section value is less than the measured spectra of 50 cm and 75 cm. Thus, it indicates that the loss of optical radiation increased with the increment of absorption path length. Therefore, the optical path length of the sensor should be calculated by agreement between the transmission loss and the acquired sensitivity of each centimeter (cm) in the direction of the optical path.

The investigation stops at 100 cm is because the result of previous study has shown almost similar pattern with other types of cell length. If the cell length exceed 100 cm, it will not affect the actual reading much other than the result just disturbed by the noise. It is because, the absorption cross section is been calculated in $\text{cm}^2/\text{molecules}$, if the cell getting longer, absorption cross section value will remain the same because the deviations in absorptivity coefficients at high concentrations ($>0.01\text{M}$) due to electrostatic interactions between molecules in close proximity thus will not affect the reading much.

4.3.6 Summary on Different Types Cell Length

Test have been conducted for SO_2 using different length of absorption cell to investigate and determine the best wavelength for an optimum absorption. Figure 4.8 below shows the absorption spectra for five different cell length compared with theoretical value lines in red in the wavelength region of 200 nm to 235 nm. The graph of different cell with length of 10 cm, 25 cm, 50 cm, 75 cm and 100 cm are represent by the color of light blue, black, green, purple and orange respectively.

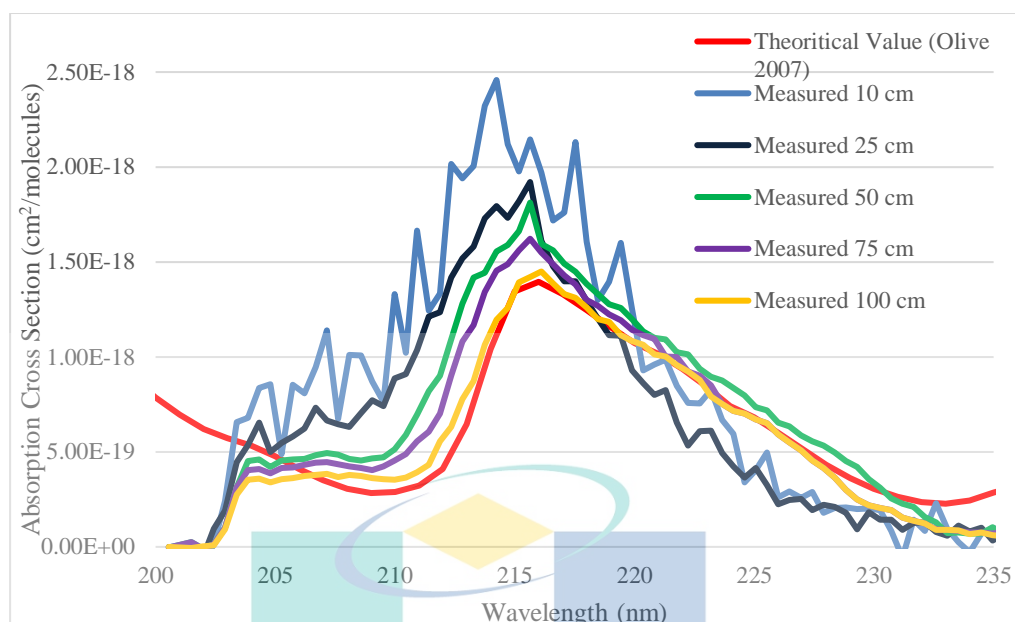


Figure 4.8 Initial experimental result compared with theoretical lines

As can be seen from Figure 4.8, the measured spectra line are getting closer to alike theoretical line as it comes to longer sensitivity. This finding broadly supports the work of studies of Ouyang et al and Inagaki et al that has stated before, a longer cell will have better sensitivity (Ouyang and Jones, 2012; Inagaki, Watanabe and Tsuchikawa, 2017). However, Wei et al stated that increment of cell length contributed to reduce of ability of a detector to detect optical radiation (Wei *et al.*, 2018). Thus, the measured spectra of 50 cm cell length has fulfil the criteria of an agreement between the loss of the transmission and the sensitivity acquired for each cm increase when it absorb the light strongly at 215.65 nm the value of absorption cross section at $1.81\text{E-}18 \text{ cm}^2/\text{molecules}$. In addition, it have lower noise with higher absorption that closely to theoretical spectra than others do.

Figure 4.8 also indicates that no absorption in the range of 200 to 203 nm for calculated SO_2 occurs. This is because no transmitted light is detected in this region by the CCD array in the spectrometer used in this experiment. The effect can be an incorrect design of the aperture (slit) or grating in which the emitted UV light in the range of 200 to 203 nm does not hit a few pixels in the spectrometer on the CCD array. Figure 4.9 shows this distinctly when the UV light source is switched on and off. Once powered, the spectrometer only displays the intensity measurement after 203 nm. This may be attributed to inadequate design of the entrance aperture (slit) or line, resulting in a UV

transmitted light not entering a few pixels in the spectrometer in that area (200-203 nm). Furthermore, the initial finding showed that the optimum wavelength to be explored is in the range of 200 and 235 nm.

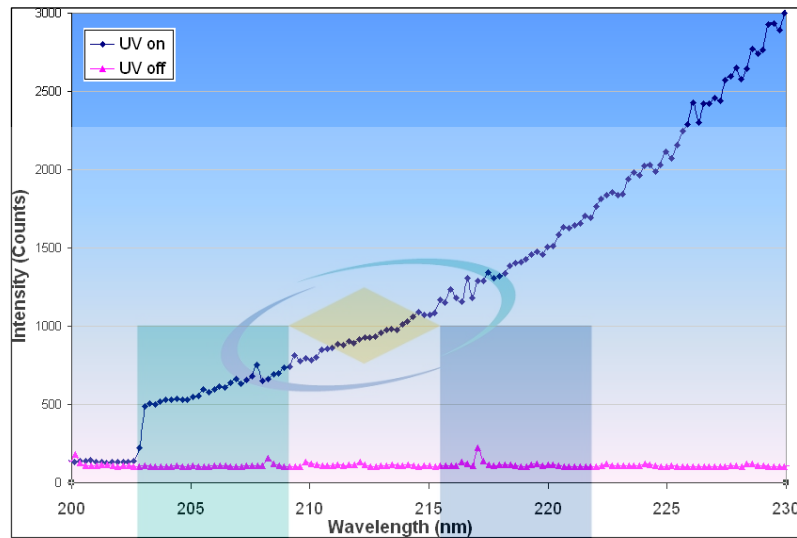


Figure 4.9 Reading of spectrometer when UV light source is switched on/off

4.4 Cross Sensitivity Experiment

The environment consists of various gasses composing the atmosphere of the earth. The atmosphere usually includes 78% N₂, 21% O₂, 0.038% CO₂ and 0.93% Argon. It also includes small amounts of other gasses, such as H₂, NO₂, CO₂ and water vapor.

In fact, cross-sensitivity is a critical limitation when measuring of gas concentration in an open environment, since the atmosphere consists of a number of gases. As issues of cross-sensitivity may influence the precision of the test, multiple methods have been used to overcome this problem, such as using gas separation techniques or measurement of a ratio. This section describes and addresses the cross-sensitivity issue of two atmospheric gases. The two primary air gases are:

- a) Oxygen
- b) Carbon Dioxide

4.4.1 Cross Sensitivity with O₂

As mentioned in section 4.3, O₂ is the second most common component in the atmosphere, with a relatively high concentration of 21%. Cross-sensitivity checking with O₂ is therefore necessary to determine the efficiency of the sensor. The experimental setup used in the cross-sensitivity testing of this study is identical to the first experiment mentioned in 4.2.1 as shown in Figure 4.10. The SpectraSuite program was used in this experiment to collect all details.

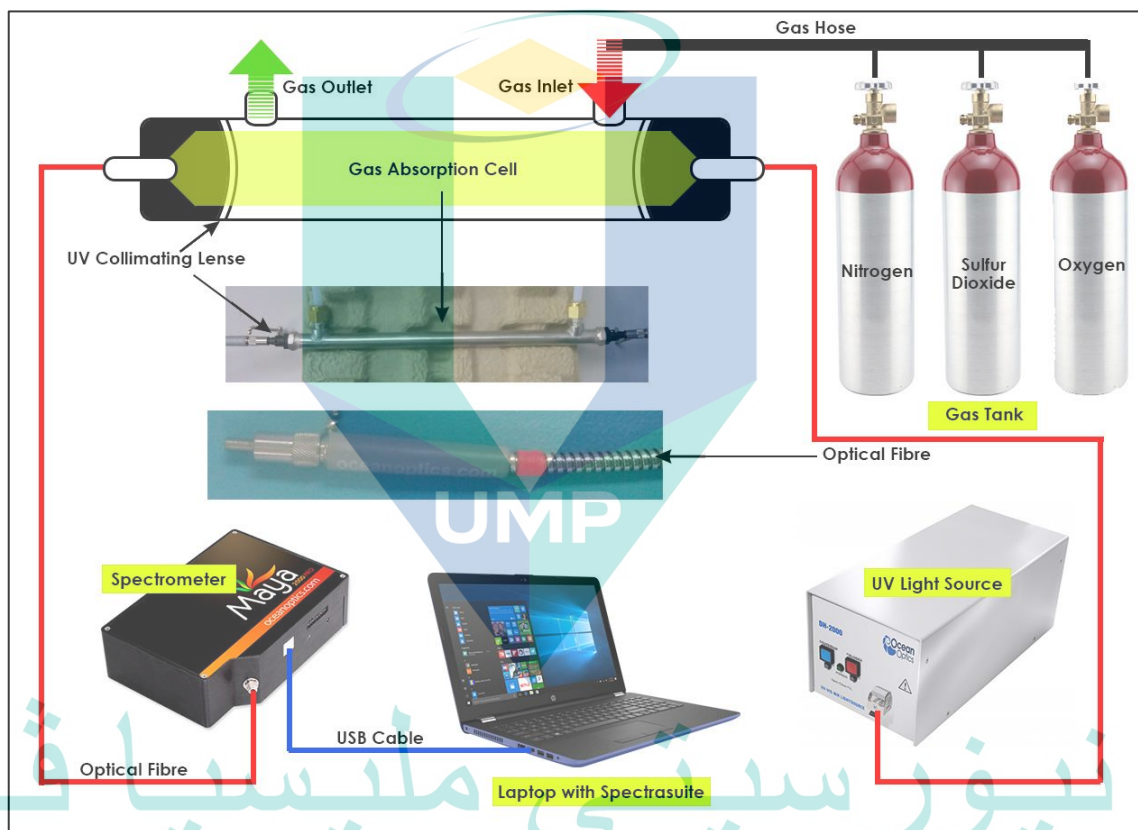


Figure 4.10 Pictorial diagram of O₂ cross-sensitivity experimental setup

For SpectraSuite the integration time was set to 2 s, although the optimal integration time was 1 s. Earlier in Chapter 3, it was mentioned that an increased integration time would contribute to a poor response time. The main objective of this cross-sensitivity study is to measure the presence of other atmospheric gases. Moreover, the response time is not the primary focus of cross-sensitivity testing. In addition, the decreased integration time would allow the input signals to be averaged more. This will increase the signal-to-noise ratio, resulting in a better cross-sensitivity check.

Before the UV light source was activated, the background intensity, I_b was measured. N_2 gas was then emitted into the gas test cell. The optical amplitude was calculated and I_o was the incident intensity. Only O_2 gas was then discharged into test cell. The intensity was once more measured and this value was seen as the transmitted intensity, I . Equation 3.1 for the absorption cross section of O_2 was included in the recorded data. The procedure has been replicated with 100 ppm SO_2 and pure O_2 .

The findings of Figure 4.11 below show the relatively small influence of O_2 on absorption lines that can be deemed negligible in the bottom noise level of the system in contrast to the SO_2 spectrum. This implies that in this 200-230 nm region, O_2 does not absorb light relative to SO_2 but is even negligible compared to SO_2 . It means that O_2 does not influence the calculation of SO_2 absorption. It therefore indicates that there is no SO_2 measuring cross-sensitivity issue in the presence of ambient O_2 .

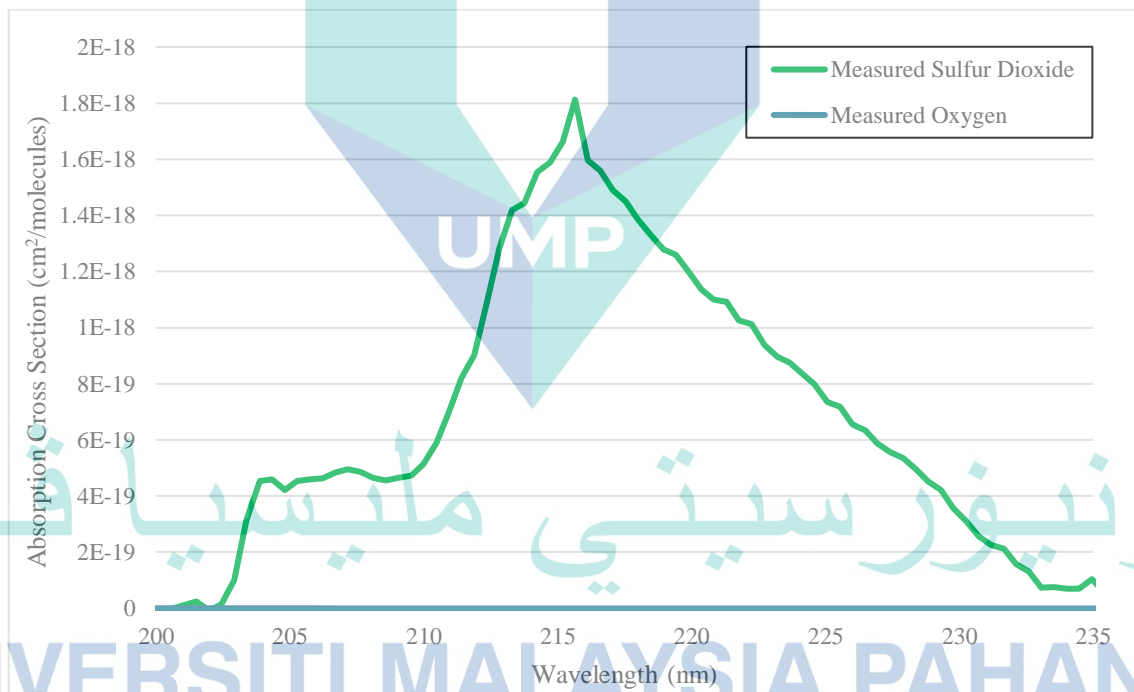


Figure 4.11 O_2 absorption lines compared to SO_2 gas

4.4.2 Cross Sensitivity with CO_2

Cross-sensitivity testing with CO_2 has performed in the same way as in Section 4.4.1 above, as shown in Figure 4.12 below. Even though CO_2 gas occurs at a low ambient concentration of just 0.038 percent or 380 ppm, cross-sensitivity experiments of CO_2 are still considered necessary. In this case, the production of CO_2 emissions is much greater

and therefore can influence the calculation of SO_2 . Nevertheless, the cross-sensitivity of CO_2 had to be examined to produce an appropriate sensing device.

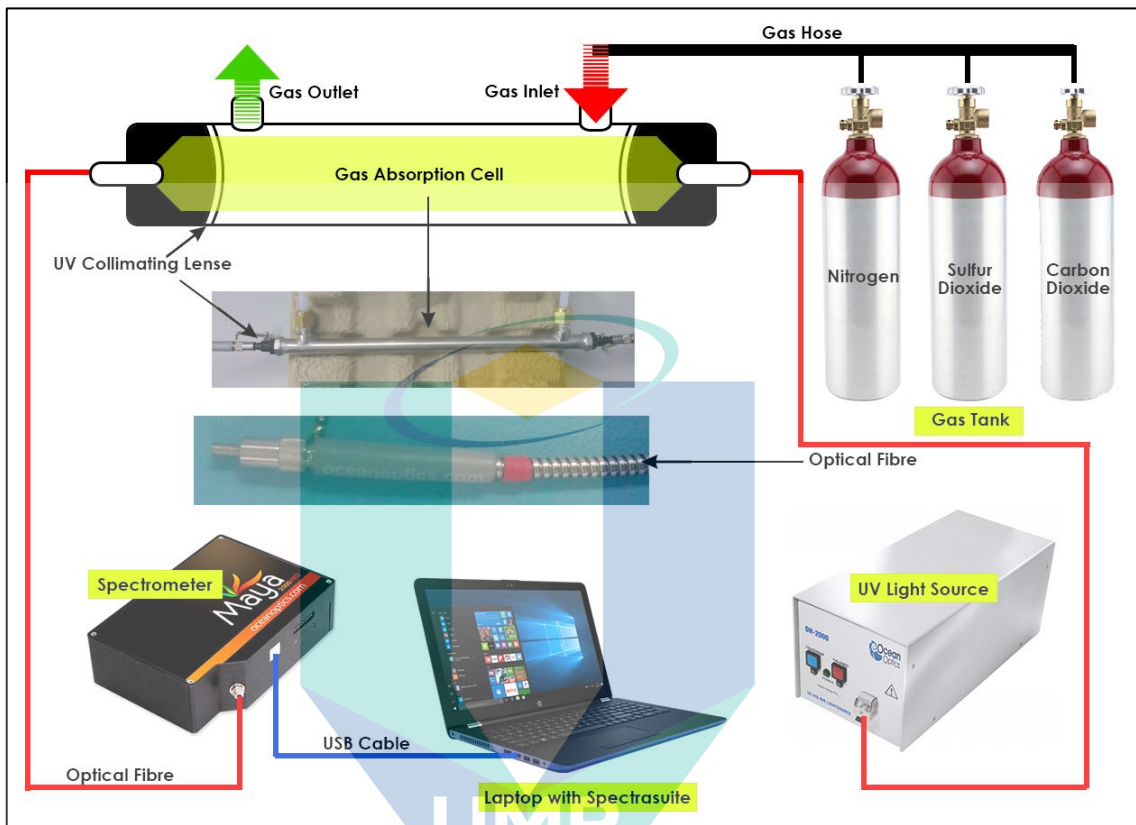


Figure 4.12 Pictorial diagram of CO_2 cross-sensitivity experimental setup

Since CO_2 is similar to the test described in section 4.3.1, the experimental set-up used in this test is almost the same as previously shown. The O_2 cylinder was substituted by a CO_2 gas cylinder. The tank holds 1% CO_2 in N_2 . One percent has been chosen to create the composition which is a much worse situation than that found in the atmosphere, because it is a much higher value than the ambient concentration (380 ppm). The collected data have again been introduced into Equation 3.1 to achieve the absorption cross-section for all gases studied.

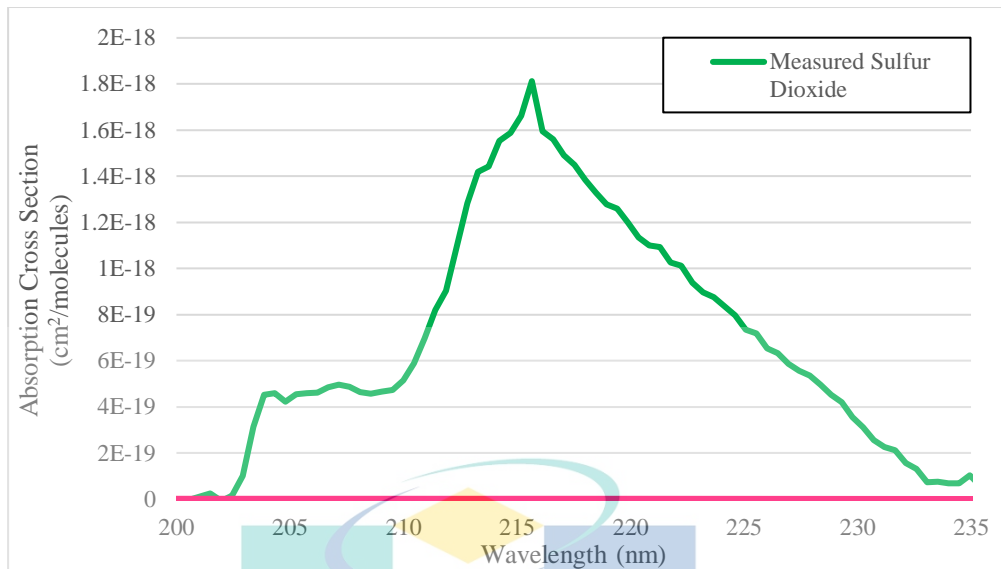


Figure 4.13 CO₂ absorption lines as compared to SO₂ gas

As shown in Figure 4.13, this analysis shows the same findings as the O₂ cross sensitivity study performed in Section 4.3.1 earlier. Apparently, CO₂ does not absorb light in the range of 200-235 nm. The absorption pattern for 100 ppm of SO₂ is also similar to that of 1% CO₂. It indicates that CO₂ activity has no significant impact in the 200-235 nm range on SO₂ absorption. It therefore supports the assumption that the CO₂ gas concentration in this region does not influence the SO₂ calculation.

4.4.3 Summary on Cross Sensitivity Experiment

Tests for CO₂ and O₂ gasses were carried out to demonstrate that no noticeable cross-sensitivity effects are found on SO₂ measures in practice. Although there have been no cross-sensitivity tests performed on water vapor, the findings can be expected that water vapor in the region between 200 and 235 nm will not influence the sulfur calculation. Therefore, there are clear advantages in calculating the cross sensitivity of SO₂ absorption within the 200-235 nm range as, as discussed above, there are no issues with cross sensitivity to specific atmospheric gases.

Moreover, the cross-sensitivity issue for all atmospheric gases can not be addressed, as there are too many gasses in the atmosphere and the volume is low and environmentally sensitive. Nevertheless, for each SO₂ study, a comparison measurement is to be carried out for all future experiments in an open environment in which other gases will occur. As a second measurement, this reference measurement is essential, and it can be used to fully justify sensor precision and efficiency.

4.5 Concentration Measurement

The main objective of this study is to successfully develop UV based detection system for SO₂ using an open path technique. Thus, concentration, ppm of SO₂ was calculated for validation purpose with absorption, σ already known previously. In order to do that, the equation for ppm which manipulated from equation for σ was used where the value of σ varies depending on the wavelength and can be obtained from previous result. The equation used for measuring the concentration is identical to equation 3.2 used for calculating the absorption. The calculation method for concentration is based on the Beer Lambert law defined in Section 3, Chapter 3.5.1. The concentration unit is converted to *ppm* as equation 4.1 below.

$$ppm = \frac{-[ln\frac{I}{I_0}][24.04]}{\sigma \times N_A \times l \times 10^{-9}} \quad 4.1$$

The only discrepancy in equation 4.1 and the absorption measurement method, as can be seen, is the location of *ppm* and σ , which are substituted. Therefore, the value of σ for the chosen wavelength must be identified. The σ value was obtained in Section 4.2.4 of the initial experiment in Figure 4.5. Depending on Table 4.1, the value of σ differs according to the calculated wavelength. Thus, the accurate σ value is indeed the value chosen for the concentration measurement at the wavelength. I_0 and I were obtained from the experiment. Table 4.1 show the calculation of SO₂ gas at selected wavelength.

Table 4.1 SO₂ gas concentration calculation at selected wavelength

Incident Intensity, I_0	Transmitted Intensity, I	I/I_0	Concentration, ppm
13493	10839	0.80328071	96.49
14278	11471	0.80340843	96.42
12586	10118	0.80391430	96.14
14793	11895	0.80409653	96.04
17307	13891	0.80262322	96.85
14121	11335	0.80272414	96.80
15507	12453	0.80309544	96.59
14998	12039	0.80271141	96.80
15959	12781	0.80086472	96.82
15440	12410	0.80377383	96.22
Average =			96.62

In this case, the selected wavelength is 215.65 nm and the value of σ is 1.81248E-18 cm²/molecules used to calculate the SO₂ gas concentration. The average value 96.62 ppm obtained is the calculated SO₂ gas concentration. This experiment used 100 ppm SO₂ gas as stated by the manufacturer. Comparatively, the calculated gas concentration is around 3.38 ppm less. One of the reason that this happened is due to noise that existed during the measurement.

As demonstrated in the previous study, noise can cause problems in deciding concentration calculation and can even contribute to incorrect concentration measurements (Dooly *et al.*, 2011). Another reason is that, the true concentration of SO₂ gas in the tank provided by the manufacturer already decreased due to the shelf life of the gas itself. However, both reason were not further investigated in this study because the value can be considered as in good agreement and used only for validation purpose. From the calculated concentration, the error rate for this sensor can be define by using the equation below:

$$\text{error rate, \%} = \frac{[\text{actual concentration}] - [\text{measured concentration}]}{\text{actual concentration}} \times 100\% \quad 4.2$$

After the value been inserted into Equation 4.2, the error rate for this sensor has been determined. The error rate found for this sensor is 3.48% which is still within acceptable limit of below 5% since this approximates widely accepted standard for statistical significance.

اونيورسيتي ملايسيا قهغ

UNIVERSITI MALAYSIA PAHANG

CHAPTER 5

CONCLUSION

5.1 Introduction

This study was conducted to analyze and improve an optical fiber sensor, utilizing UV light as a source of light. A fiber optic sensor was designed to identify and quantify the concentration of SO₂ concentration. This sensor has been described in detail in terms of construction, layout, application and its benefits and advantages using an open path optical absorption technique. This chapter describes the contributions of the work for the creation of this optical fiber sensor. Therefore, a plan and recommendations are given for future work.

5.2 Conclusions

The main objective of this study is to develop the UV based detection system for SO₂ using an open path OFS and the new system should be possible to be used for environmental monitoring in enclosed building. In an initial experiment, the optical fibre sensor showed good agreement with theoretical absorption values from the MPI-Mainz database. Analysis of SO₂ gas spectral resulted in absorption wavelength at the region of 200 nm – 235 nm and it indicate an important point. The major point is that the system is able to detect SO₂ via the open path technique applied. The absorption spectral is unique for each of the compound, thus this system also might be able to distinguish different sulphuric compound. Then, another significant point is the choice of UV as the light source is most appropriate. This wavelength range fell under the UV-C region, the shortest wavelength of UV.

There is no interference issue of SO₂ gas when cross sensitivity testing was carried out. Some detection methods previously are sensitive to interference from other compounds or environmental. The cross sensitivity assessment that was carried out previously only O₂ and CO₂ but not with another atmospheric gas that may exist in the environment. This assessment also indicates that the wavelength region of 200 nm to 235

nm is the best potential band selected for the development of the SO₂ UV based detection system.

Concentration of SO₂ gas was obtained with calculating using derivation of Beer Lambert Law equation for quantitative validation purpose. The calculation that used the previous result of absorption acquired from the peak value demonstrated that this detection system is objective and provide measurable result. Accordingly, the system is not just for plain detection of SO₂ existence but also can indicate the intensity of the SO₂. The objective achieved in this study are as in the Table 5.1 below.

Table 5.1 Objectives of the research

Objectives of The Research	Remark
Design the SO ₂ gas detection using an open-path cell length	Have the measured spectra line that identical to the theoretical spectra
Investigate the best wavelength for an optimum absorption	215.65 nm
Develop SO ₂ sensor with no cross sensitivity	No cross-sensitivity with CO ₂ and O ₂
The optimum cell length	50 cm
The best absorption cross section	1.81248E-18 cm ² /molecules
Validation of Concentration	96.62 ppm
% Error	3.48 %

5.3 Future Work

Future work for this sensor will look at installing and testing the sensor into the enclosed room of food preservation or enclosed space of sulfuric acid manufacture industry and by using real-time monitoring with LabVIEW software. Further tests will look at a wider variety of gas mixtures and testing other gases within the UV range. In addition, to lower the cost, DUV LED will be use as it may be commercially available in the future.

REFERENCES

- Adams, J. B. (1997) 'Food additive-additive interactions involving sulphur dioxide and ascorbic and nitrous acids: A review', *Food Chemistry*, pp. 401–409. doi: 10.1016/S0308-8146(96)00283-X.
- Al-Jalal, A. A. *et al.* (2019) 'Measurement of low concentrations of NO₂ gas by differential optical absorption spectroscopy method', *Measurement: Journal of the International Measurement Confederation*. Elsevier B.V., 146, pp. 613–617. doi: 10.1016/j.measurement.2019.07.022.
- Ali, M. F., Ali, B. M. E. and Speight, J. G. (2005) *Handbook of Industrial Chemistry*. 1st edn. CBS.
- Amann, M., Klimont, Z. and Wagner, F. (2013) 'Regional and global emissions of air pollutants: Recent trends and future scenarios', *Annual Review of Environment and Resources*. Annual Reviews, 38(1), pp. 31–55. doi: 10.1146/annurev-environ-052912-173303.
- Amelio, G. F., Tompsett, M. F. and Smith, G. E. (1970) 'Experimental Verification of the Charge Coupled Device Concept', *Bell System Technical Journal*, 49(4), pp. 593–600. doi: 10.1002/j.1538-7305.1970.tb01791.x.
- Ampuero, S. and Bosset, J. O. (2003) 'The electronic nose applied to dairy products: A review', *Sensors and Actuators, B: Chemical*, pp. 1–12. doi: 10.1016/S0925-4005(03)00321-6.
- Antony, R. *et al.* (2014) 'Detection principles and development of microfluidic sensors in the last decade', *Microsystem Technologies*. Springer Berlin Heidelberg, 20(6), pp. 1051–1061. doi: 10.1007/s00542-014-2165-0.
- Arata, J., Terakawa, S. and Fujimoto, H. (2013) 'Fiber Optic Force Sensor for Medical Applications within a Backbone-shape Structure', *Procedia CIRP*, 5, pp. 66–69. doi: 10.1016/j.procir.2013.01.013.
- Australian Government Department of the Environment and Heritage (2005) *Air Quality Fact Sheet: Sulfur dioxide*. Available at: <https://www.environment.gov.au/protection/publications/factsheet-sulfur-dioxide-so2> (Accessed: 3 December 2019).
- Azman, F. (2019) *Bukan hanya gas metana dikesan dalam Sungai Kim Kim? | Astro Awani*. Available at: <http://www.astroawani.com/berita-malaysia/bukan-hanya-gas-metana-dikesan-dalam-sungai-kim-kim-201007> (Accessed: 11 August 2020).
- Azmi, H., Mohd Kamil, H. and Balkis, A. (2002) 'Keracunan Sulfur Dioksida Di Kalangan Orang Awam Di Kawasan Perindustrian, Kemaman, Negeri Terengganu', *Malaysian Journal of Public Health Medicine*, 2(1), pp. 31–35. Available at: <http://www.myjournal.my/public/article-view.php?id=62514> (Accessed: 11 August 2020).

- Bahareh, G. and Hooman, N. (2008) 'Fiber Optic Sensors', *International Journal of Electrical, Computer, Energetic, Electronic and Communication Engineering*, 2, pp. 1107–1117.
- Balaram Sahoo, Nimai Charan Nayak, Asutosh Samantaray, P. K. P. (2012) *Inorganic Chemistry*. PHI Learning Private Limited.
- Barrett, J. (2002) *Atomic Structure and Periodicity, Atomic Structure and Periodicity*. Royal Society of Chemistry. doi: 10.1039/9781847550187.
- Barsan, N., Koziej, D. and Weimar, U. (2007) 'Metal oxide-based gas sensor research: How to?', *Sensors and Actuators, B: Chemical*, 121(1), pp. 18–35. doi: 10.1016/j.snb.2006.09.047.
- Bartlett, J. K. and Skoog, D. A. (1954) 'Colorimetric Determination of Elemental Sulfur in Hydrocarbons', *Analytical Chemistry*. doi: 10.1021/ac60090a014.
- Beasley, G. B. and Panayiotou, C. A. (2019) 'CCCC and LASER-TEC educational Raman spectrometer demo', in, p. 141. doi: 10.1117/12.2523866.
- Bent, H. A. (2004) *Question Why does helium have the ending '-ium' usually re-served for metals?*
- Berger, F. *et al.* (1997) 'Tin dioxide-based gas sensors for SO₂ detection: a chemical interpretation of the increase in sensitivity obtained after a primary detection', *Sensors and Actuators B: Chemical*, 45(3), pp. 175–181. doi: 10.1016/S0925-4005(97)00284-0.
- Betty, C. A., Choudhury, S. and Arora, S. (2015) 'Tin oxide-polyaniline heterostructure sensors for highly sensitive and selective detection of toxic gases at room temperature', *Sensors and Actuators B*, 220, pp. 288–294. doi: 10.1016/j.snb.2015.05.074.
- Bharadwaj, V. (2014) 'COLOURS: A SCIENTIFIC APPROACH', *International Journal of Research -GRANTHAALAYAH*, pp. 1–6. Available at: http://granthaalayah.com/Composition_of_colours/Articles/27_IJRG14_CC11_141.pdf (Accessed: 12 December 2019).
- Binyehmed, F. M., Abdullah, A. M. and Zainal, Z. (2016) 'Trend and Status of SO₂ Pollution as a Corrosive Agent at Four Different Monitoring Stations in the Klang Valley', *International Journal of Advanced Scientific and Technical Research*.
- Björn, L. O. (2008) 'The nature of light and its interaction with matter', in *Photobiology: The Science of Life and Light: Second Edition*. Springer New York, pp. 1–39. doi: 10.1007/978-0-387-72655-7_1.
- Bogumil, K. *et al.* (2003) 'Measurements of molecular absorption spectra with the SCIAMACHY pre-flight model: instrument characterization and reference data for atmospheric remote-sensing in the 230–2380 nm region', *Journal of Photochemistry and Photobiology A: Chemistry*. Elsevier, 157(2–3), pp. 167–184. doi: 10.1016/S1010-6030(03)00062-5.

- Briz, S. *et al.* (2007) 'Remote sensing by open-path FTIR spectroscopy. Comparison of different analysis techniques applied to ozone and carbon monoxide detection', *Journal of Quantitative Spectroscopy and Radiative Transfer*, 103(2), pp. 314–330. doi: 10.1016/j.jqsrt.2006.02.058.
- Bunge, F. *et al.* (2019) 'Microfluidic oxygen sensor system as a tool to monitor the metabolism of mammalian cells', *Sensors and Actuators, B: Chemical*. Elsevier, 289, pp. 24–31. doi: 10.1016/j.snb.2019.03.041.
- Burlakov, V. D. *et al.* (2010) 'A differential-absorption lidar for ozone sensing in the upper atmosphere-lower stratosphere', *Instruments and Experimental Techniques*, 53(6), pp. 886–889. doi: 10.1134/S0020441210060229.
- Busa, L. S. A. *et al.* (2016) 'Simple and sensitive colorimetric assay system for horseradish peroxidase using microfluidic paper-based devices', *Sensors and Actuators, B: Chemical*. Elsevier, 236, pp. 433–441. doi: 10.1016/j.snb.2016.06.013.
- Butt, C. R. M., Gole, M. J. and Dyck, W. (2000) 'Chapter 10 Helium', *Handbook of Exploration Geochemistry*, 7(C), pp. 303–352. doi: 10.1016/S0168-6275(00)80034-3.
- Buzanovskii, V. A. (2018) 'Determination of Sodium in Blood', *Review Journal of Chemistry*. Pleiades Publishing Ltd, 8(2), pp. 197–222. doi: 10.1134/s2079978018020012.
- Canadian Centre for Occupational Health and Safety (CCOHS) (2016) *Ultraviolet Radiation*. Available at: https://www.ccohs.ca/oshanswers/phys_agents/ultravioletradiation.html (Accessed: 17 October 2017).
- Carlier, J., Li, Y. and Lutton, J. (1997) 'Reliability evaluation of large telecommunication networks', *Discrete Applied Mathematics*, 76(1–3), pp. 61–80. doi: 10.1016/S0166-218X(96)00117-5.
- Carson, C. (2000) 'The origins of the quantum theory', *Beam Line*, pp. 6–19. Available at: <https://poseidon01.ssrn.com/delivery.php?ID=5630061100270850180860810971050681101020130670920700871260021091000170950770781261130991221160020190250280020811071140180880691260320130320390920011211230290810000950570390030910641230721270161040751211090720080> (Accessed: 11 December 2019).
- Chakraborty, N. *et al.* (2008) 'Measurement of CO₂, CO, SO₂, and NO emissions from coal-based thermal power plants in India', *Atmospheric Environment*. Elsevier Ltd, 42(6), pp. 1073–1082. doi: 10.1016/j.atmosenv.2007.10.074.
- Chao, Y. *et al.* (2005) 'Amperometric sensor for selective and stable hydrogen measurement', *Sensors and Actuators, B: Chemical*. doi: 10.1016/j.snb.2004.09.042.
- Chatterjee, C. and Sen, A. (2015) 'Sensitive colorimetric sensors for visual detection of carbon dioxide and sulfur dioxide', *Journal of Materials Chemistry A*. doi: 10.1039/c4ta06321j.

- Chaudhary, V. and Kaur, A. (2015) 'Solitary surfactant assisted morphology dependent chemiresistive polyaniline sensors for room temperature monitoring of low parts per million sulfur dioxide', *Polymer International*. John Wiley and Sons Ltd, 64(10), pp. 1475–1481. doi: 10.1002/pi.4944.
- Cheryl B. Bast; George M. Woodall; Lorren Koller (2010) *Acute Exposure Guideline Levels for Selected Airborne Chemicals: Volume 8*. 8th edn. National Academies Press. Available at: https://www.researchgate.net/publication/255220210_Sulfur_Dioxide_Acute_Exposure_Guideline_Levels (Accessed: 3 October 2019).
- Cleary, J., Slater, C. and Diamond, D. (2007) 'Field-deployable microfluidic sensor for phosphate in natural waters', in *Proceedings of IEEE Sensors*. doi: 10.1109/ICSENS.2007.4388573.
- Clifford, P. K. and Tuma, D. T. (1982) 'Characteristics of semiconductor gas sensors I. Steady state gas response', *Sensors and Actuators*, 3(C), pp. 233–254. doi: 10.1016/0250-6874(82)80026-7.
- Coburn, C., Fan, D. and Forrest, S. R. (2019) 'Organic Charge-Coupled Device', *ACS Photonics*, 6(8), pp. 2090–2095. doi: 10.1021/acsp Photonics.9b00596.
- Colls, J. and Tiwary, A. (2010) *Air pollution: measurement, modelling and mitigation, Choice Reviews Online*. doi: 10.5860/choice.47-4447.
- Council of the European Union (1980) *Council directive on air quality limit values and guide values for sulphur dioxide and suspended particulates - 80/779/EEC*. Publications Office of the European Union.
- Culshaw, B. and Kursey, A. (2008) 'Fiber-Optic Sensing: A Historical Perspective', *JOURNAL OF LIGHTWAVE TECHNOLOGY*, 26(9), pp. 1064–1078.
- Currie, J. ., Essalik, A. and Marusic, J.-C. (1999) 'Micromachined thin film solid state electrochemical CO₂, NO₂ and SO₂ gas sensors', *Sensors and Actuators B: Chemical*, 59(2–3), pp. 235–241. doi: 10.1016/S0925-4005(99)00227-0.
- Curtis, L. S. (2007) *Natural Cycles, Lori S. Curtis*.
- Custom Fiber Optic Patch Cables (no date). Available at: https://www.thorlabs.us/newgrouppage9.cfm?objectgroup_id=2410. (Accessed: 17 December 2018).
- Dahiya, S. and Myllyvirta, L. (2019) *Global SO₂ emission hotspot database RANKING THE WORLD'S WORST SOURCES OF SO₂ POLLUTION Content*. Available at: https://storage.googleapis.com/planet4-international-stateless/2019/08/e40af3dd-global-hotspot-and-emission-sources-for-so2_16_august-2019.pdf (Accessed: 3 December 2019).
- Daly, A. and Zannetti, P. (2007) 'An Introduction to Air Pollution – Definitions , Classifications , and History', in *Ambient Air Pollution*, pp. 1–14.

- Das, S *et al.* (2008) 'Vanadium doped tin dioxide as a novel sulfur dioxide sensor', *Talanta*, 75, pp. 385–389. doi: 10.1016/j.talanta.2007.11.010.
- Dasan, M. *et al.* (2019) 'Optically Multiplexed Systems: Wavelength Division Multiplexing', in *Multiplexing*. IntechOpen. doi: 10.5772/intechopen.88086.
- Dastoorpoor, M. *et al.* (2019) 'Air pollution and hospital admissions for cardiovascular diseases in Ahvaz, Iran', *Science of the Total Environment*. Elsevier B.V., 652, pp. 1318–1330. doi: 10.1016/j.scitotenv.2018.10.285.
- Dauer, V. (2000) 'Optical constants of lithium fluoride thin films in the far ultraviolet', *Journal of the Optical Society of America B*. The Optical Society, 17(2), p. 300. doi: 10.1364/josab.17.000300.
- Davenport, W. *et al.* (2006) 'Sulphuric Acid Manufacture', *Southern African Pyrometallurgy 2006*, pp. 5–8.
- Delmdahl, R. and Pätzelt, R. (2008) 'Pulsed laser deposition-UV laser sources and applications', *Applied Physics A: Materials Science and Processing*, 93(3), pp. 611–615. doi: 10.1007/s00339-008-4716-7.
- Demtröder, W. (1999) 'Laser Applications in Electronic Spectroscopy', in *Encyclopedia of Spectroscopy and Spectrometry*. Elsevier, pp. 1113–1123. doi: 10.1006/rwsp.2000.0148.
- Deng, J. *et al.* (2001) 'Optical fiber sensor-based detection of partial discharges in power transformers', *Optics & Laser Technology*, 33(5), pp. 305–311. doi: 10.1016/S0030-3992(01)00022-6.
- Detto, M. *et al.* (2011) 'Comparing laser-based open- and closed-path gas analyzers to measure methane fluxes using the eddy covariance method', *Agricultural and Forest Meteorology*, 151(10), pp. 1312–1324. doi: 10.1016/j.agrformet.2011.05.014.
- Devia, D. M., Rodriguez-Restrepo, L. V and Restrepo-Parra, E. (2015) 'Methods Employed in Optical Emission Spectroscopy Analysis: a Review', *Ingeniería y Ciencia*, 11(21), pp. 239–267. doi: 10.17230/ingciencia.11.21.12.
- Diffey, B. L. (2002) 'Sources and measurement of ultraviolet radiation', *Methods*, 28(1), pp. 4–13. doi: 10.1016/S1046-2023(02)00204-9.
- Divol, B., Du Toit, M. and Duckitt, E. (2012) 'Surviving in the presence of sulphur dioxide: Strategies developed by wine yeasts', *Applied Microbiology and Biotechnology*, pp. 601–613. doi: 10.1007/s00253-012-4186-x.
- DOE's Report | Department of Environment (no date). Available at: <https://www.doe.gov.my/portalv1/en/awam/maklumat-umum/laporan-jabatan-alam-sekitar> (Accessed: 11 August 2020).
- Dooly, G. *et al.* (2011) 'In-situ low concentration monitoring of ammonia using an optical fibre sensor', in *Proceedings of IEEE Sensors*, pp. 242–245. doi: 10.1109/ICSENS.2011.6127153.

- Dooly, G., Fitzpatrick, C. and Lewis, E. (2008) 'Optical sensing of hazardous exhaust emissions using a UV based extrinsic sensor', *Energy*. Elsevier Ltd, 33(4), pp. 657–666. doi: 10.1016/j.energy.2007.11.009.
- Dooly, G., Lewis, E. and Fitzpatrick, C. (2007) 'On-board monitoring of vehicle exhaust emissions using an ultraviolet optical fibre based sensor', *Journal of Optics A: Pure and Applied Optics*, 9(6). doi: 10.1088/1464-4258/9/6/S05.
- Eastham, P. (2012) 'Quantum theory of light and matter The questions'.
- EC (1999) 'Council Directive 1999/30/EC of, 22 April, 1999. Relating to limit values for sulphur dioxide, nitrogen dioxide and oxides of nitrogen, particulate matter and lead in ambient air (The First Daughter Directive). From the Official Journal of the European Co', <https://webarchive.nationalarchives.gov.uk/eu-exit/https://eur-lex.europa.eu/legal-content/EN/TXT/?uri=CELEX:01999L0030-20100611>. Queen's Printer of Acts of Parliament.
- EC (2000) *Guidance on Assessment under the EU Air Quality Directives-FINAL DRAFT Guidance on Assessment under the EU Air Quality Directives Final draft*. Available at: <http://ec.europa.eu/environment/air/pdf/guidanceunderairquality.pdf> (Accessed: 11 August 2020).
- EC (2008) 'Directive 2008/50/EC of the European Parliament and of the Council of 21 May 2008 on ambient air quality and cleaner air for Europe', <https://webarchive.nationalarchives.gov.uk/eu-exit/https://eur-lex.europa.eu/legal-content/EN/TXT/?uri=CELEX:02008L0050-20150918>. Queen's Printer of Acts of Parliament.
- Environment: Definition of Environment in Oxford Dictionary (British & World English)* (no date).
- Eshaghi, Z. (2011) 'Photodiode Array Detection in Clinical Applications; Quantitative Analyte Assay Advantages, Limitations and Disadvantages', in *Photodiodes - Communications, Bio-Sensings, Measurements and High-Energy Physics*. InTech. doi: 10.5772/18244.
- European Environment Agency (2016) *European Union emission inventory report 1990–2014 under the UNECE Convention on Long-range Transboundary Air Pollution (LRTAP)*, EEA Technical report. doi: 10.2800/18374.
- European Parliament and Council (2008) 'Directive 2008/1/EC of the Parliament and the Council of 15 January 2008 concerning integrated pollution prevention and control (Codified version)', *Official Journal of the European Union*. Publications Office of the European Union, L 24, pp. 8–29.
- European Parliament And The Council Of The European Union (2001) 'Directive 2001/81/EC of the European Parliament and of the Council of 23 October 2001 on national emission ceilings for atmospheric pollutants', *Official Journal of the European Communities*. Publications Office of the European Union, (L 309), pp.

22–30. doi: <http://eur-lex.europa.eu/LexUriServ/LexUriServ.do?uri=OJ:L:2001:309:0022:0030:EN:PDF>.

Fergus, J. W. (2008) ‘A review of electrolyte and electrode materials for high temperature electrochemical CO₂ and SO₂ gas sensors’, *Sensors and Actuators B: Chemical*, 134(2), pp. 1034–1041. doi: 10.1016/j.snb.2008.07.005.

Fidanboylu and Efendioglu, H. S. (2009) ‘Fiber optic sensors and their applications’, *Symposium A Quarterly Journal In Modern Foreign Literatures*, pp. 1–6.

Finkenzeller, U. and Labs, D. (1979) ‘Deuterium lamp as a UV continuum source from 160 nm to 320 nm for space applications’, *Appl Opt*, 18(23), pp. 3938–3941. doi: 10.1364/AO.18.003938.

Fischer, R. E., Tadic-Galeb, B. and Yoder, P. R. (2008) ‘Optical System for the UV’, in *Optical System Design*. 2nd Editio. McGraw Hill, p. 255. doi: 10.1016/b978-0-12-408660-9.x5001-6.

Flaud, J. M. *et al.* (2005) ‘Quantitative spectroscopy and atmospheric measurements’, in *NATO Security through Science Series C: Environmental Security*, pp. 107–121. doi: 10.1007/978-1-4020-5090-9_7.

Fossum, E. R. and Hondongwa, D. B. (2014) ‘A review of the pinned photodiode for CCD and CMOS image sensors’, *IEEE Journal of the Electron Devices Society*. doi: 10.1109/JEDS.2014.2306412.

Fu, Q., Wan, H. and Qiu, F. (2010) ‘Pipeline leak detection based on fiber optic early-warning system’, *Procedia Engineering*, 7, pp. 88–93. doi: 10.1016/j.proeng.2010.11.013.

Gan, T. and Hu, S. (2011) ‘Electrochemical sensors based on graphene materials’, *Microchimica Acta*, 175(1–2), pp. 1–19. doi: 10.1007/s00604-011-0639-7.

Gangaiya, P. and Mahendra, N. (2008) *Chemical Bioavailability in Terrestrial Environment, Developments in Soil Science*. Elsevier (Developments in Soil Science). doi: 10.1016/S0166-2481(07)32024-2.

Gao, Z. X. *et al.* (2008) ‘A simple microfluidic chlorine gas sensor based on gas-liquid chemiluminescence of luminol-chlorine system’, *Analytica Chimica Acta*. Elsevier, 622(1–2), pp. 143–149. doi: 10.1016/j.aca.2008.05.067.

Gauthier, R. C. (1993) ‘External birefringent fibre-optic heart-rate monitor’, *Optics & Laser Technology*, 25(1), pp. 9–15. doi: 10.1016/0030-3992(93)90150-E.

General Fiber Information (no date).

Ghetia, S., Gajjar, R. and Trivedi, P. (2013) ‘Classification of Fiber Optical Sensors’, *International Journal of Electronics Communication and Computer Technology (IJECCCT)*, 3(4), pp. 442–445.

- Ghidini, S., Varrà, M. O. and Zanardi, E. (2019) 'Approaching authenticity issues in fish and seafood products by qualitative spectroscopy and chemometrics', *Molecules*, 24(9). doi: 10.3390/molecules24091812.
- Ghimbeu, C. M. *et al.* (2010) 'Detection of H₂S, SO₂, and NO₂ using electrostatic sprayed tungsten oxide films'. doi: 10.1016/j.mssp.2010.01.001.
- Gibbs, D. P. *et al.* (1994) 'Simultaneous detection of multiple greenhouse gases using open-path spectrometers', in *International Geoscience and Remote Sensing Symposium (IGARSS)*, pp. 690–692. doi: 10.1109/igarss.1994.399229.
- Giddey, S., Badwal, S. P. S. and Kulkarni, A. (2013) 'Review of electrochemical ammonia production technologies and materials', *International Journal of Hydrogen Energy*, pp. 14576–14594. doi: 10.1016/j.ijhydene.2013.09.054.
- Girardin, D. *et al.* (1997) 'Modelling of SO₂ detection by tin dioxide gas sensors', *Sensors and Actuators B: Chemical*, 43(1–3), pp. 147–153. doi: 10.1016/S0925-4005(97)00149-4.
- Gonzalez, Gonzalo Abad Amir, H. S. *et al.* (2019) 'Five decades observing Earth's atmospheric trace gases using ultraviolet and visible backscatter solar radiation from space', *Journal of Quantitative Spectroscopy and Radiative Transfer*. Pergamon. doi: 10.1016/J.JQSRT.2019.04.030.
- Goushcha, A. and Tabbert, B. (2007) 'Optical Detectors', in *Springer Handbook of Lasers and Optics*. Springer New York, pp. 503–562. doi: 10.1007/978-0-387-30420-5_9.
- Grant, W. B., Kagann, R. H. and McClenny, W. A. (1992) 'Optical Remote Measurement of Toxic Gases', *Journal of the Air and Waste Management Association*, 42(1), pp. 18–30. doi: 10.1080/10473289.1992.10466965.
- Green, L. F. (1976) 'Sulphur dioxide and food preservation-A review', *Food Chemistry*, pp. 103–124. doi: 10.1016/0308-8146(76)90003-0.
- Guerreiro, C. B. B., Foltescu, V. and de Leeuw, F. (2014) 'Air quality status and trends in Europe', *Atmospheric Environment*. Elsevier Ltd, 98, pp. 376–384. doi: 10.1016/j.atmosenv.2014.09.017.
- Gwimbi, P. (2017) 'Monitoring SO₂ emission trends and residents' perceived health risks from PGM smelting at Selous Metallurgical Complex in Zimbabwe', *International Journal for Equity in Health*. BioMed Central Ltd., 16(1). doi: 10.1186/s12939-017-0696-6.
- Hadi, M. (2011) *An Ultra Violet Optical Fibre Based Sensor For Ammonia Detection in the Agricultural Sector*.
- Hardesty, J. H. and Attili, B. (2010) *Spectrophotometry and the Beer-Lambert Law: An Important Analytical Technique in Chemistry, Collin College*.

- Hirayama, H. (2018) 'Recent Progress in AlGaIn Deep-UV LEDs', in *Light-Emitting Diode - An Outlook On the Empirical Features and Its Recent Technological Advancements*. InTech. doi: 10.5772/intechopen.79936.
- Ho, K. C. and Hung, W. T. (2001) 'An amperometric NO₂ gas sensor based on Pt/Nafion® electrode', *Sensors and Actuators, B: Chemical*, 79(1), pp. 11–16. doi: 10.1016/S0925-4005(01)00782-1.
- Hoera, C. *et al.* (2018) 'A chip-integrated optical microfluidic pressure sensor', *Sensors and Actuators, B: Chemical*. Elsevier, 255, pp. 2407–2415. doi: 10.1016/j.snb.2017.08.195.
- Hopkins, J. L. (2014) *Using commercial amateur astronomical spectrographs*. Available at: <http://dx.doi.org/10.1007/978-3-319-01442-5> (Accessed: 17 December 2019).
- Houck, M. M., Crispino, F. and McAdam, T. (2018) 'Detecting', in *The Science of Crime Scenes*. Elsevier, pp. 149–165. doi: 10.1016/b978-0-12-849878-1.00015-6.
- Iftiqar, S. M. *et al.* (2012) 'Fabrication of Crystalline Silicon Solar Cell with Emitter Diffusion, SiN_x Surface Passivation and Screen Printing of Electrode', in *Photodiodes - From Fundamentals to Applications*. InTech. doi: 10.5772/51065.
- Inagaki, T., Watanabe, T. and Tsuchikawa, S. (2017) 'The effect of path length, light intensity and co-Added time on the detection limit associated with NIR spectroscopy of potassium hydrogen phthalate in aqueous solution', *PLoS ONE*. Public Library of Science, 12(5). doi: 10.1371/journal.pone.0176920.
- Inaoka, M. (2005) 'Environmental Pollution Control Measures', in *Japan's Experiences in Public Health and Medical Services*. Japan International Cooperation Agency (JICA), pp. 145–164.
- International Energy Agency (2016) *World Energy Outlook 2016 Special Report: Energy and Air Quality*, International Energy Agency. doi: <http://www.worldenergyoutlook.org/publications/weo-2016/>.
- ISO International Standard 21348 (2007) *Space Environment (Natural and Artificial)*. Available at: <http://www.spacewx.com>.
- Izquierdo-Casas, P. M. *et al.* (2012) 'Colloidal silver complex as an alternative to sulphur dioxide in winemaking', *Food Control*, 23, pp. 73–81. doi: 10.1016/j.foodcont.2011.06.014.
- James, S. W. and Tatam, R. P. (no date) 'Fibre Optic Sensors with Nano-Structured Coatings', *Journal of Optics A: Pure and Applied Optics*, 8(7), pp. S430–S444.
- Jamieson, J. (1982) 'Fibre-optic military communications', *Computer Communications*, 5(4), pp. 171–175. doi: 10.1016/0140-3664(82)90111-6.
- Jiang, H. *et al.* (2013) 'Multilayer fiber optic sensors for in situ gas monitoring in harsh environments', *Sensors and Actuators B: Chemical*, 177, pp. 205–212. doi: 10.1016/j.snb.2012.10.122.

- Juang, J. and Radharamanan, R. (2009) 'Evaluation of Ring Laser and', American S.
- Kali Charan Sahu (2007) *Textbook of Remote Sensing and Geographical Information Systems*. Atlantic Publisher & Distributors (P) LTD. Available at: [https://books.google.com.my/books?id=tdP2NELOdHcC&pg=PA30&dq=Absorption+of+ultraviolet+\(UV\)+in+the+atmosphere+is+chiefly+due+to+electronic+transitions+of+the+atomic+and+molecular+oxygen+and+nitrogen.+Due+to+the+ultraviolet+absorption,+some+of+the+oxygen+a](https://books.google.com.my/books?id=tdP2NELOdHcC&pg=PA30&dq=Absorption+of+ultraviolet+(UV)+in+the+atmosphere+is+chiefly+due+to+electronic+transitions+of+the+atomic+and+molecular+oxygen+and+nitrogen.+Due+to+the+ultraviolet+absorption,+some+of+the+oxygen+a) (Accessed: 17 July 2019).
- Kang, S. J. and Donnelly, V. M. (2007) 'Optical absorption and emission spectroscopy studies of ammonia-containing plasmas', *Plasma Sources Science and Technology*, 16(2), pp. 265–272. doi: 10.1088/0963-0252/16/2/008.
- Kaspers, O. P., Sterenborg, H. J. C. M. and Amelink, A. (2008) 'Controlling the optical path length in turbid media using differential path-length spectroscopy: Fiber diameter dependence', *Applied Optics*. OSA - The Optical Society, 47(3), pp. 365–371. doi: 10.1364/AO.47.000365.
- Kenneth Hopkins, F. *et al.* (2018) 'Photodiode array for characterizing optical fibers', *Applied Optics*. The Optical Society, 57(3), p. 409. doi: 10.1364/ao.57.000409.
- Khokhar, M. F., Platt, U. and Wagner, T. (2008) 'Temporal trends of anthropogenic SO₂ emitted by non-ferrous metal smelters in Peru and Russia estimated from Satellite observations', *Atmospheric Chemistry and Physics Discussions*. Copernicus GmbH, 8(5), pp. 17393–17422. doi: 10.5194/acpd-8-17393-2008.
- Kim, J. *et al.* (2019) 'A disposable microfluidic flow sensor with a reusable sensing substrate', *Sensors and Actuators, B: Chemical*. Elsevier, 288, pp. 147–154. doi: 10.1016/j.snb.2019.02.088.
- Kim, K. H. and Kim, M. Y. (2001) 'Comparison of an open path differential optical absorption spectroscopy system and a conventional in situ monitoring system on the basis of long-term measurements of SO₂, NO₂, and O₃', *Atmospheric Environment*, 35(24), pp. 4059–4072. doi: 10.1016/S1352-2310(01)00216-3.
- Kim, M. *et al.* (2013) 'Integrated microfluidic-based sensor module for real-time measurement of temperature, conductivity, and salinity to monitor reverse osmosis', *Desalination*. Elsevier, 317, pp. 166–174. doi: 10.1016/j.desal.2013.03.007.
- King, R. B. (2005) *Encyclopedia of Inorganic Chemistry*. 2nd editio. Wiley.
- Kitamura, R., Pilon, L. and Jonasz, M. (2007) 'Optical constants of silica glass from extreme ultraviolet to far infrared at near room temperature', *Applied Optics*. OSA - The Optical Society, 46(33), pp. 8118–8133. doi: 10.1364/AO.46.008118.
- Kreutz, M. E. *et al.* (2001) 'Communication architectures for system-on-chip', in *Proceedings - 14th Symposium on Integrated Circuits and Systems Design, SBCCI 2001*. Institute of Electrical and Electronics Engineers Inc., pp. 14–19. doi: 10.1109/SBCCI.2001.952997.

- Krivetskiy, V. *et al.* (2018) 'Selective detection of individual gases and CO/H₂ mixture at low concentrations in air by single semiconductor metal oxide sensors working in dynamic temperature mode', *Sensors and Actuators, B: Chemical*. Elsevier B.V., 254, pp. 502–513. doi: 10.1016/j.snb.2017.07.100.
- Kumar, A. *et al.* (2019) 'Numerical model for the chemical adsorption of oxygen and reducing gas molecules in presence of humidity on the surface of semiconductor metal oxide for gas sensors applications', *Materials Science in Semiconductor Processing*. Elsevier Ltd, 90, pp. 236–244. doi: 10.1016/j.mssp.2018.10.020.
- Kumar, R., Avasthi, D. K. and Kaur, A. (2017) 'Fabrication of chemiresistive gas sensors based on multistep reduced graphene oxide for low parts per million monitoring of sulfur dioxide at room temperature', *Sensors and Actuators B*, 242, pp. 461–468. doi: 10.1016/j.snb.2016.11.018.
- Lagalante, A. F. (1999) 'Atomic absorption spectroscopy: A tutorial review', *Applied Spectroscopy Reviews*, pp. 173–189. doi: 10.1081/asr-100100844.
- Landsbergen, D., Shiang, J. and Byrnes, P. (1994) 'Fiber optic highways and network bridges: Planning for the telecommunications infrastructure needs of the city in the 21st century', *Telematics and Informatics*, 11(3), pp. 255–274. doi: 10.1016/0736-5853(94)90010-8.
- Lecler, S. and Meyrueis, P. (2012) 'Intrinsic Optical Fiber Sensor', *Fiber Optic Sensors*. doi: 10.5772/27079.
- Lesser, M. (2014) 'Charge coupled device (CCD) image sensors', in *High Performance Silicon Imaging: Fundamentals and Applications of CMOS and CCD sensors*. Elsevier Inc., pp. 78–97. doi: 10.1533/9780857097521.1.78.
- Lesser, M. (2015) 'A Summary of Charge-Coupled Devices for Astronomy', *Publications of the Astronomical Society of the Pacific*. IOP Publishing, 127(957), pp. 1097–1104. doi: 10.1086/684054.
- Li, C. *et al.* (2017) 'India Is Overtaking China as the World's Largest Emitter of Anthropogenic Sulfur Dioxide', *Scientific Reports*. Nature Publishing Group, 7(1). doi: 10.1038/s41598-017-14639-8.
- Li, X. *et al.* (2012) 'Rapid, on-site identification of explosives in nanoliter droplets using a UV reflected fiber optic sensor.', *Analytica chimica acta*, 751, pp. 112–8. doi: 10.1016/j.aca.2012.09.022.
- Liu, C.-C. *et al.* (2017) 'Rapid integrated microfluidic paper-based system for sulfur dioxide detection'. doi: 10.1016/j.cej.2017.02.023.
- Liu, L. H. *et al.* (2012) 'Adduct of magnesium tetraphenylporphyrin with aniline for colorimetric detection of SO₂', *Chinese Chemical Letters*. doi: 10.1016/j.ccllet.2011.10.018.
- Lu, G., Ocola, L. E. and Chen, J. (2009) 'Reduced graphene oxide for room-temperature gas sensors', *Nanotechnology*. IOP Publishing, 20(44), p. 445502. doi: 10.1088/0957-4484/20/44/445502.

- Lu, X. *et al.* (2005) ‘Solid-state amperometric hydrogen sensor based on polymer electrolyte membrane fuel cell’, *Sensors and Actuators, B: Chemical*, 107(2), pp. 812–817. doi: 10.1016/j.snb.2004.12.022.
- Lu, Z., Zhang, Q. and Streets, D. G. (2011) ‘Sulfur dioxide and primary carbonaceous aerosol emissions in China and India, 1996-2010’, *Atmospheric Chemistry and Physics*, pp. 9839–9864. doi: 10.5194/acp-11-9839-2011.
- Lupan, O., Chow, L. and Chai, G. (2009) ‘A single ZnO tetrapod-based sensor’, *Sensors and Actuators, B: Chemical*, 141(2), pp. 511–517. doi: 10.1016/j.snb.2009.07.011.
- Makgato, S. S. and Chirwa, E. M. N. (2017) ‘Waterberg coal characteristics and SO₂ minimum emissions standards in South African power plants’, *Journal of Environmental Management*. Academic Press, 201, pp. 294–302. doi: 10.1016/j.jenvman.2017.06.049.
- Martini, V. *et al.* (2012) ‘Microfluidic gas sensor with integrated pumping system’, in *Sensors and Actuators, B: Chemical*. Elsevier, pp. 45–50. doi: 10.1016/j.snb.2011.01.011.
- Martono, S., Febriani, I. and Rohman, A. (2018) ‘Application of liquid chromatography-photodiode array detector for analysis of whitening agents in cream cosmetics’, *Journal of Applied Pharmaceutical Science*, 8(5), pp. 143–147. doi: 10.7324/JAPS.2018.8520.
- Maushake, P. (2008) ‘Calcium Fluoride Crystals’, *Optik & Photonik*, 3(2), pp. 46–47. doi: 10.1002/opph.201190192.
- Mei, L., Zhao, G. and Svanberg, S. (2014) ‘Differential absorption lidar system employed for background atomic mercury vertical profiling in South China’, *Optics and Lasers in Engineering*, 55, pp. 128–135. doi: 10.1016/j.optlaseng.2013.10.028.
- Merlo, S., Norgia, M. and Donati, S. (2002) ‘Fiber gyroscope principles’, *Handbook of Optical Fibre Sensing Technology*.
- Mirzaei, A. *et al.* (2013) ‘Transient response of buried oil pipelines fiber optic leak detector based on the distributed temperature measurement’, *International Journal of Heat and Mass Transfer*, 65, pp. 110–122. doi: 10.1016/j.ijheatmasstransfer.2013.05.062.
- Misra, S. C. K., Mathur, P. and Srivastava, B. K. (2004) ‘Vacuum-deposited nanocrystalline polyaniline thin film sensors for detection of carbon monoxide’, *Sensors and Actuators A: Physical*, 114(1), pp. 30–35. doi: 10.1016/j.sna.2004.02.026.
- Mohaghegh Montazeri, M., O’Brien, A. and Hoorfar, M. (2019) ‘Understanding microfluidic-based gas detectors: A numerical model to investigate fundamental sensor operation, influencing phenomena and optimum geometries’, *Sensors and Actuators B: Chemical*. doi: 10.1016/j.snb.2019.126904.

- Mohajan, H. K. (2014) 'Chinese Sulphur Dioxide Emissions and Local Environment Pollution', *International Journal of Scientific Research in Knowledge*. IJSR Publications, 2(6), pp. 265–276. doi: 10.12983/ijsrk-2014-p0265-0276.
- Molebny, V. *et al.* (2016) 'Laser radar: historical prospective—from the East to the West', *Optical Engineering*. SPIE-Intl Soc Optical Eng, 56(3), p. 031220. doi: 10.1117/1.oe.56.3.031220.
- Mondal, B. *et al.* (2015) 'Quantitative recognition of flammable and toxic gases with artificial neural network using metal oxide gas sensors in embedded platform', *Engineering Science and Technology, an International Journal*. Elsevier B.V., 18(2), pp. 229–234. doi: 10.1016/j.jestch.2014.12.010.
- Mörmann, D. *et al.* (2003) 'GEM-based gaseous photomultipliers for UV and visible photon imaging', in *Nuclear Instruments and Methods in Physics Research, Section A: Accelerators, Spectrometers, Detectors and Associated Equipment*, pp. 93–98. doi: 10.1016/S0168-9002(03)00760-5.
- Morris, D. P. (2009) 'Optical Properties of Water', in *Encyclopedia of Inland Waters*. Elsevier Inc., pp. 682–689. doi: 10.1016/B978-012370626-3.00069-7.
- Muramoto, Y., Kimura, M. and Nouda, S. (2015) 'Development and future of ultraviolet light-emitting diodes ~uV-LED will replace UV lamp~', in *2015 IEEE Summer Topicals Meeting Series, SUM 2015*, pp. 13–14. doi: 10.1109/PHOSST.2015.7248169.
- NASA. (2016) *Global Sulfur Dioxide Monitoring Home Page*. Available at: <https://so2.gsfc.nasa.gov/measures.html> (Accessed: 4 December 2019).
- NASA (no date) *Atmospheric Chemistry (AURA)*. Available at: <https://aura.gsfc.nasa.gov/omi.html> (Accessed: 4 December 2019).
- Nguyen, T. X. *et al.* (2014) 'An Intrinsic Fiber-Optic Sensor for Structure Lightning Current Measurement', *23rd International Lightning Detection Conference, 5th International Lightning Meteorology Conference*.
- Norazmi, N. *et al.* (2018) 'UV Detection on Artificial Uric Acid Using UV-Vis Spectrometer', *Journal of Lasers, Optics & Photonics*, 05(01), p. 179. doi: 10.4172/2469-410x.1000179.
- O'Keeffe, S. *et al.* (2010) 'Real-time monitoring of agricultural ammonia emissions based on optical fibre sensing technology', in *Proceedings of IEEE Sensors*, pp. 1140–1143. doi: 10.1109/ICSENS.2010.5690821.
- Ocean Optics (2019) *Home - Ocean Optics*. Available at: <https://oceanoptics.com/> (Accessed: 18 July 2019).
- Ohtsu, M., Kotani, H. and Tagawa, H. (1983) 'Spectral Measurements of NH₃ and H₂O for Pollutant Gas Monitoring by 1.5 μm InGaAsP/InP Lasers', *Japanese Journal of Applied Physics*. Japan Society of Applied Physics, 22(Part 1, No. 10), pp. 1553–1557. doi: 10.1143/jjap.22.1553.

Olive, B. S. (2007) *Absorption Spectrum of Sulfur Dioxide*, MPI-Mainz UV/VIS Spectral Atlas. doi: 10.5194/essd-5-365-2013.

Olive, B. S. (2015) *Absorption spectra of benzene, toluene, and sulfur dioxide*, MPI-Mainz UV/VIS Spectral Atlas. doi: 10.5194/essd-5-365-2013.

Oliveira, C. N. P., Khoury, H. J. and Santos, E. J. P. (2016) 'PiN photodiode performance comparison for dosimetry in radiology applications', *Physica Medica*. Associazione Italiana di Fisica Medica, 32(12), pp. 1495–1501. doi: 10.1016/j.ejmp.2016.10.018.

Orna, M. V. (2013) 'Discovery of the Physics of Color', in, pp. 11–28. doi: 10.1007/978-3-642-32642-4_2.

Ouyang, B. and Jones, R. L. (2012) 'Understanding the sensitivity of cavity-enhanced absorption spectroscopy: Pathlength enhancement versus noise suppression', *Applied Physics B: Lasers and Optics*, 109(4), pp. 581–591. doi: 10.1007/s00340-012-5178-3.

P.S. Kalsi (2004) *Spectroscopy of Organic Compounds*. 6th edn. New Age International Publisher. Available at: https://books.google.com.my/books?id=QWq47QCIOM0C&printsec=frontcover&source=gbs_ge_summary_r&cad=0#v=onepage&q&f=false (Accessed: 18 July 2019).

Pendse, D. R. and Chin, A. K. (2001) 'Cathodoluminescence and Transmission Cathodoluminescence', in *Encyclopedia of Materials: Science and Technology*. Elsevier, pp. 1–7. doi: 10.1016/b0-08-043152-6/00190-x.

Percuoco, R. (2013) 'Plain Radiographic Imaging', in *Clinical Imaging: With Skeletal, Chest, & Abdominal Pattern Differentials: Third Edition*. Elsevier Inc., pp. 1–43. doi: 10.1016/B978-0-323-08495-6.00001-4.

Perry, D. L. (2011) *Handbook of Inorganic Compounds*. 2nd edn. CRC press.

Pirronello, V. and Manicó, G. (1998) 'Radiation physics', *Earth, Moon and Planets*. Elsevier, 80(1–3), pp. 261–283. doi: 10.1023/A:1006382300634.

Platt, U. (2017) 'Air Monitoring by Differential Optical Absorption Spectroscopy', in *Encyclopedia of Analytical Chemistry*. Chichester, UK: John Wiley & Sons, Ltd, pp. 1–28. doi: 10.1002/9780470027318.a0706.pub2.

Point and nonpoint sources of water pollution (no date).

Pollution: Definition of Pollution in Oxford Dictionary (British & World English) (no date).

Ponce Wong, R. D., Posner, J. D. and Santos, V. J. (2012) 'Flexible microfluidic normal force sensor skin for tactile feedback', *Sensors and Actuators, A: Physical*. doi: 10.1016/j.sna.2012.03.023.

- Pospíšilová, M., Kuncová, G. and Trögl, J. (2015) 'Fiber-optic chemical sensors and fiber-optic bio-sensors', *Sensors (Switzerland)*, pp. 25208–25259. doi: 10.3390/s151025208.
- Rahman Khan, R. and Siddiqui, M. J. . (2014) *Review on effects of Particulates; Sulfur Dioxide and Nitrogen Dioxide on Human Health, Int. Res. J. Environment Sci. International Science Congress Association*. Available at: www.isca.me (Accessed: 2 December 2019).
- Ramdzan, A. N. *et al.* (2016) 'Development of a microfluidic paper-based analytical device for the determination of salivary aldehydes', *Analytica Chimica Acta*. Elsevier, 919, pp. 47–54. doi: 10.1016/j.aca.2016.03.030.
- Rasmussen, A. *et al.* (2001) 'Simulation and optimization of a microfluidic flow sensor', *Sensors and Actuators, A: Physical*. Elsevier, 88(2), pp. 121–132. doi: 10.1016/S0924-4247(00)00503-3.
- Ray, S. and Kim, K. H. (2014) 'The pollution status of sulfur dioxide in major urban areas of Korea between 1989 and 2010', *Atmospheric Research*. Elsevier Ltd, 147–148, pp. 101–110. doi: 10.1016/j.atmosres.2014.05.011.
- Richard, K. (2000) 'Carbon Monoxide Detector', *Carbon Monoxide Toxicity*. 1st edn. Edited by D. G. Penney. CRC press, (714), p. 584.
- Rogers, E. I. *et al.* (2010) 'Amperometric gas detection using room temperature ionic liquid solvents', in *ECS Transactions*, pp. 473–502. doi: 10.1149/1.3484806.
- Rößner, M. R. *et al.* (2012) 'Broadband light source for fiber-optic measurement system in spaceborne applications', *Acta Astronautica*, 70, pp. 95–99. doi: 10.1016/j.actaastro.2011.07.018.
- Rouse, J. A. (2018) 'Three Dimensional Computer Modeling of Electron Optical Systems', *Advances in Imaging and Electron Physics*. doi: 10.1016/bs.aiep.2018.09.001.
- S.C.Gad (2014) 'Sulfur Dioxide', *Encyclopedia of Toxicology (Third Edition)*. Academic Press, pp. 420–423. doi: 10.1016/B978-0-12-386454-3.00933-7.
- Sahney, S., Benton, M. J. and Ferry, P. A. (2010) 'Links between global taxonomic diversity, ecological diversity and the expansion of vertebrates on land.', *Biology Letters*, 6(4), pp. 544–577. doi: 10.1098/rsbl.2009.1024.
- Salaha, M. I. *et al.* (2008) 'A natural alternative to sulphur dioxide for red wine production: Influence on colour, antioxidant activity and anthocyanin content', *Journal of Food Composition and Analysis*, 21, pp. 660–666. doi: 10.1016/j.jfca.2008.03.010.
- Salahudin, S. N., Abdullah, M. M. and Newaz, N. A. (2013) 'Emissions : Sources , Policies and Development in Malaysia', *International Journal of Education and Research*, 1.

- Saldanha, P. L. and Monken, C. H. (2011) 'Interaction between light and matter: A photon wave function approach', *New Journal of Physics*, 13. doi: 10.1088/1367-2630/13/7/073015.
- Saleh, A. A., A Mustafa, A. B. and Osman, A. A. (2015) 'Feasibility of Laying Fiber-Optic Cables underwater along River Nile Basin-Sudan Study Case', *IOSR Journal of Computer Engineering Ver. V*, 17(1), pp. 2278–661. doi: 10.9790/0661-17154852.
- Salim, M. R. *et al.* (2018) 'Highly responsive CO₂ detection by an improved & compact gas sensor using mid-IR spectroscopy', *Journal of Telecommunication, Electronic and Computer Engineering*, 10(2–8), pp. 1–7.
- De Sanctis, A. *et al.* (2018) 'Graphene-based light sensing: Fabrication, characterisation, physical properties and performance', *Materials*. doi: 10.3390/ma11091762.
- Sanders, M. *et al.* (2014) 'An enhanced LSPR fiber-optic nanoprobe for ultrasensitive detection of protein biomarkers.', *Biosensors & bioelectronics*, 61, pp. 95–101. doi: 10.1016/j.bios.2014.05.009.
- Sathiyamoorthi, R. *et al.* (2004) 'Study of electrochemical based gas sensors for fluorine and chlorine', *Sensors and Actuators, B: Chemical*, 99(2–3), pp. 336–339. doi: 10.1016/j.snb.2003.11.031.
- Sberveglieri, G. (1995) 'Recent developments in semiconducting thin-film gas sensors', *Sensors and Actuators: B. Chemical*, 23(2–3), pp. 103–109. doi: 10.1016/0925-4005(94)01278-P.
- SCHENK, B. and RAAKE, D. (1999) *Local Strain and Temperature Measurement, Local Strain and Temperature Measurement*. Elsevier. doi: 10.1016/B978-1-85573-424-1.50025-3.
- Scholar, B. (2012) 'Fiber Optics And Its Types For Sensing Applications In Various Fields', *International Journal of Engineering*, 1(7), pp. 1–7. Available at: <http://www.ijert.org/browse/september-2012-edition?download=994:fiber-optics-and-its-types-for-sensing-applications-in-various-fields&start=70>.
- Schütze, C. *et al.* (2013) 'Ground-based Remote Sensing with Open-path Fourier-transform Infrared (OP-FTIR) Spectroscopy for Large-scale Monitoring of Greenhouse Gases', *Energy Procedia*, 37, pp. 4276–4282. doi: 10.1016/j.egypro.2013.06.330.
- Sebastián, E., Armiens, C. and Gómez-Elvira, J. (2010) 'Pyrometer model based on sensor physical structure and thermal operation', *Applied Thermal Engineering*, 30(16), pp. 2403–2411. doi: 10.1016/j.applthermaleng.2010.06.010.
- Shamir, A. (2006) 'An overview of Optical Gyroscopes Theory, Practical Aspects, Applications and Future Trends'.
- Sharma, R. K. (2017) 'Various Spectroscopic Techniques', in Gurjar, B. R. and Kumar, P. (eds) *Environmental Pollution Monitoring, Modeling and Control*. 1st edn. Studium Press LLC, U.S.A., pp. 181–206.

- Shi, Q. *et al.* (2016) 'Self-powered liquid triboelectric microfluidic sensor for pressure sensing and finger motion monitoring applications', *Nano Energy*. Elsevier, 30, pp. 450–459. doi: 10.1016/j.nanoen.2016.10.046.
- Shimizu, Y. *et al.* (2001) 'Improvement of SO₂ sensing properties of WO₃ by noble metal loading', *Sensors and Actuators, B: Chemical*, 77(1–2), pp. 35–40. doi: 10.1016/S0925-4005(01)00669-4.
- Shivang Ghetia, Ruchi Gajjar and P Trivedi (2013a) 'Classification of Fiber Optical Sensors', *International Journal of Electronics Communication and Computer Technology*, 3(4), pp. 442–445. Available at: www.ijecct.org (Accessed: 12 December 2019).
- Shivang Ghetia, Ruchi Gajjar and P Trivedi (2013b) 'Classification of Fiber Optical Sensors', *International Journal of Electronics Communication and Computer Technology*.
- Shonnard, D. R. and Allen, D. T. (2010) 'An Introduction to Environmental Issues and Sustainability', in, pp. 1–35.
- Silvester, D. S. (2011) 'Recent advances in the use of ionic liquids for electrochemical sensing', *Analyst*. Royal Society of Chemistry, pp. 4871–4882. doi: 10.1039/c1an15699c.
- Simmons, M. K. (no date) *Sulfur Dioxide Fact Sheet*, U.S. Department of Labor, Occupational Safety and Health Administration.
- Singh, J. *et al.* (2012) 'Sulfur dioxide and nitrogen dioxide adsorption on zinc oxide and zirconium hydroxide nanoparticles and the effect on photoluminescence', *Applied Surface Science*, 258(15), pp. 5778–5785. doi: 10.1016/j.apsusc.2012.02.093.
- Singh, M. and Issar, S. (2017) *Indonesia's Coal Power Emission Norms*. Available at: <https://icel.or.id/wp-content/uploads/Policy-Paper.-ICEL-CSE-REEI-2017-Indonesias-Coal-Power-Emission-Norms-Lessons-from-India-China.pdf> (Accessed: 4 December 2019).
- Smith, B. C. (2002) *Quantitative Spectroscopy: Theory and Practice*, *Quantitative Spectroscopy: Theory and Practice*. Academic Press. doi: 10.1016/b978-0-12-650358-6.x5000-3.
- SO₂ MATERIAL SAFETY DATA SHEET* (no date).
- SO₂ SAFETY DATA SHEET* (no date).
- Srivastava, R. K. *et al.* (1994) 'Sensing mechanism in tin oxide-based thick-film gas sensors', *Sensors and Actuators: B. Chemical*, 21(3), pp. 213–218. doi: 10.1016/0925-4005(94)01248-2.
- Stewart, J. J. P. (2019) 'An examination of the nature of localized molecular orbitals and their value in understanding various phenomena that occur in organic chemistry', *Journal of Molecular Modeling*. Springer Verlag, 25(1). doi: 10.1007/s00894-018-3880-8.

Stotts, L. B. (2019) *Free Space Optical Systems Engineering: Design and Analysis (Stotts, L.B.) [Book Review]*, *IEEE Aerospace and Electronic Systems Magazine*. Institute of Electrical and Electronics Engineers (IEEE). doi: 10.1109/maes.2019.2914984.

Sulfur Dioxide: Science behind this anti-microbial, anti-oxidant, wine additive | Practical Winery & Vineyard Journal (no date).

Sulfur Dioxide (no date) *Canadian Centre for Occupational Health and Safety*.

Sung, L.-Y. and Lu, C.-J. (2014) 'A single-beam titration method for the quantification of open-path Fourier transform infrared spectroscopy', *Journal of Quantitative Spectroscopy and Radiative Transfer*, 145, pp. 43–49. doi: 10.1016/j.jqsrt.2014.04.016.

Taieb, D. and Ben Brahim, A. (2013) 'Electrochemical method for sulphur dioxide removal from flue gases: Application on sulphuric acid plant in Tunisia', *Comptes Rendus Chimie*, 16, pp. 39–50. doi: 10.1016/j.crci.2012.08.009.

Taniyasu, Y., Kasu, M. and Makimoto, T. (2006) 'An aluminium nitride light-emitting diode with a wavelength of 210 nanometres', *Nature*. Nature Publishing Group, 441(7091), pp. 325–328. doi: 10.1038/nature04760.

Tao, S. X., Chan, H. W. and Van Der Graaf, H. (2016) 'Secondary electron emission materials for transmission dynodes in novel photomultipliers: A review', *Materials*. MDPI AG. doi: 10.3390/ma9121017.

Taylor, G. A. and Thacker, J. C. (1982) 'Fibre optics systems for space applications', *Optics & Laser Technology*, 14(2), pp. 93–97. doi: 10.1016/0030-3992(82)90008-1.

Thakral, S. and Manhas, P. (2011) 'Fiber Optic Sensors Technology & their applications', *International Journal of Electronics & Communication Technology*, 2(2), pp. 126–128.

The European Parliament and the Council of the European Union (1998) *Directive 98/70/EC - Quality of petrol and diesel fuels*, *Official Journal of the European Union*. Available at: <https://www.eea.europa.eu/policy-documents/directive-98-70-ec-quality> (Accessed: 11 August 2020).

Thoeniss, T. and Mewes, S. (2014) 'UV Light - Demands On Optical Systems', (March 2008), pp. 17–22.

Tiffenberg, J. *et al.* (2017) 'Single-Electron and Single-Photon Sensitivity with a Silicon Skipper CCD', *Physical Review Letters*, 119(13). doi: 10.1103/PhysRevLett.119.131802.

Tiwari, M. K., Bajpai, S. and Dewangan, U. K. (2019) 'Environmental Issues in Thermal Power Plants-Review in Chhattisgarh Context', *J. Mater. Environ. Sci*, 10(11), pp. 1123–1134. Available at: <http://www.jmaterenvironsci.com> (Accessed: 5 December 2019).

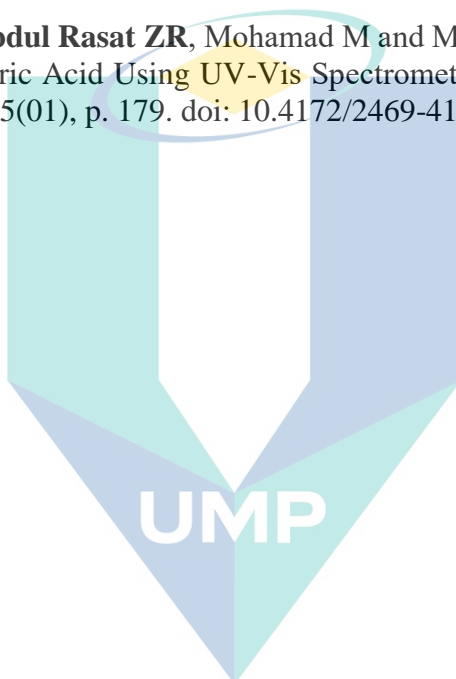
- Tomchenko, A. A. *et al.* (2003) 'Semiconducting metal oxide sensor array for the selective detection of combustion gases', *Sensors and Actuators B: Chemical*, 93(1–3), pp. 126–134. doi: 10.1016/S0925-4005(03)00240-5.
- Toniolo, R. *et al.* (2010) 'A sensor based on electrodes supported on ion-exchange membranes for the flow-injection monitoring of sulphur dioxide in wines and grape juices.', *Talanta*, 80(5), pp. 1809–15. doi: 10.1016/j.talanta.2009.10.024.
- Trottier, S. *et al.* (2009) 'Atmospheric monitoring for the Pembina Cardium CO₂ Monitoring Project using open path laser technology', *Energy Procedia*, 1(1), pp. 2307–2314. doi: 10.1016/j.egypro.2009.01.300.
- Tyagi, P. *et al.* (2016a) 'Metal oxide catalyst assisted SnO₂ thin film based SO₂ gas sensor', *Sensors and Actuators B*, 224, pp. 282–289. doi: 10.1016/j.snb.2015.10.050.
- Tyagi, P. *et al.* (2016b) 'Metal oxide catalyst assisted SnO₂ thin film based SO₂ gas sensor', *Sensors and Actuators, B: Chemical*. Elsevier, 224, pp. 282–289. doi: 10.1016/j.snb.2015.10.050.
- Tyagi, P. *et al.* (2017) 'SnO₂ thin film sensor having NiO catalyst for detection of SO₂ gas with improved response characteristics', *Sensors and Actuators, B: Chemical*. Elsevier B.V., 248, pp. 998–1005. doi: 10.1016/j.snb.2017.02.168.
- UNECE (2007) *Review of the 1999 Gothenburg Protocol. ECE.EB.AIR 2007/10: United Nations Economic Commission for Europe, Geneva, Switzerland*. Available at: <https://digitallibrary.un.org/record/610518?ln=en> (Accessed: 11 August 2020).
- Uneme, Y., Tamura, S. and Imanaka, N. (2013) 'Sulfur dioxide gas sensor based on Zr⁴⁺ and O²⁻ ion conducting solid electrolytes with lanthanum oxysulfate as an auxiliary sensing electrode', *Sensors and Actuators B: Chemical*, 177, pp. 529–534. doi: 10.1016/j.snb.2012.11.010.
- US EPA, O. (no date) 'Sulfur Dioxide Trends'. *UV-visible absorption spectra* (no date). Available at: <https://www.chemguide.co.uk/analysis/uvvisible/theory.html> (Accessed: 18 July 2019).
- Vahedian, M. *et al.* (2017) 'Ambient air pollution and daily hospital admissions for cardiovascular diseases in Arak, Iran', *ARYA Atherosclerosis*. Isfahan University of Medical Sciences(IUMS), 13(3), pp. 117–134.
- Vahlsing, C. and Smith, K. R. (2012) 'Global review of national ambient air quality standards for PM₁₀ and SO₂ (24 h)', *Air Quality, Atmosphere and Health*, pp. 393–399. doi: 10.1007/s11869-010-0131-2.
- Vestreng, V. *et al.* (2009) 'Evolution of NO_x emissions in Europe with focus on road transport control measures', *Atmospheric Chemistry and Physics*. Copernicus GmbH, 9(4), pp. 1503–1520. doi: 10.5194/acp-9-1503-2009.

- Vukmirica, V. (2008) 'Interferometric Fiber Optic Gyroscope: Principle of Operation and Basic Parameters Determination', (3), pp. 83–91.
- Wang, C. *et al.* (2010) 'Metal oxide gas sensors: Sensitivity and influencing factors', *Sensors*, pp. 2088–2106. doi: 10.3390/s100302088.
- Wang, J. (2006) *Analytical Electrochemistry, Third Edition, Analytical Electrochemistry, Third Edition*. John Wiley and Sons. doi: 10.1002/0471790303.
- Wang, J., Zhu, B. and Niu, S. (2008) 'Differential optical absorption spectroscopy system for suburb of NanJing atmospheric pollution monitoring', in *2nd International Conference on Bioinformatics and Biomedical Engineering, iCBBE 2008*. IEEE Computer Society, pp. 4070–4074. doi: 10.1109/ICBBE.2008.518.
- Wang, M. *et al.* (2011) 'Using a mobile laboratory to characterize the distribution and transport of sulfur dioxide in and around Beijing', *Atmospheric Chemistry and Physics*, 11, pp. 11631–11645. doi: 10.5194/acp-11-11631-2011.
- Wang, S. and Chen, B. (2016) 'Accounting of SO₂ emissions from combustion in industrial boilers', in *Energy Procedia*. Elsevier Ltd, pp. 325–329. doi: 10.1016/j.egypro.2016.06.141.
- Wedzicha, B. L. (1991) 'Sulfur-Dioxide - the Most Versatile Food Additive', *Chemistry in Britain*, 27, pp. 1030–1032.
- Wei, P. S. *et al.* (2018) 'Absorption coefficient of carbon dioxide across atmospheric troposphere layer', *Heliyon*. Elsevier Ltd, 4(10). doi: 10.1016/j.heliyon.2018.e00785.
- Wesely, M. L. and Hicks, B. B. (1977) 'Some Factors that Affect the Deposition Rates of Sulfur Dioxide and Similar Gases on Vegetation', *Journal of the Air Pollution Control Association*, 27(11), pp. 1110–1116.
- Wetchakun, K. *et al.* (2011) 'Semiconducting metal oxides as sensors for environmentally hazardous gases', *Sensors and Actuators B: Chemical*, 160(1), pp. 580–591. doi: 10.1016/j.snb.2011.08.032.
- Worrell, W. L. and Liu, Q. G. (1984) 'A new sulphur dioxide sensor using a novel two-phase solid-sulphate electrolyte', *Journal of Electroanalytical Chemistry and Interfacial Electrochemistry*, 168(1–2), pp. 355–362. doi: 10.1016/0368-1874(84)87109-9.
- Wysokiński, K. *et al.* (2015) 'Study on the sensing coating of the optical fibre CO₂ sensor', *Sensors (Switzerland)*, 15, pp. 31888–31903. doi: 10.3390/s151229890.
- Xiong, L. and Compton, R. G. (2014) 'Amperometric gas detection: A review', *International Journal of Electrochemical Science*. Electrochemical Science Group, 9(12), pp. 7152–7181.
- Xu, G. *et al.* (2016) 'Evaluation of air pollutant emissions from scattered coal burning and electric heating in Beijing-Tianjin-Hebei region', *Research of Environmental Sciences*. doi: 10.13198/j.issn.1001-6929.2016.12.01.

- Xu, Y. (2011) 'Improvements in the operation of SO₂ scrubbers in Chinas coal power plants', *Environmental Science and Technology*, 45(2), pp. 380–385. doi: 10.1021/es1025678.
- Yamashita, Y. *et al.* (2013) 'A 340-nm-band ultraviolet laser diode composed of GaN well layers', *Optics Express*, 21(3), p. 3133. doi: 10.1364/oe.21.003133.
- Yan, S. Z. and Chyan, L. S. (2010) 'Performance enhancement of BOTDR fiber optic sensor for oil and gas pipeline monitoring', *Optical Fiber Technology*, 16(2), pp. 100–109. doi: 10.1016/j.yofte.2010.01.001.
- Yin, M. jie *et al.* (2018) 'Recent development of fiber-optic chemical sensors and biosensors: Mechanisms, materials, micro/nano-fabrications and applications', *Coordination Chemistry Reviews*. doi: 10.1016/j.ccr.2018.08.001.
- Yio, S. *et al.* (2008) 'Fiber Optic Sensors', *International Journal of Electrical, Computer, Energetic, Electronic and Communication Engineering*, 2(6), pp. 1107–1117.
- Yousif, E. and Haddad, R. (2013) 'Photodegradation and photostabilization of polymers, especially polystyrene: Review', *SpringerPlus*. doi: 10.1186/2193-1801-2-398.
- Yubero, C., García, M. C. and Calzada, M. D. (2008) 'Using a halogen lamp to calibrate an optical system for UV-VIS radiation detection', *Optica Applicata*, 38(2), pp. 353–363.
- Zanger, H. and Zanger, C. (1991) *Fiber optics : communication and other applications*, *International Journal of Innovative Research in Engineering & Science ISSN*.
- Zhang, C. *et al.* (2019) 'Room temperature conductive type metal oxide semiconductor gas sensors for NO₂ detection', *Sensors and Actuators, A: Physical*. Elsevier B.V., pp. 118–133. doi: 10.1016/j.sna.2019.02.027.
- Zhang, J. X. J. and Hoshino, K. (2019) 'Optical transducers: Optical molecular sensing and spectroscopy', in *Molecular Sensors and Nanodevices*. Elsevier, pp. 231–309. doi: 10.1016/b978-0-12-814862-4.00005-3.
- Zhang, Z. *et al.* (2019) 'A 271.8 nm deep-ultraviolet laser diode for room temperature operation', *Applied Physics Express*, 12(12), p. 124003. doi: 10.7567/1882-0786/ab50e0.
- Zheng, N. *et al.* (2018) 'Observations of atmospheric trace gases in China using a compact LED long path DOAS system', *Atmospheric Pollution Research*. Elsevier B.V., 9(2), pp. 379–387. doi: 10.1016/j.apr.2017.10.004.
- Zhou, Q. *et al.* (2016) 'Hydrothermal Synthesis and Responsive Characteristics of Hierarchical Zinc Oxide Nanoflowers to Sulfur Dioxide', *Journal of Nanotechnology*. Hindawi Limited, 2016. doi: 10.1155/2016/6742104.
- Zhou, Q. *et al.* (2019) 'High sensitive and low-concentration sulfur dioxide (SO₂) gas sensor application of heterostructure NiO-ZnO nanodisks', *Sensors and Actuators B: Chemical*, 298, p. 126870. doi: 10.1016/j.snb.2019.126870.

APPENDIX A
LIST OF PUBLICATIONS

1. **A. R. Zul Rasyied**, N. N. Mazlee, M. R. Salim, S. Nurulain, H. Manap (2018) ‘The potential development of oxygen optical fibre gas sensor for automotive industry’, *Journal of Telecommunication, Electronic and Computer Engineering*, 10(1–3), pp. 1–4.
2. N Norazmi , **ZR Abdul Rasat**, M Mohamad, and H Manap (2017) ‘Uric acid detection using uv-vis spectrometer’, *IOP Conference Series: Materials Science and Engineering*, 257(1). doi: 10.1088/1757-899X/257/1/012031.
3. Norazmi N, **Abdul Rasat ZR**, Mohamad M and Manap H (2018) ‘UV Detection on Artificial Uric Acid Using UV-Vis Spectrometer’, *Journal of Lasers, Optics & Photonics*, 05(01), p. 179. doi: 10.4172/2469-410x.1000179.



اونيورسيتي ملايسيا قهغ

UNIVERSITI MALAYSIA PAHANG

APPENDIX B DH2000-BAL SPECIFICATION SHEET



UV-NIR Spectral Range with Balanced Output

We've applied our expertise in patterned dichroic filters to an innovation in light source technology to create the only combined-spectrum illumination source available that eliminates saturation and signal-to-noise problems associated with the D-alpha line in the deuterium source. The DH-2000-BAL Deuterium Tungsten Halogen Light Source combines deuterium and tungsten halogen light sources in a single optical path, producing a powerful, stable output from 215-2000 nm.

About the D-alpha Line

All deuterium tungsten halogen sources have a D-alpha line, revealed as a sharp peak in the visible portion of the spectrum, that produces "unbalanced" output in the deuterium and tungsten halogen sources. Correcting for this peak – a sharp spectral feature near 655 nm -- is difficult. For example, if you adjust spectrometer integration time to reduce the intensity of this saturated peak, the efficiency of the system at ultraviolet wavelengths drops significantly, compromising the signal-to-noise of the spectrum. Also, spectrometer efficiency is typically greatest in the same general spectral range as the 655 nm line, exaggerating its effects.

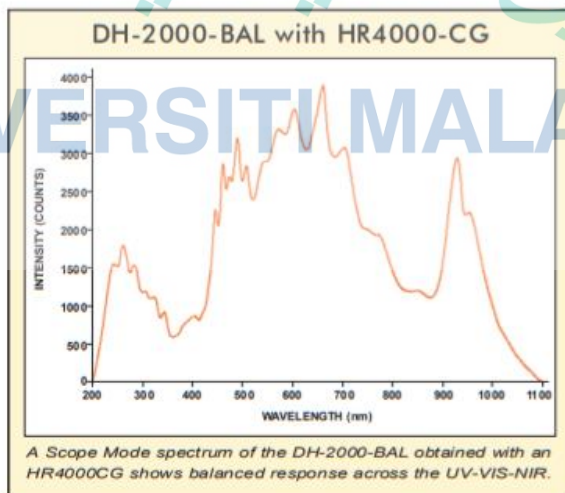
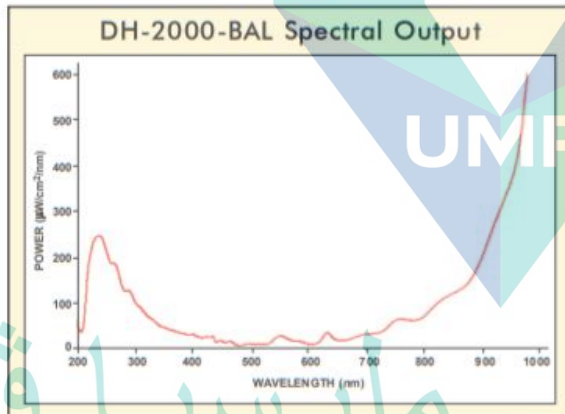
Proprietary Filtering Technology

Using the same high-precision patterned dichroic filter technology that distinguishes our Linear Variable Filters (page 80), the DH-2000-BAL:

- balances the intensity of the deuterium and tungsten halogen sources;
- eliminates the D-alpha, D-beta and Fulcher lines;
- eliminates problems associated with saturation; and
- produces a "smoother" spectrum across the entire wavelength range.

Optical Fibers

We recommend using our solarization-resistant optical fibers with the DH-2000-BAL. See pages 123 and 125 for details.



DH-2000-BAL

Specifications

Dimensions:	150 mm x 135 mm x 319 mm
Weight:	3.8 kg
Power consumption:	25 W (deuterium); 20 W (tungsten halogen)
Wavelength range:	215-400 nm (deuterium); 360-2000 nm (tungsten halogen)
Humidity:	5-95% non-condensing at 40 °C
Lamp voltage:	Ignition 350 V/20"
Tungsten bulb voltage:	Adjustable from 4.5 to 11.5 volts
Lamp current:	Operating 85 W/0.3A
Lamp lifetime:	1,000 hours
Current voltage drift:	<0.01% per hour
Voltage stability:	<5 x 10 ⁻⁶ peak-to-peak (0.1-10.0 Hz)
Operating temperature:	5 °C - 35 °C
Power requirements:	85-264 V 50/60 Hz
Power consumption:	190 W maximum
Warm-up time:	40 min. (deuterium); 20 min. (tungsten halogen)
Electronic certifications:	CE; VDI/VE 0160; EN 61010

APPENDIX C
SPECTROMETER SPECIFICATION SHEET

Maya2000 Series Components Table

Ocean Optics permanently secures all components in the Maya2000 Series Spectrometers at the time of manufacture. Only Ocean Optics technicians can replace interchangeable components, where noted.

Item	Name	Description
1	SMA Connector	Secures the input fiber to the spectrometer. Light from the input fiber enters the optical bench through this connector.
2	Slit	A dark piece of material containing a rectangular aperture, which is mounted directly behind the SMA Connector. The size of the aperture regulates the amount of light that enters the optical bench and controls spectral resolution. You can also use the Maya2000 Series Spectrometer without a Slit. In this configuration, the diameter of the fiber connected to the spectrometer determines the size of the entrance aperture. Only Ocean Optics technicians can change the Slit.
3	Filter	Restricts optical radiation to pre-determined wavelength regions. Light passes through the Filter before entering the optical bench. Both bandpass and longpass filters are available to restrict radiation to certain wavelength regions. Only Ocean Optics technicians can change the Filter.
4	Collimating Mirror	Focuses light entering the optical bench towards the Grating of the spectrometer. Light enters the spectrometer, passes through the SMA Connector, Slit, and Filter, and then reflects off the Collimating Mirror onto the Grating.
5	Grating	Diffraction light from the Collimating Mirror and directs the diffracted light onto the Focusing Mirror. Gratings are available in different groove densities, allowing you to specify wavelength coverage and resolution in the spectrometer. Only Ocean Optics technicians can change the Grating.
6	Focusing Mirror	Receives light reflected from the Grating and focuses the light onto the CCD Detector or L2 Detector Collection Lens (depending on the spectrometer configuration).
7	Detector with QFLV Filter	Eliminates second-order effects and is used with an HC-1 Grating in a 200-950 nm wavelength system in a Maya2000 Series spectrometer.
8	Back-thinned Area Detector	Provides 90% (Maya200) or 75% (Maya2000 Pro) quantum efficiency and bins pixels in a vertical column to acquire light from the entire height of the spectrometer's slit image. This improves light collection and signal-to-noise significantly. This 2D area detector is back-thinned (back-illuminated) and does not require the detector upgrade that is normally applied to other detectors. Only Ocean Optics technicians can add or remove the Detector.

Maya2000 Series Spectrometers Specifications

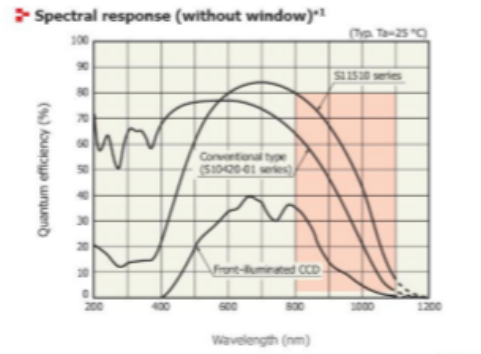
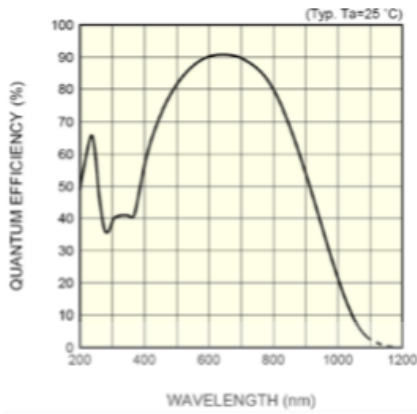
The following sections provide specification information for the CCD detector in the Maya2000 Series spectrometers, as well as for each model Maya2000 Series Spectrometer itself.

CCD Detector Specifications

Specification	Maya2000	Maya2000 Pro	Maya200Pro VIS-NIR
Detector	Hamamatsu S9840, back-thinned FFT-CCD	Hamamatsu S10420, back-thinned FFT-CCD	Hamamatsu S11510, back-thinned FFT-CCD
Thermoelectric cooling	No		
Number of pixels	All: 2080 x 20 Active: 2048 x 14	All: 2068 x 70 Active: 2048 x 64	
Spectral range	200-1100 nm with window, Deep UV option available (150nm). Deep UV option includes purge port and window removal. 175-1100 nm with HC1 grating.		
Pixel size	14 μ m square		
Pixel well depth	130 Ke-	200 Ke-	
Column height	196 μ m square	896 μ m square	
Detector active area (mm)	28.672 horizontal x 0.196 vertical	28.672 horizontal x 0.896 vertical	
Quantum efficiency: Peak QE QE @ 250 nm	>90% 55%	75% at 600 nm 60%	85% at 700 nm

اونيور سیتی ملیسیا قهغ

UNIVERSITI MALAYSIA PAHANG



*1: Spectral response with quartz glass is decreased according to the spectral transmittance characteristic of window material.

Quantum Efficiency of S9840 Detector

Quantum Efficiency of S10420 and S11510 Detectors

Maya2000 Series Spectrometer Specifications

Specification	Maya2000	Maya2000 Pro	Maya2000Pro VIS-NIR
Dimensions (LxWxH)	148.6 mm (5.85 in.) x 109.3 mm (4.30 in.) x 50.4 mm (1.98 in.)		
Weight	0.96 kg (2.12 lbs.)		
Temperature Operation Storage	-0 °C to +50 °C -30 °C to +70 °C		
Humidity	0 – 90% noncondensing		
Power consumption	500 mA @ 5 VDC		
Supply Voltage	4.5 – 5.5 V		
Power-up Time	~ 2s depending on code size		
Gratings	14 gratings available		
Entrance aperture	5, 10, 25, 50, 100 or 200 μ m wide slits		
Order-sorting filters	.6 OF series available		
Focal length (input)	f/4, 101 mm		
Optical resolution (FWHM)	Depends on grating and size of entrance aperture		

Specification	Maya2000	Maya2000 Pro	Maya2000Pro VIS-NIR
Stray light	<0.05% at 600 nm; <0.10% at 435 nm		
A/D converter	16 bit, 150 kHz+		
Dynamic range Spec Typical	5000:1 8000:1+		8000:1 12000:1+
Signal-to-noise ratio	350:1		450:1
Non-linearity Uncorrected Corrected	~4% <1.0%		~10.0% <1.0%
Fiber optic connector	SMA 905 to single-strand optical fiber (0.22 NA)		
Integration time	6 ms to 10 seconds		6 ms to 5 seconds
Interfaces			USB 2.0

System Compatibility

You can use the Maya2000 Series' USB connectivity with any computer that meets the requirements for the spectrometer operating software being used (Windows 98/Me/2000/XP, Mac OS X and Linux). See [About SpectraSuite Software](#).

UMP

اونيورسيتي ملايسيا قهغ

UNIVERSITI MALAYSIA PAHANG

APPENDIX D UVNS OPTICAL FIBRE SPECIFICATION SHEET

CeramOptec[®]

Innovative Fiber Optics...Every Step of the Way™

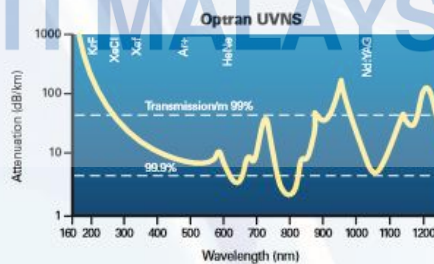
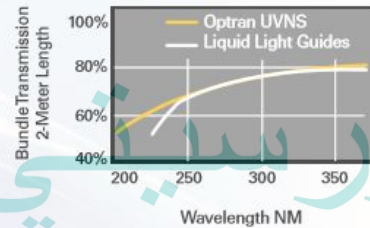
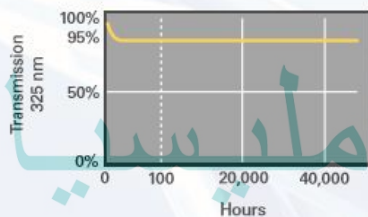
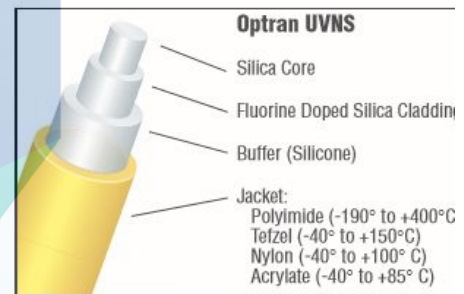
Leading the Way in Long-Term Performance

Setting new standards through breakthrough research and development is at the heart of our business. As the manufacturer of the world's first UV Non-Solarizing (UVNS) optical fiber, CeramOptec continues to find ways to break down the barriers for simplifying UV spectroscopy and sensing applications.

For long-term performance, Optran UVNS fibers and PowerLightGuide bundles set the standard. Tested for well over 40,000 continuous, unfiltered hours, our Optran UVNS fibers exhibit level, steady transmission at 95% of the original input!

Setting the Standards in Deep UV

Optran UVNS all silica optical fibers offer exceptional throughput in wavelengths ranging from 160 to 1200 nm—without solarization. When used in our PowerLightGuide™ Fused-End Bundles, our Optran UVNS fibers allow typical bundle transmission to be 50% higher than any other manufacturer of fused silica UV fiber products. CeramOptec's PowerLightGuide bundles are fused at the ends to eliminate inter-fiber spaces—while maintaining the fibers' NA. Please see our PowerLightGuide Bundle data sheet for more information about our non-solarizing bundles—a solid solution to UV Spectroscopy and Liquid Light Guides.



Applications

■ Industrial/Scientific

Replacement for UV Liquid Light Guides
Spectroscopy
Sensors
UV photolithography
Laser welding/soldering/markings
Laser delivery
Nuclear plasma diagnostics
Analytical instruments

Laser diode pigtailings
Pyrometry
Semiconductor capital equipment
Thomson scattering
UV illumination and monitoring
UV Raman spectroscopy
UV curing

■ Medical

Medical diagnostics
Laser delivery

Photodynamic therapy
Medical treatments such as UV psoriasis treatment

Features

Broad UV/VIS/NIR spectral range: 160 – 1200 nm
High laser damage resistance
Broad temperature range
High core to clad ratio
Large core diameters to 1700 μm
Biocompatible materials

Radiation resistance: 10^9 rad. total
Sterilizable by ETO and other methods
Manufactured at GMP and ISO 9001 compliant facility
Specialty coatings available for high temperatures, high vacuum, and harsh chemicals
All dielectric, non-magnetic construction

Properties

Step index profile
Pure silica core
Available NAs:
Low NA – 0.12 ± 0.02
Standard NA – 0.22 ± 0.02
Optran Plus™ $0.28 - 0.28 \pm 0.02$
Optran Plus™ $0.30 - 0.30 \pm 0.02$
Standard proof test: 70 kpsi
Core/clad ratios available: 1:1.06, 1:1.1, 1:1.15, 1:1.2, 1:1.25, 1:1.4

Minimum bend radius:
100 x clad radius (momentary)
300 x clad radius (long term)
Laser damage threshold:
XeCl 18.0 mJ/mm² (200ns pulse) at 308 nm
XeCl 8.0 mJ/mm² (20ns pulse) at 308 nm
Nd:YAG 5.4 J/mm² (1 ms pulse) at 1060 nm
Nd:YAG 1.3 kW/mm² (CW) at 1060 nm

Optran UVNS (0.22 NA) Standard Core Sizes (0.28 and 0.30 NA Also Available)

50	200	400	600	1000	1500
100	300	500	800	1250	1700

Notes:

Custom sizes are available upon request.

NA is measured at the 95% intensity angle.

CeramOptec strives to ensure the accuracy of all information provided; however, we imply no warranties and disclaim any liability in connection with the use of this information.

Tefzel® is a registered DuPont product.

Please contact our Sales Engineering representatives:

North America

CeramOptec Industries, Inc.
515A Shaker Road; East Longmeadow, MA 01028
Tel: 800-934-2377
413-525-0600
Fax: 413-525-1112
Email: salesengineering@ceramoptec.com

West Coast Office

Tel: 408-362-0100
Fax: 408-629-1657
Email: salesengineering@ceramoptec.com

Europe

CeramOptec GmbH
Siemensstr. 44; 53121 Bonn, Germany
Tel: +49 (0) 228-979670
Fax: +49 (0) 228-9796799
Email: info@ceramoptec.de

Innovative Fiber Optics...Every Step of the Way

CeramOptec was founded in 1986 and today is a global leader in the production of stock and custom silica / silica, plastic-clad silica, and hard polymer-clad silica optical fibers; fused capillary tubing; DPSS lasers; diode modules; and low loss bundles and assemblies for UV, VIS, and IR transmission, medical laser delivery, sensors, plasma fusion, and spectroscopy.

With several facilities worldwide, we are able to provide our customers with local, prompt, and reliable service and products. By maintaining complete control over the entire manufacturing process—from preform manufacturing to finished fiber product—we are able to provide the highest quality control, custom solutions, and competitive pricing to our customers.

Please visit <http://www.ceramoptec.com> for more information.

CeramOptec is a subsidiary of biolitec™ AG.

Please visit <http://www.biolitec.com> for more information.

©2003 CeramOptec Industries, Inc.

ML-135 REV. A (05/03)

APPENDIX E COLLIMATING LENS

Operating Instructions: Collimating Lenses



74-UV, 74-VIS Collimating Lenses

In order to obtain accurate data, the light entering the sample and the light collected after exiting the sample must be well collimated. The 74-UV and 74-VIS COLLIMATING LENSES screw onto the end of SMA-terminated optical fibers and other sampling optics to convert divergent beams of radiation (light) into a parallel beam.

Application Tips

- ◆ Using a collimating lens is easy. Screw a collimating lens onto the end of any SMA-terminated port to collect, shape, or focus light.
- ◆ Collimating lenses are useful for any optical setup that requires the acceptance or transmission of parallel beams of light at the illumination source, at the entrance optics, or at both ends (illumination and read) of the setup. That's important because the optical fibers Ocean Optics specifies for use with its spectrometers and light sources have a field of view (FOV) of $\sim 25^\circ$ -- an acceptance angle that may not be appropriate for some experiments. Collimating lenses are adjustable, providing FOV angles from collimation (near 0°) to $\sim 45^\circ$. Without the collimating lenses, the light would disperse more than is required for efficient transmission and collection of the signal.

Specifications

Lens diameter:	5 mm
Lens length:	10 mm
f-number:	f/2
74-UV material:	Dynasil 1100 quartz (200 nm - $2 \mu\text{m}^*$)
74-VIS material:	BK 7 glass (360 nm - $2 \mu\text{m}^*$)
Lens barrel:	stainless steel with black oxide finish
Threads:	UNC 3/8-24

* Though the product can be used to $2 \mu\text{m}$, it can be configured to "see" only to 1100 nm with our S2000 spectrometer.

Adjusting the Focus for Collimating Lenses

In order to obtain accurate data, the light entering and exiting a sample by means of a fiber/collimating lens assembly must be well collimated. The following is a description of how to adjust the focus of light so that accurate data is collected by the spectrometer. (All collimating lenses are already adjusted at the time of manufacture such that light emerging from a $200 \mu\text{m}$ fiber/collimating lens assembly is collimated.)

Adjust the focus of the collimating lens on your light source.

1. Connect the fiber that you are going to use as the illumination fiber in your setup to the light source. Ensure the connection is tight. The female SMA connector of the fiber must be screwed all the way into the male connector of the lamp.
2. Turn on the lamp and inspect the light beam emitted from the other end of the fiber by pointing the fiber at a light-colored object such as a white piece of paper. The distance is not too critical but should be at least 3 inches from the surface. Loosen the set screw on the fiber barrel of the light source with an Allen wrench.

3. After the set screw has been loosened, slide the inner barrel of the collimating lens on the light source until you see an even intensity across the beam spot. The spot of light should be uniform; there should be no fluctuations in intensity and color. There should not be any dimmer rings of light surrounding the center spot.
4. Once the inner barrel is positioned so that a well-focused, uniform spot of light is obtained, tighten the set screw with the Allen wrench. Do not put down the fiber and then tighten the set screw. Try to continue to hold the fiber 3 inches from the surface while you tighten so that if the inner barrel of the collimating lens slips and distorts the spot of light, you will be able to readjust the focus. Now the collimating lens on the light source is focused for the fiber.

Adjust the focus of the next collimating lens in your setup.

5. For this part of the procedure, the illumination fiber is still connected to the lamp and its collimating lens and the lamp is still on. Now take the second collimating lens in your setup (removed from the illumination side of a cuvette holder, for example) and screw it onto the *other* end of the illumination fiber. Make sure the fiber and the second collimating lens are completely connected. Point this end of the fiber at least 2 meters away from a wall. If the beam spot on the wall is too faint, you may need to dim the room lights.
6. Loosen the set screw that holds the barrel of this second collimating lens in place and slide the barrel until the spot of light focused on the wall has crisp edges. You are looking for the sharpest and cleanest image possible. Tighten the set screw. Do not put the fiber down and then tighten the set screw. Try to continue to hold the fiber with the spot of light focused on the wall while you tighten the set screw so that if the inner barrel of the collimating lens slips and distorts the image while tightening, you will be able to readjust the focus. Now that the second collimating lens has been refocused, remove it from the end of the fiber and install it back into your setup (back into a cuvette holder, for example).

Continue to adjust the focus of the other collimating lenses in your setup.

7. You have completed adjusting the focus of the collimating lenses in the illumination part of your setup. Continue to adjust the focus of the other collimating lenses in your setup. If the read fiber is the same diameter size as the illumination fiber, repeat step 6 with each collimating lens in your setup. If the read fiber is a different diameter size than that of the illumination fiber, you need to remove the illumination fiber from the light source, connect the read fiber to the light source, and repeat step 6 for every collimating lens on the read part of your setup.

UMP

اونيورسيتي ملايسيا قهق

UNIVERSITI MALAYSIA PAHANG

APPENDIX F SPECTROMETER CALIBRATION

Calibrating the Spectrometer

Preparing for Calibration

To recalibrate the wavelength of your spectrometer, you need the following components:

- A light source capable of producing spectral lines

Note

Ocean Optics' HG-1 Mercury-Argon lamp is ideal for recalibration. If you do not have an HG-1, you need a light source that produces several (at least 4-6) spectral lines in the wavelength region of your spectrometer.

- A Maya2000Pro Series spectrometer
- An optical fiber (for spectrometers without a built-in slit, a 50- μm fiber works best)
- A spreadsheet program (Excel or Quattro Pro, for example) or a calculator that performs third-order linear regressions

Note

If you are using Microsoft Excel, choose **Tools | Add-Ins** and check **AnalysisToolPak** and **AnalysisToolPak-VBA**.

Calibrating the Wavelength of the Spectrometer

► Procedure

Perform the steps below to calibrate the wavelength of the spectrometer:

1. Place the spectrometer operating software into Scope mode and take a spectrum of your light source. Adjust the integration time (or the A/D conversion frequency) until there are several peaks on the screen that are not off-scale.
2. Move the cursor to one of the peaks and position the cursor so that it is at the point of maximum intensity.
3. Record the pixel number that is displayed in the status bar or legend (located beneath the graph). Repeat this step for all of the peaks in your spectrum.
4. Use the spreadsheet program or calculator to create a table like the one shown in the following figure. In the first column, place the exact or true wavelength of the spectral lines that you used.

In the second column of this worksheet, place the observed pixel number. In the third column, calculate the pixel number squared, and in the fourth column, calculate the pixel number cubed.

Independent Variable	Dependent Variables			Values Computed from the Regression Output	
True Wavelength (nm)	Pixel #	Pixel # ²	Pixel # ³	Predicted Wavelength	Difference
253.65	175	30625	5359375	253.56	0.09
296.73	296	87616	25934336	296.72	0.01
302.15	312	97344	30371328	302.40	-0.25
313.16	342	116964	40001688	313.02	0.13
334.15	402	161604	64964808	334.19	-0.05
365.02	490	240100	117649000	365.05	-0.04
404.66	604	364816	220348864	404.67	-0.01
407.78	613	375769	230346397	407.78	0.00
435.84	694	481636	334255384	435.65	0.19
546.07	1022	1044484	1067462648	546.13	-0.06
576.96	1116	1245456	1389928896	577.05	-0.09
579.07	1122	1258884	1412467848	579.01	0.06
696.54	1491	2223081	3314613771	696.70	-0.15
706.72	1523	2319529	3332642667	706.62	0.10
727.29	1590	2528100	4019679000	727.24	0.06
738.40	1627	2647129	4306878883	738.53	-0.13
751.47	1669	2785561	4649101309	751.27	0.19

- Use the spreadsheet or calculator to calculate the wavelength calibration coefficients. In the spreadsheet program, find the functions to perform linear regressions.
 - If using Quattro Pro, look under **Tools | Advanced Math**
 - If using Excel, look under **Analysis ToolPak**
- Select the true wavelength as the dependent variable (Y). Select the pixel number, pixel number squared, and the pixel number cubed as the independent variables (X). After executing the regression, you will obtain an output similar to the one shown below. Numbers of importance are noted.

Regression Statistics

Multiple R 0.999999831
 R Square 0.999999663 ← R Squared
 Adjusted R Square 0.999999607
 Standard Error 0.125540214
 Observations 22

	<u>Coefficients</u>	<u>Standard Error</u>	
Intercept	190.473993	0.369047536	← First coefficient
X Variable 1	0.36263983	0.001684745	
X Variable 2	-1.174416E-05	8.35279E-07	
X Variable 3	-2.523787E-09	2.656608E-10	← Second coefficient
			← Third coefficient

اونيورسيتي ماليزيا قهق

UNIVERSITI MALAYSIA PAHANG

7. Record the Intercept, as well as the First, Second, and Third Coefficients. Additionally, look at the value for R squared. It should be very close to 1. If not, you have most likely assigned one of your wavelengths incorrectly.

Keep these values at hand.

Saving the New Calibration Coefficients: USB Mode

Ocean Optics programs wavelength calibration coefficients unique to each Maya2000Pro Series Spectrometer onto an EEPROM memory chip in the spectrometer.

You can overwrite old calibration coefficients on the EEPROM using the Maya2000Pro Series Spectrometer via the USB port.

► Procedure

To save wavelength calibration coefficients using the USB mode, perform the following steps:

1. Ensure that the Maya2000Pro Series is connected to the PC and that you have closed all other applications.
2. Point your browser to <http://www.oceanoptics.com/technical/softwaredownloads.asp> and scroll down to **Microcode**. Select **USB EEPROM Programmer**.
3. Save the setup file to your computer.
4. Run the **Setup.exe** file to install the software. The **Welcome** screen appears.
5. Click the **Next** button. The **Destination Location** screen appears.
6. Accept the default installation location, or click the **Browse** button to specify a directory. Then, click the **Next** button. The **Program Manager Group** screen appears.
7. Click the **Next** button. The **Start Installation** screen appears.
8. Click the **Next** button to begin the installation. Once the installation finishes, the **Installation Complete** screen appears.
9. Click the **Finish** button and reboot the computer when prompted.
10. Navigate to the **USB EEPROM Programmer** from the Start menu and run the software.
11. Click on the desired spectrometer displayed in the left pane of the **USB Programmer** screen.
12. Double-click on each of the calibration coefficients displayed in the right pane of the USB Programmer screen and enter the new values acquired in Steps 5 and 6 of the [Calibrating the Wavelength of the Spectrometer](#) section in this appendix.
13. Repeat Step 12 for all of the new values.
14. Click on the **Save All Values** button to save the information, and then **Exit** the USB Programmer software.

The new wavelength calibration coefficients are now loaded onto the EEPROM memory chip on the Maya2000Pro Series Spectrometer.